Development of a hollow fiber membrane microfluidic system to predict human pharmacokinetics in vitro

Msc thesis in Biomedical Engineering

Sarah Braem

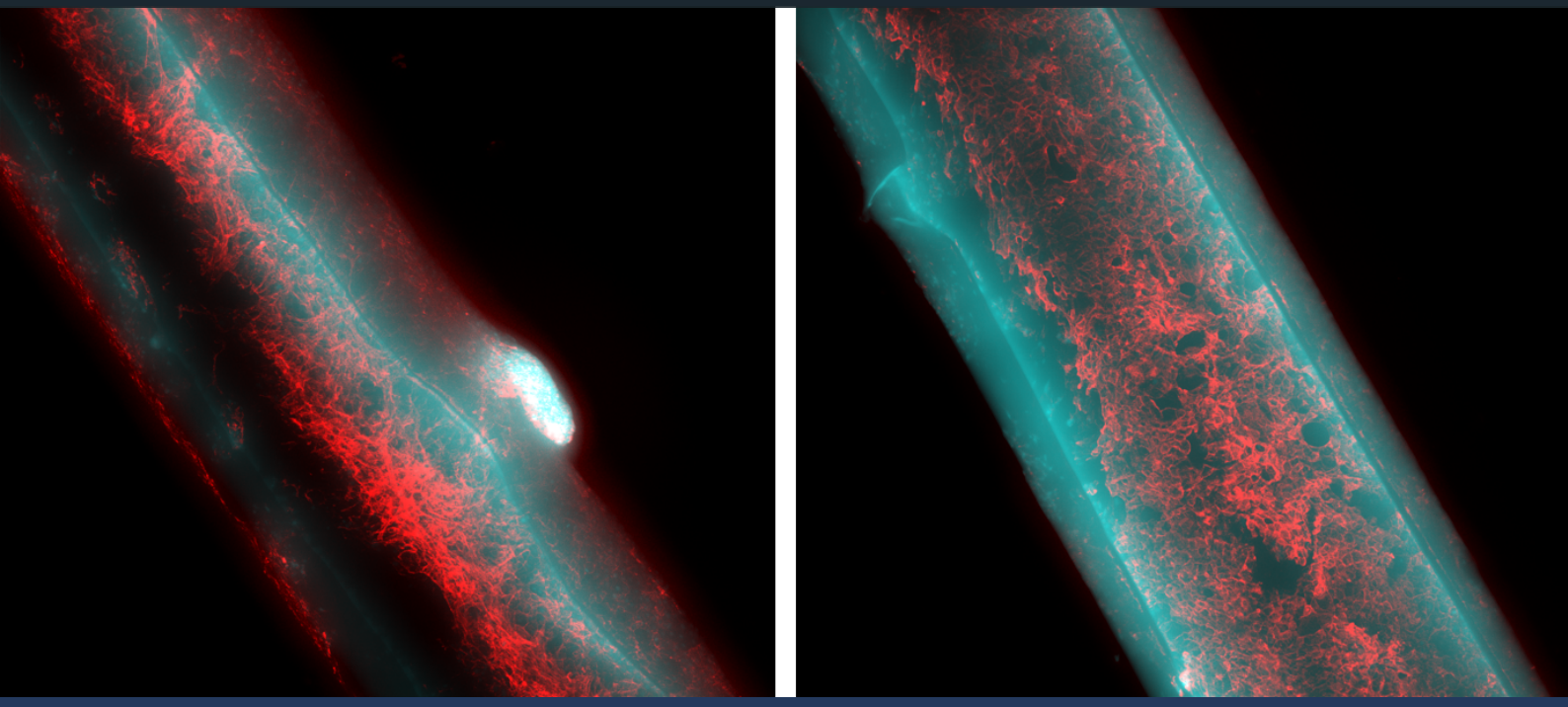

TU Delft

Development of a hollow fiber membrane microfluidic system to predict human pharmacokinetics in vitro

Msc thesis in Biomedical Engineering

Thesis report

by

Sarah Braem

to obtain the degree of Master of Science
at the Delft University of Technology
to be defended publicly on May 17, 2023 at 15:30

Thesis committee:

Chair:	Prof. dr. ir. R. Dekker
Supervisors:	dr. M. Keuper-Navis
	dr. J. Donkers
External examiners:	Dr. B. Spee
	Prof. dr P. M. Sarro
Place:	Faculty of Mechanical Engineering, Delft
Project Duration:	September 2022 - May 2023
Student number:	4564847

An electronic version of this thesis is available at `http://repository.tudelft.nl/`.

Faculty of Mechanical Engineering · Delft University of Technology

Abstract

Drug efficacy and side effects are significantly impacted by the first-pass metabolism, a sequence of events that occurs in the stomach and the liver after oral ingestion. Accurate prediction of this mechanism is crucial for a faster and more cost-efficient drug development process. Replicating the first-pass metabolism *in vitro* using standard cell culture techniques is challenging due to its complexity involving simultaneous transport and organ-organ interactions in both the gut and liver tissue. A more precise *in vitro* to *in vivo* translation of drug distribution, efficacy, and toxicity may be provided by organ-on-a-chip (OoC) models, thereby creating the ability to partially replace currently-used animal models. More specifically, gut-liver-on-a-chip models can aid with *in vitro* predictions of oral drug administration and the first-pass metabolism. Therefore, the aim of this thesis was to develop an OoC system that could accommodate both intestinal and hepatic cell sources. A hollow fiber membrane (HFM) as a cell scaffold was a critical component of the chip design in order to more accurately reproduce the three-dimensional native environment of the cells. Additionally, the system would need to exhibit the ability to be interconnected quickly and easily, thereby creating the possibility to develop a MOoC system in a plug-and-play manner in a later stage of development, enabling the ultimate realization of organ-organ interactions.

Preface

I would like to express my gratitude to everyone who has contributed to completing my thesis.

Firstly, I would like to thank my supervisors Marit Keuper-Navis and Roland Dekker for their guidance, advice, and support throughout the entire process. Their expertise and insights have been invaluable in shaping my research and helping me to reach the finish line.

I would like to sincerely thank the Department of MHR at TNO for their support throughout the process and for providing access to the resources that made my research possible. My special thanks go out to Hossein Eslami Amirabadi for assisting me with all my technical issues and for the great insights and interesting conversations during the whole project, Angelique van Santen for assisting me with the 3D printing process, Maria Kloukinioti and Marta Hanczar for the lab and mental support, and finally Joanne Donkers for guiding me through the final parts of my thesis.

Lastly, I would like to thank my friends and family for their patience, understanding, and support. Special thanks go out to Loïc Struyvelt and Marijne van den Ende for their eternal encouragement and belief in me, which have helped me to overcome the challenges and obstacles that I faced throughout my thesis.

Contents

Nomenclature

List of Abbreviations

3D Three-dimensional

ACAT Model Advanced Compartmental Absorption and Transit (ACAT) model

ADR Adverse Drug Reaction

AM Additive Manufacturing

AV Arteriovenous reservoir

BSA Bis(trimethylsilyl)acetamide

CAT Model Compartmental Absorption and Transit Model

CYP Cytochrome P450 enzymes

DLP Digital Light Processing

DMD Digital Micro Mirror Device

ECM Extracellular Matrix

ER Efflux Ratio

FA Fraction absorbed

FD4 Fluorescent Dextran 4 kDa

GDFS gravity-driven flow

GI Gastrointestinal Tract

HBSS Hanks' Balanced Salt Solution

HFM Hollow Fibre Membrane

hiPSCs Human Induced Pluripotent Stem Cells

ICO Intrahepatic cholangiocyte organoids

IEBC Intestinal Explant Barrier Chip

IPS Induced Pluripotent Stem Cell

L-Dopa L-3,4-di-hydroxyphenylalanine

LDH Lactate Dehydrogenase

MAD Maximum Absorbable Dose

MOoC Multi-Organ-on-a-Chip

NSA Non-specific Adsorption

OoC Organ-on-a-Chip

PDFS pump-driven flow

PDMS Polydimethylsiloxane

PEG poly(ethylene glycol)

PES Polyether Sulfone

PFA Perfluoroalkoxy alkanes

PLA Polylactic

PP Portal Vein

PV Hepatic Vein

SLA Stereolithography

SLM Selective Laser Melting

SLS Selective Laser Sintering

TEER Transepithelial Electrical Resistance

ZO-1 Zonula occludens-1

List of Symbols

η Viscosity

τ Fluid flow

A	Surface area
C_H	Driving force concentrations
$CL_{int,G}$	Internal clearance of the gut
CL_{perm}	Permeation clearance
E_G	Extraction ratio of the gut
E_H	Extraction ratio of the liver
F	Oral bioavailability
F_G	Gastrointestinal bioavailability
F_H	Hepatic bioavailability
F_{abs}	Fraction absorbed
F_S	percentage of the dosage that, following oral administration, enters the systemic circulation as an unaltered drug
h	Height
P_{app}	*In vitro* apparent permeability
P_{eff}	*In vivo* effective permeability
Q	Volumetric flow rate
Q_{gut}	Hybrid between intestinal blood flow and permeability
Q_{villi}	Rate of villous blood flow
S	Solubility
TT_{si}	Transit time of the gut
w	Width
C_{in}	Drug concentration in the blood entering the liver
C_{out}	Drug concentration in the blood that leaves the liver
CL_H	Hepatic clearance
$CLint$	Intrinsic clearance of the liver
Q_H	Flow of blood through the liver
f	Proportion of the drug in the blood that is unbound to plasma proteins or free to interact with hepatic enzymes

List of Figures

List of Tables

1 Introduction

1.1. Predicting Human Pharmacokinetics in Vitro

The development of orally administered drugs is a lengthy, laborious, and costly process. Despite an extensive preclinical screening process and a significant investment of resources, almost 90% of drugs entering Phase I clinical trials ultimately fail due to efficacy or unforeseen side effects. One of the main factors contributing to the poor translation of drug candidates into practical use is the lack of model systems that accurately mimic the normal function of human organs and their response to drug molecules. Traditionally, animal models or conventional static two-dimensional (2D) cell culture models are used in the earliest phases of drug development but these are often not reliable. Static cell culture methods fail to mimic the complexity of native tissue environments because they differ significantly from biological tissues, with the most significant difference being their 2D rather than three-dimensional (3D) architecture. Therefore, a new approach that delivers reliable drug toxicity data is required. The organ-on-a-chip model (OoC) is a new technology that can mimic the complexity of native tissues *in vitro*, and many distinctive OoC devices have been developed recently. However, various elements of typical human tissue are still missing in current OoC models. Single-organ systems lack the intricate intercellular and interorgan communication that takes place *in vivo*, making them unable to accurately represent the enterohepatic circulation and metabolism that are responsible for breaking down toxic compounds. Therefore, despite the fact that phylogenetic differences between species frequently prevent animal models from accurately simulating human physiology, and despite the ethical concerns and high costs associated with their use, animal models continue to be the gold standard for drug testing because, as of yet, *in vitro* models have been unable to accurately reproduce the native conditions [1].

Consequently, new models are required to recreate the dynamic microenvironment of the organs involved in the drug clearance process which allow for better recapitulation of the 3D native tissues present *in vivo*. Orally administered drugs undergo a series of steps after ingestion, called the first-pass metabolism. In this process, drugs are first absorbed in the gut, followed by metabolism in the liver before entering the systemic circulation [2, 3]. Accurately predicting the first-pass metabolism is crucial for making the drug development process more cost- and time-efficient, as many drug candidates fail due to unanticipated toxicity or ineffectiveness, which is greatly

influenced by the first-pass metabolism [3]. To achieve a better understanding of the mechanisms involved in this mechanism, new multi-organ microfluidic (MOoC) systems are required. These systems can better mimic the first-pass metabolism than single OoC devices due to their more complicated configurations, which allow for the replication of complex organ-organ interactions and cross-signaling *in vitro* [3, 4]. As the liver and the gut are the most important organs involved in the first-pass metabolism, individual gut- and liver-on-a-chip models that are able to replicate the native 3D environment of cells should be linked to provide a more accurate model of the first-pass metabolism [3].

The aim of this thesis was to develop an OoC system that could accommodate both intestinal and hepatic cell sources. The inclusion of a hollow fiber membrane (HFM), which is employed as a scaffold for the cells to generate a 3D structure that more closely reflects their *in vivo* architecture, was a crucial design requirement of the system. Additionally, the system would need to exhibit the ability to be interconnected quickly and easily, thereby creating the possibility to develop a MOoC system in a plug-and-play manner, enabling the ultimate realization of organ-organ interactions at a later stage of development. Although some MOoCs have been developed that link the gut and the liver, none of these take into account the pathway by which a drug is secreted after it passes the liver. The incorporation of a two-compartment model, in which one compartment represents the systemic circulation and the second compartment represents the bile, is therefore a crucial addition to this system. This allows for the precise tracking of the pathway of a drug and its metabolites after they leave the hepatic circulation. When compared to previous systems, this addition is a significant improvement since, even if a compound may become toxic after metabolization by the liver, if it is secreted into the bile after exiting the liver, the component would leave the body and would not be considered harmful. Consequently, in contrast to current MOoC models, these drugs would not be immediately rejected in the first phase of development, allowing for a higher throughput of drugs in the first phases of the development process.

1.2. Research Formulation and Design Requirements

The following research objective was determined for this project:

Research Objective

Development of a microfluidic system for intestinal and hepatic cell sources which can house a hollow fiber membrane and that can be easily interconnected to predict human pharmacokinetics *in vitro*.

The most important design requirements to reach this objective were:

- The facile inclusion and removal of a HFM into the device.
- The development of a two-compartment model, which can be employed for both the hepatic as well as the intestinal model with the possibility to sample in both compartments.
- The ability to easily interconnect single devices in a plug-and-play configuration.
- The possibility to culture cells on the HFM outside of the chip environment to avoid cell attachment to the chip material.

1.3. Relevance of Research

The development of the chip in this project is part of the research for a larger consortium project, namely "*Drug disposition On-a-Chip: a multi-organ-on-chip model tailored to mimic pharmacokinetics in vitro*". This overarching project, which combines knowledge from the academic world with the public industry, consists of four phases: the first step is to generate the individual organ chips involved in the drug disposition process (liver, kidney, intestine, and bile duct). Secondly, these organ chips need to be fluidically interconnected. The third phase is validating the operation of the linked organ-on-a-chip devices using drugs with known pharmacokinetic behavior. Finally, data is required to demonstrate that readouts from this newly constructed technology may be used to effectively mimic how drugs are disposed of in humans. Therefore, this thesis project is a part of the initial phase of developing a MOoC model to simulate human pharmacokinetics *in vitro*. The University of Utrecht supervises the initiative (NL). The Netherlands Organization for Applied Scientific Research (NL), TNO (NL), Novartis (CH), and Cell4 Pharma (NL) are the consortium partners.

The societal relevance of this project will be described by means of connecting the project goals to the overarching Sustainability Goals of the United Nations [5]. The relevant goals for this project have been selected and are illustrated in Figure 1.1.

Goal 3: Good Health and Well-being: The development of OoC models can contribute to speeding up the drug development process and aid in the more rapid detection of a higher volume of new drug candidates. OoC technology enables researchers to create more effective treatments for a range of diseases, thereby improving the health and well-being of people and society as a whole.

Goal 5: Gender Equality: Clinical trials have traditionally focused mostly on men, and little is known about how drugs and treatments affect women. Researchers can contribute to ensuring that women receive the same degree of care and consideration as men by employing OoC models to examine the impact of drugs and treatments on female biology. This is especially important when investigating diseases and issues that give rise to gender-specific symptoms and disease development such as e.g. heart disease and cancer. The development of OoC technology may lead to a more inclusive test panel as female cell sources can be easily included in the testing models. Thereby, researchers can better comprehend these gender-specific distinctions and provide more individualized therapies. Concludingly, OoC technology has the potential to significantly advance gender equality in healthcare by providing more accurate and detailed information about how drugs and treatments affect women.

Goal 9: Industry, Innovation, and Infrastructure: OoC technology is a revolutionary and innovative method that has the potential to transform the medical field and drug research.

Goal 10: Reduced Inequality: Historically, medical research has focused on white, male participants as test subjects, resulting in an enormous discrepancy in the knowledge of how different populations can react to medical treatments. Promoting inclusion in the creation and use of novel technologies like OoCs is essential to resolve this problem. This involves broadening the diversity of the study population and taking into account the specific needs and perspectives of other populations. By doing so, everyone can benefit from new technologies, regardless of race, gender, or other variables. The development of OoC technology can therefore lead to a more inclusive test panel as cell sources from many different ethnicities can be easily included in the

testing models.

Goal 12: Responsible Consumption and Production: By reducing material waste during manufacture, the chip in this project will be made responsibly. In order to enhance the sustainability of the usage of OoC technology, the chip will also be designed to enable sterilization and reuse of all components. Additionally, the application of OoC technology is consistent with the 3Rs (Replacement, Reduction, and Refinement) of research. The 3Rs aim to encourage researchers to minimize the number of animals used in studies, increase the well-being of animals used in research, and identify alternatives to animal testing wherever feasible. By reducing the need for animal testing, OoC technology has the potential to significantly reduce animal use in research while still allowing for the development of safe and effective drugs and therapies.

Goal 17: Partnerships for the Goals: This initiative is part of a consortium effort that brings together several organizations. It enables the integration of OoC technological knowledge and expertise from numerous parties, combining knowledge from the academic world with the public industry.

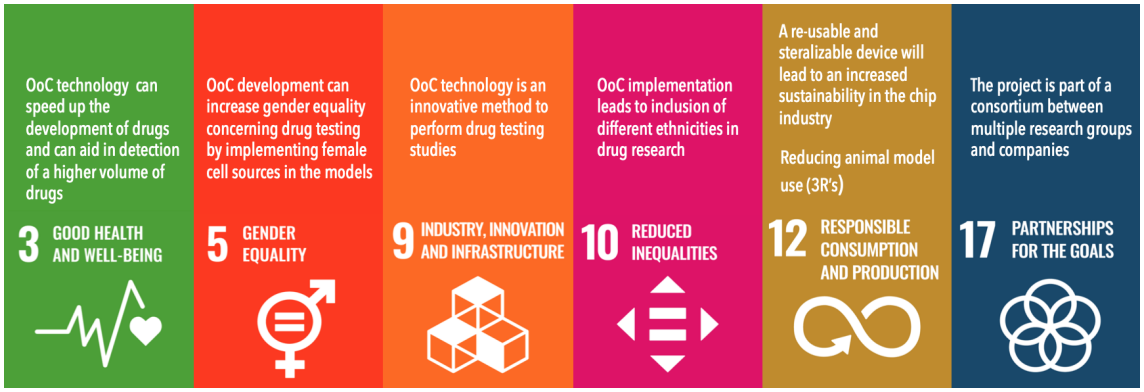

Figure 1.1: Correlating project goals with UN sustainability goals.

1.4. Structure of the Report

The purpose of this report is to provide an overview of the steps that were taken into creating and optimizing a new OoC model to predict human pharmacokinetics *in vitro*. This thesis report will be divided into two main parts including the design and technical work (chapters 3, 4 and 5) and the biological work (chapters 6 and 7). The report is organized as follows; Firstly, Chapter 2 provides a literature review concerning the most important concepts that were used as a guide in the development process. The design criteria for the creation of the HFM chip system are then included in Chapter 3. The overview and renders of the final design are included in Chapter 4, which also discusses the design and development process. Subsequently, chapter 5 offers the technical validation of the chip design. The cell investigations are then shown in Chapter 6, after which the biological validation is presented in Chapter 7. At the end of each chapter, a chapter discussion and conclusion will be provided. Finally, chapter 8 provides a general discussion and recommendations for the future directions of the project, and Chapter 9 concludes the thesis project as a whole.

2

Theoretical Background

2.1. Working Mechanism of the Gut

Understanding gut anatomy and physiology is essential for this project. The principal function of the gut is to absorb and digest nutrients and contribute to a good water balance in the body [6]. At the same time, it also serves as a protective epithelial barrier because it prevents compounds like pathogens and bacteria from entering the body [7]. Furthermore, the gut is also a key player in the immune and endocrine systems [8, 9, 10]. Because of its myriad of functions, the gut also plays a crucial role in the proper functioning of many other organs [11].

Another important aspect that relates to understanding the physiology of the gut is that the epithelial cells of the gut are colonized by large numbers of micro-organisms which are together called the microbiota [12]. The largest density of these organisms is found in the gastrointestinal tract (GI), and because of this, the gut is the most important study topic in microbial research [12]. These bacteria have many different functions, which are for the most part situated in the large intestine, and comprise things like the prevention of bacterial overgrowth, resistance to pathogens, training and development of the immune system, and many more [12].

When designing a gut-on-a-chip model, one has to realize that the gut possesses this great variability because, anatomically, it looks very different at the beginning than at the end [6]. The gut consists of three main parts: the small intestine, the large intestine, and the rectum [6]. All these parts have specific anatomical and physiological characteristics and possess different functions [6]. So, to properly study the mechanisms of the gut, models for each of these parts of the gut are needed [6].

2.1.1. The Small Intestine

Absorption and digestion are the main functions of the small intestine [13]. The small intestine is the primary digestive organ of the body and absorbs almost all nutrients, and more than 95% of the water [14]. Digestion occurs with the help of bile, and pancreatic enzymes [13]. Absorption is highest in this part of the gut because the small intestine is highly adapted for the absorption of nutrients [13]. The intestinal epithelium is extensively folded, which enhances the absorptive surface enormously [6, 13].

The intestinal epithelium has three structural modifications called circular folds, villi, and microvilli [13]. Because of the circular folds, there is more time to achieve full nutrient absorption [13]. The villi are essential for absorbing digested food molecules to the capillary blood, and the lacteal [13]. On the surface of the microvilli, enzymes called the brush border enzymes are present, which are responsible for the digestion of proteins and carbohydrates in the small intestine [13].

The intestinal epithelium consists of five main types of cells: enterocytes (responsible for absorption of nutrients and electrolytes), enteroendocrine cells (excretion of hormones), goblet cells (mucus-secreting cells), Paneth cells (secretory cells), and stem cells (continuously dividing cells in the depth of the crypts of which daughter cells can differentiate into all of the other cell types) [13]. When designing a gut-on-a-chip model, all these types of cells must be represented in the model. To achieve this, one should be able to culture the five types of human gut cells in the small intestine from stem cells on a microfluidic chip [6]. However, even if the desired cell types can be cultured on the chip, still one crucial aspect of normal intestine function is lacking; namely, peristalsis [6].

Peristalsis is a propulsive movement of alternating contractions and relaxations of muscle layers that mix substances and squeeze them through the internal pathway [13]. Because this movement significantly contributes to intestinal function and health, it is vital to incorporate this property into a model to represent intestinal function adequately [7]. Conventional models lack the property to reproduce peristaltic movement and thereby cannot reproduce the intestinal folds, and villus structures crucial to the standard intestine function [7]. In organ-on-a-chip models, this problem can be overcome by introducing a laminar fluid flow that mimics the peristaltic movement of the gut, and in some cases, the cells are even stretched and relaxed to mimic the behavior even closer [7]. This capability to form a 3D structure in the gut-on-a-chip model results in a model that can better represent the small intestine function than conventional models, which do not comprise this capability.

2.1.2. The Large Intestine

The large intestine primarily absorbs most of the remaining water from food residues that are indigestible, stores these components for a short period, and finally eliminates them from the body as feces [13]. Furthermore, it also takes up metabolites and vitamins produced by bacteria. These ferment carbohydrates that could not be absorbed in the small intestine and synthesize some vitamins like B complex vitamins and vitamin K [13]. The bacterial flora (also called gut microbiome) of the large intestine comprises over a thousand different types of bacteria and is of essential importance for human health and for enteral and nonenteral disease development [13, 7].

However, because the gut microbiome is crucial for the normal functioning of the large intestine, it is challenging to create proper representative models for this part of the gut [6, 7]. This is mainly due to the difficulty in co-culturing these bacteria with the living epithelium of the large intestine for longer than one day using conventional models and even when using intestinal organ cultures [7]. In conventional models, bacteria rapidly overgrow the living epithelium of the gut, which tremendously limits the period in which the model can be used [7]. In organ-on-a-chip models, this overgrowth is prevented by introducing a continuous laminar fluid flow in the large intestine model, which results in a more extended period to use the model [6, 7].

Another critical aspect of the large intestine is that the inside (or lumen) of the large intestine is oxygen-deprived [6]. Many of the gut microbiome bacteria would not even survive an environment where oxygen is present [6]. Nevertheless, the epithelial layer of the large intestine on the side of the blood does require oxygen which is typically provided by oxygen transport via the blood [6]. These features do not facilitate the production of a representative model for the large intestine, but these hurdles can be overcome by using an organ-on-a-chip model.

2.1.3. Modeling gut-on-a-chip devices

Although there are many different organ-on-a-chip models, many of them share similar features [11]. Mostly, the chips are gas permeable and optically transparent such that gases like carbon dioxide and oxygen can quickly diffuse, and observations and imaging are facilitated [11]. Inside the body of the chip, the channels are housed next to other embedded elements like, for example, electrodes or sensors [11].

For a gut-on-a-chip model, the chip mainly comprises two microfluidic channels separated by a flexible and porous membrane [11]. The top microfluidic channel (at the luminal side) is an oxygen-poor channel in which bacteria can be added and gut epithelial cells can be cultured [6, 11]. These cells are first seeded under static conditions within the channel to make sure there is proper adherence of the cells, and later on, a medium is forced through the channel by the use of a particular pump (peristaltic, syringe, or pressure pump) [11]. The flow is added to mimic the dynamic microenvironment that is found in the native environment of the cells [11]. Furthermore, a second microfluidic channel on the bottom mimics a blood vessel with vascular endothelial cells that line the vessel and is an oxygen-rich environment [6, 11].

In between the channels is a porous membrane that separates the two channels and on which the gut epithelial cells can grow [6]. As mentioned before, these two microfluidic channels are isolated from each other by a flexible and porous membrane that has as its primary function to permit the transport of soluble molecules between the two channels [11]. Although a membrane is used in most gut-on-a-chip models, more recent research sometimes eliminates the membrane to approximate the native tissue even better [15]. Finally, the channels are surrounded by vacuum chambers responsible for the simulation of peristaltic movement and deformation. This deformation has been shown to help in the maturation and formation of 3D tissue structures in gut-on-a-chip models [11].

As for the cells used for modeling the gut, the most widely used cell line is the Caco-2 cell line, which was derived from colon cancer [16]. Despite not having a small intestine origin, when appropriately differentiated, it has been shown to exhibit p-glycoprotein transporter and brush border enzymes, among other small intestine-specific characteristics [16]. In conventional 2D cultures, the Caco-2 cell line is employed in a transwell format, where the cells are cultivated on a semipermeable membrane in an insert that is housed inside the receiving compartment. The Caco-2 cell line exhibits a number of flaws despite being a still-commonly-used model, including erroneous absorption kinetics for hydrophilic substances transported along the paracellular pathway and the absence of important metabolizing enzymes and mucin proteins [16]. The unusual, three-dimensional structure of the gut epithelium, known as the villi and crypts, is one of the distinguishing features of the gut [16]. These protrusions and indentations in the gut epithelium affect the proliferation and differentiation of the gut cells in the intestinal epithelium as well as the

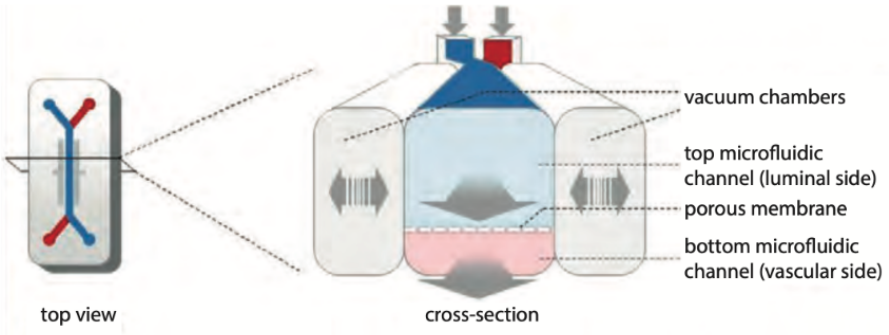

Figure 2.1: Example of a typical gut-on-a-chip device consisting of two microfluidic channels (one on the luminal side and one on the blood side, separated by a porous membrane and with a vacuum chamber that simulates peristalsis [6].

absorptive surface area. It has been hypothesized that 2D monolayer cultures on a flat surface are one of the primary drawbacks of the conventional Caco-2 paradigm [16]. The 2D monolayer culture fails to replicate the complicated spatial gradient of chemicals and the expression of important proteins, including alkaline phosphatases, dipeptidases, CYP enzymes, and transporter proteins. It also fails to mimic the real absorptive surface area of the gut epithelium [16].

However, when these cells are cultured in a fluidic environment inside a microfluidic device, where the cells can grow on a semipermeable membrane between the two compartments of the chip, the cells spontaneously produce microscale structures resembling the gut villi [17]. The introduction of a flow also allows the cells to differentiate into the four main intestinal cell types, including enterocytes, Paneth cells, goblet cells and enteroendocrine cells [18]. Further research showed that the combination of fluidic shear and cyclic strain in the microfluidic device allowed the cells to produce villi structures [17]. Nowadays, multiple cell stimuli methods have been used to stimulate cells to create mature cell tissue *in vitro*. However, biomimetic shear stress provided by the presence of a fluid flow can still be seen as one of the most important stimuli for forming mature tissue in the models [11]. Next to this, it is important to note that for gut-on-a-chip devices used for drug permeability studies, a separated fluid flow to both the apical and basolateral side of the cells in the microfluidic device is a crucial requirement [19]. This second and separate fluid flow is used to mimic the transport of intestinal material inside the intestine on one side of the device (apical or luminal surface) and the blood supply on the other side (basolateral or serosal surface) [20]. In this way, the cells reside in a dynamic environment while continuously being perfused with fresh nutrients and waste products are removed simultaneously [20].

Next to fluid flow, strain resulting from peristaltic movement also induces the formation of crypts and villi [11]. On top of this, the strain also induces the formation of a brush layer, tight junctions, and a mucous layer [11]. Remarkably, these mechanical stimuli seem to influence the gut epithelial cells, and their micro-organisms [21]. When mechanical stimuli like fluid flow and peristaltic strain are present in the model, the invasion of micro-organisms increases [21].

Although 2D cell cultures in combination with microfluidics can better mimic the native intestinal tissue than conventional 2D models, it has been reported that when a 3D structure-based system was used as a gut model, drug absorption and cellular differentiation were more closely resembled

than in traditional 2D cell culture methods [17]. So, in order to more closely mimic the *in vivo* gastrointestinal system, cell sources comprising 3D characteristics and a dynamic environment should be combined in a microfluidic system [17].

One example of an intestine-on-a-chip that is of significant importance for this research is the Intestinal Explant Barrier Chip (IEBC). This is a gut-on-a-chip system that has been developed by TNO and which is generated using high-resolution stereolithography (SLA) 3D printing with a resin that is used in dental applications to ensure biocompatibility of the chip [19]. The suitability of the resin that was used to produce this chip was verified by measuring the recovery of seven marketed and FDA-approved drugs [19]. The average recovery of these drugs was between 86-90% and the number of drugs that resided in the tissue was less than 1% [19]. These findings confirm that the material of the IEBC is suitable to study the transport of small molecules through the digestive tract without losing a significant amount of the test drugs to non-specific binding (adsorption) or uptake (absorption) by the materials in the microfluidic system [19]. Furthermore, the system can incorporate tissue explants or 3D organoid cultures between two microchannels, creating a dynamic microenvironment similar to the one found *in vivo* [19]. The IEBC comprises a snap-fit mechanism to fix a tissue explant or organoid culture between its two microchannels (Figure 2.2). This mechanism consists of a sealing rubber, a support net, a tissue explant or organoid culture, a fixing insert, and is closed by a 3D printed removable cap [19]. SLA 3D printing was also used to create the mechanics of the chip. Common fluidic ports can be printed on the chip, such as barbed connectors or threaded holes for finger-tight connectors [19]. These ports link the chip to a microfluidic recirculation system, in which a peristaltic pump circulates media around the tissue explant on both sides (Figure 2.3) [19].

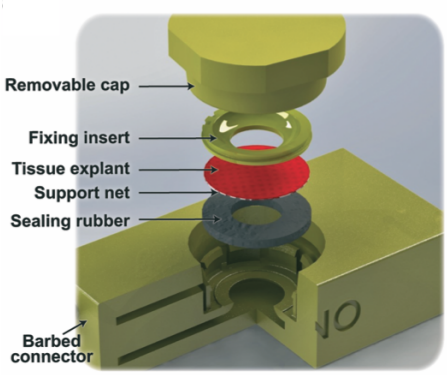

Figure 2.2: Overview of the parts of the IEBC mechanism. The IEBC consists of a removable cap, a fixing insert, a tissue explant or monolayer with Caco-2 cells or organoids, a support net, and a sealing rubber. Figure adapted from *Amaribadi et al.* [19].

Although this system has been validated and shows clear benefits over other intestine-on-a-chip systems, one of its major disadvantages is the 2D configuration of the cells on the insert. Cells are cultured in static conditions on a flat membrane in a similar manner as they are in a conventional 2D Transwell configuration. Although a combination of 2D cell cultures with microfluidics can better mimic the native intestinal tissue over conventional static Transwell 2D models, the flat membrane lacks the support for the cells to form intestinal tube-like structures [17, 18]. It is important to note that local geometrical properties partly regulate the proliferation and differentiation of biological

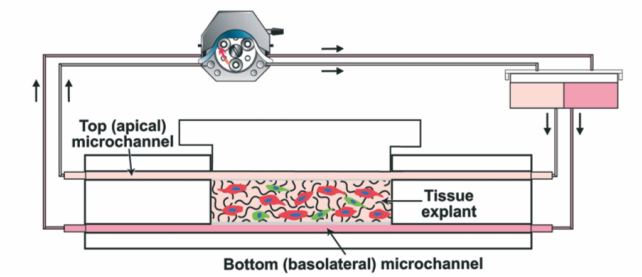

Figure 2.3: The IEBC microfluidic recirculation system is shown schematically. The reservoirs are filled with medium. The peristaltic pump extracts medium from the reservoirs and returns it to the reservoirs by recirculation. The tissue explant or organoids are positioned between two microfluidic channels in the IEBC, that represent the basolateral and apical sides of the intestine Figure adapted from *Amaribadi et al.* [19].

tissues [18].

Hollow fiber membranes (HFM), such as those made of the reliable and affordable biocompatible substance polyether sulfone (PES), have demonstrated promise as an *in vitro* platform for the formation of tube-like tissue structures to mimic various organs [18, 22] (Figure 2.4 A). Compared to cells grown on Transwell inserts, the HFM support cells to develop in 3D tubules, more closely simulating the biological structure of the intestine and promoting Caco-2 cell differentiation [18]. Caco-2 cells that are seeded on the HFM show a clear tubular structure with apparent villi after exposure to flow for seven days (Figure 2.5). To enhance Caco-2 differentiation even more, HFMs are coated by ECM elements including Human collagen IV and L-3,4-di-hydroxyphenylalanine (L-Dopa) as these contribute to differentiation and cell signaling (Figure 2.4 B) [18]. The addition of ECM components has been shown to contribute to further differentiation of Caco-2 cells because they increasingly induced the activity of brush border enzymes [18]. By combining a 3D microenvironment with microfluidics and an induced flow, drug absorption, and cellular differentiation can be more closely resembled than in traditional 2D cell culture methods with induced flow [17, 18].

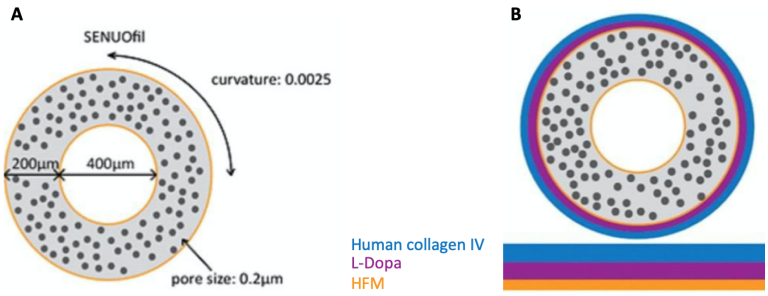

Figure 2.4: (A) Hollow fiber membrane by SENUOfil with a pore size of 0.2 µm, a curvature of 0.0025 an inner diameter of 400 µm, an outer diameter of 600 µm and a thickness of 200 µm [18]. **(B)** HFMs are coated with ECM components including Human collagen IV and L-Dopa to enhance Caco-2 differentiation [18]. Figure adapted from *Jochems et al.* [18].

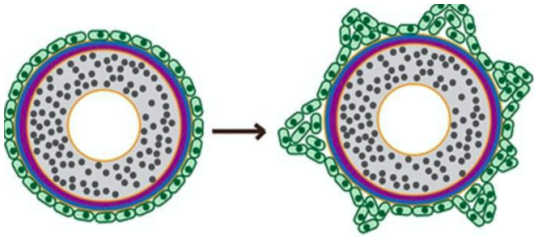

Figure 2.5: Influence of shear stress on the Caco-2 cells that are seeded on the HFM. After being exposed for seven days to shear stress, the Caco-2 cells show a clear tubular structure with apparent villi [18]. Figure adapted from *Jochems et al.* [18].

Therefore, a novel microfluidic device was developed by *Langerak et al.* in which the HFM could be incorporated to create a 3D dynamic microenvironment [23]. The device was designed to examine drug transport and the metabolic functions of the intestine, with the possibility to use the system to mimic other organ models in the future [23]. The material used for the generation of this device was an inert biocompatible polylactic (PLA) [23]. This device consists of a body of PLA and transparent glass on the top and bottom. The HFM can fit and be glued into the device and is thereby connected to the in- and outlets for the flow, which is generated by a peristaltic pump (Figure 2.6). Cells could be seeded on the outside of the fiber and the shear stress induced by the flow will lead to a tight monolayer of Caco-2 cells [23]. In this system, there is a fluid flow on the outside of the fiber as well as through the fiber, which are both generated by the peristaltic pump [19].

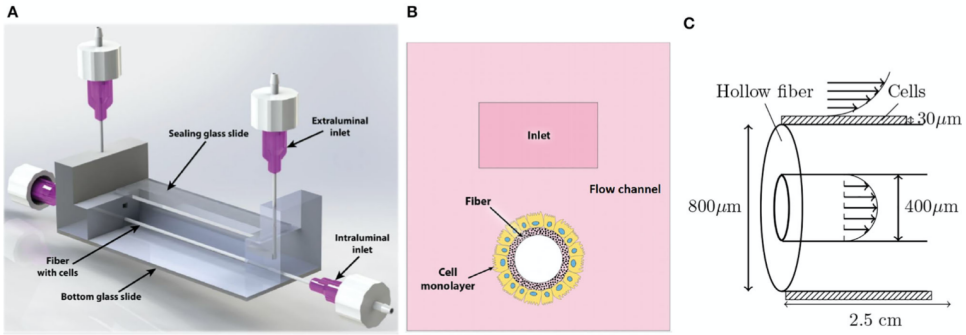

Figure 2.6: **(A)** the microfluidic chip with the inlets and outlets, the fiber, and the top and bottom made of clear glass. A peristaltic pump is used to drive fluid flow, and its inlets and outputs are linked to the intra- and extraluminal inlets and outlets of the chip individually. **(B)** Cross-section of the HFM chip. **(C)** Detailed overview of the HFM with seeded cells. The shaded layer indicates the cell monolayer, on which shear stress is exerted because of the passing fluid flow [23]. Figure adapted from *Langerak et al.* [23].

Although this system can house the HFM and can apply shear stress that is generated by a fluid flow on the cells, there are still some major drawbacks concerning its usability. One of the most important downsides of this system is the open culture chamber. Because of this open chamber, the system is prone to infections and spillage. Next to this, due to the open nature of the chamber, there is a significant pressure difference between the environment inside and outside of the fiber. This pressure difference showed to disrupt the barrier function of the cells on

the HFM after a certain period of time. Furthermore, because the HFM is glued inside the chip before cell culturing, a large number of cells were seen to attach to the bottom glass plate of the device during culturing. These cells are unwanted because they can absorb drug compounds during an experiment and thereby can negatively influence the results and consequently lead to mistakes in readouts. Additionally, gluing the fiber in the chip serves another function as the glue is used as a seal between the apical and basolateral compartments of the chip. Nevertheless, for the glue to serve as a proper seal, the compartment should be perfectly sealed off by glue, such that all liquid is blocked. Therefore, in practice, leakage was frequently observed since gluing the fiber proved to be prone to human mistakes, which resulted in an insufficient compartment seal. Finally, the perfusion time of this device is a maximum of ten minutes, which is again a significant limitation in the system's usability for drug perfusion studies as the required perfusion times for these studies range from hours to a day. Therefore, a new microfluidic device should be developed to overcome the aforementioned limitations.

2.2. Working Mechanism of the Liver

The liver, the largest organ in the human body, performs a variety of functions and is vital to maintaining overall health and regular body processes [24, 25]. Conversion or metabolism of nutrients, drugs, harmful chemicals, and toxins occurs mostly in the liver. Next to this, the liver serves as storage for e.g. iron, glycogen, and vitamins [26]. It regulates the blood sugar and ammonia levels and the synthesis of various hormones [6, 27]. Hepatocytes, the cell type that is seen most commonly in the liver, carry out the majority of liver functions. Stellate cells, which are involved in fat storage and fibrosis, and Kupffer cells, which are part of the immune system, also contribute to the proper functioning of the liver and are thereby often involved in the disruption of the liver function [6]. Because of its important role in the first-pass metabolism, predicting hepatic clearance is crucial for setting the first human dose and assisting in the choice of dosing regiments within the therapeutic window during preclinical drug development [28]. The liver often possesses a remarkable ability to regenerate itself after enduring chemical and physical damage. However, damage brought on by adverse drug reactions and chronic illnesses may limit its capacity to carry out its physiological functions [25]. Adverse drug reactions (ADRs) are known to be significant contributors to liver damage and failure [27]. ADRs are, therefore, next to safety concerns, key factors in the discontinuation of drug development projects and the withdrawal of drugs from the market [27]. Consequently, accurate models are required to reliably model drug response and liver disease.

The ability of the liver to metabolize and remove a substance as it travels through the liver is known as hepatic clearance. Hepatic clearance, therefore, indicates the quantity of drug that is lost during its passage through the liver relative to its plasma concentration. The liver uses both metabolism and biliary excretion to clear a drug, so hepatic clearance relies on both of these phenomena (Figure 2.7). Therefore, factors like hepatic blood flow, drug plasma protein binding, liver enzyme, and transporter activity all influence hepatic clearance.

Predicting human hepatic clearance is crucial for pharmacokinetic studies since it affects both the effectiveness and safety of a drug by controlling the exposure of the drug in the body [29]. Hepatic clearance also aids in predicting dose, bioavailability, and half-life and is a key factor in prioritizing compounds for *in vivo* assessment if these show the desired drug-like characteristics

in vitro, such as sufficient oral bioavailability, reduced systemic clearance, and a long enough half-life to allow for once-daily oral dosing [29].

The ability of the liver to eliminate drugs depends on three main factors [30, 31]:

1. the proportion of the drug in the blood that is unbound to plasma proteins or free to interact with hepatic enzymes (f)
2. the flow of blood through the liver (Q_H), which indicates the delivery of drugs to the liver
3. the capacity of hepatic enzymes to metabolize a particular compound, which is also called *"Intrinsic clearance"* (CLint)

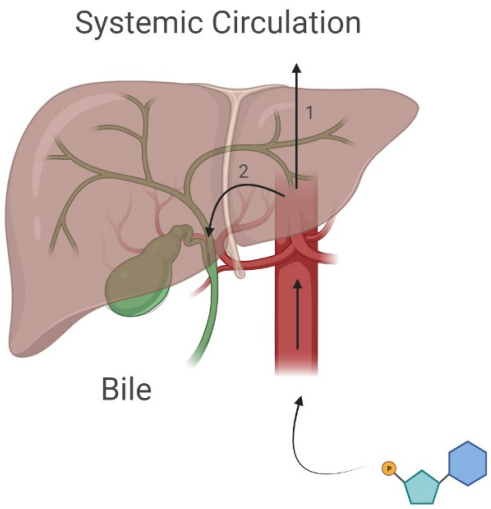

Figure 2.7: Schematic overview of hepatic clearance of a drug compound. A drug compound enters the liver and is either metabolized and thereafter excreted to the bile (1) or the systemic circulation (2) or it is not metabolized and thereafter secreted to the bile or systemic circulation. A drug compound and its metabolites can thus be excreted to either the systemic circulation or the bile when leaving the liver. Figure generated with *BioRender*.

It is important to realize that the liver receives blood with a relatively high drug concentration before the blood enters the liver. After passage through the liver, the blood will contain a relatively low drug concentration [30, 31]. The extraction ratio is an indication of how efficiently the liver can remove a drug from the blood as it passes through the liver. It is thus the difference between the drug concentration in the blood entering the liver (C_{in}) and the concentration in blood that leaves the liver (C_{out}) proportionate to the concentration of the drug in the blood before entering the liver [29].

$$E_H = \frac{C_{in} - C_{out}}{C_{in}} = \frac{fCLint}{Q_H + fCLint} \quad (1)$$

With C_{in} the initial drug concentration before entering the liver, C_{out} the final drug concentration after passing the liver, f the proportion of the drug in the blood that is unbound to plasma proteins or free to interact with hepatic enzymes, CLint the intrinsic clearance, and Q_H the hepatic blood flow.

Thus, if the blood would be completely cleared of the drug, the final concentration of the drug would be zero, leading to a value of one for the extraction ratio. Contrarily, if the liver is inefficient at removing a drug, the final concentration of the drug would remain quite high proportionally to the initial concentration, resulting in a low extraction ratio [29]. Classification of the extraction ratio ranges from low (<0.3), middle (0.3-0.7) to high (>0.7) depending on the proportion of the drug that is removed during one passage in the liver [29].

The hepatic clearance (CL_H) is then the product of the extraction ratio and the blood flow to the liver, leading to Rowland's equation:

$$CL_H = Q_H E_H = Q_H \frac{C_{in} - C_{out}}{C_{in}} = Q_H \frac{fCLint}{Q_H + fCLint} \quad (2)$$

The above equations are an approximation of the hepatic clearance and are valid when the well-stirred model is applied. According to the well-stirred model, the liver is a single compartment with complete blood mixing and the drug is evenly distributed throughout the liver (Figure 2.8) [29, 32]. The drug concentration can thus be approximated by a constant (Figure 2.9 A) [29, 32]. Although this model is an oversimplification of the *in vivo* physiological situation, it is a useful tool to approximate this complex phenomenon. Next to the well-stirred model, there are two other approximation models that are frequently used to translate the *in vitro* measurements of hepatic clearance to the native physiological situation, namely the parallel tube model and the dispersion model [29].

According to the parallel-tube concept, the liver is made up of a collection of similar tubes that are lined up side by side, with metabolizing enzymes and biliary excretion activities uniformly distributed throughout the tubes and no blood mixing between them [29, 32]. Therefore, the drug concentrations are assumed to decline gradually throughout the liver by a first-order mechanism and can be approximated by a first-order function (Figure 2.9 B) [32]. In the case of the parallel tube model, the formula for hepatic clearance becomes:

$$CL_H = Q_H ln \frac{C_{in}}{C_{out}} \quad (3)$$

The parallel-tube and well-stirred models are the two boundary models of the structural characteristics and blood flow patterns of the liver [29, 32]. According to the dispersion model, the liver is an intermediate of these two extremes and is a meshed organ with internal blood dispersion, the degree of which may be determined by the so-called dispersion number (D_N), which represents the degree of blood mixing. There are thus an unlimited number of dispersion models between the parallel tube mode and the well-stirred model, each of which is defined by a particular dispersion number (D_N) that can range from zero (the parallel tube mode) to infinity (the well-stirred model) [29, 32].

An example of such a dispersion model is displayed in Figure 2.9 C. In the case of the dispersion model, the formula for hepatic clearance becomes [29, 32]:

$$CL_H = Q_H \frac{C_{in} - C_{out}}{C_{average}} \quad (4)$$

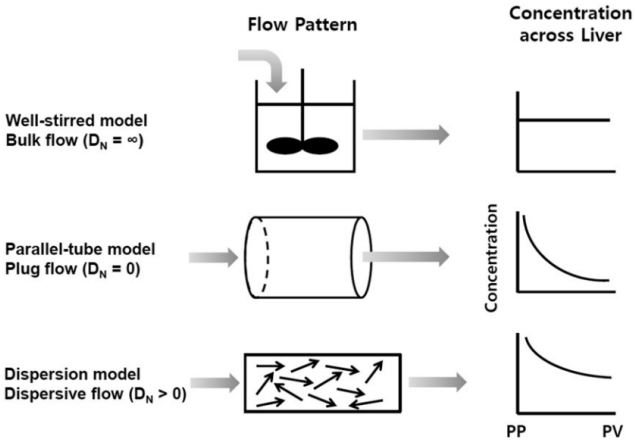

Figure 2.8: Hepatic clearance models. From left to right: well-stirred model, parallel tube model, and dispersion model (PP = portal vein, PV = hepatic vein). Figure adapted from *Cho et al.* [32].

Examining each model in Figure 2.9 reveals that, despite using the same (C_{in}) and (C_{out}), the drug concentration profile varies significantly between them, leading to different hepatic drug exposures (area under the curve) and various average driving force concentrations (C_H) that are in charge of hepatic drug elimination [32, 29].

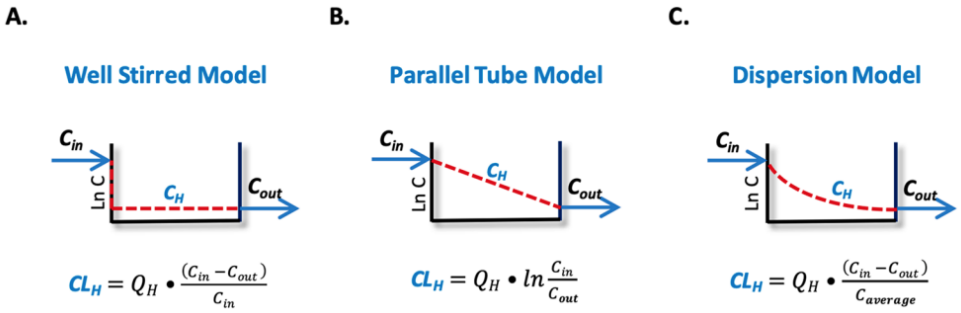

Figure 2.9: Hepatic clearance models with their corresponding formulas for the hepatic clearance. **(A)** The well-stirred model assumes a constant drug distribution throughout the liver, **(B)** the parallel tube model assumes a linear drug distribution approximation, **(C)** and the dispersion model is intermediate between the two previous models. Figure adapted from *Sodhi et al.* [29].

Because it is one of the processes involved in hepatic clearance, reproducing the liver metabolism *in vitro* has received significant attention lately. Drugs pass via the intestine and liver on their way to the systemic circulation and are processed by intestinal, microbial, and hepatic enzymes [4, 33]. Drugs can be transported directly from the GI tract to the liver without being spread through the body because of the hepatic portal system. In this system, the portal vein is used to transport venous drainage from the majority of the GI tract, the spleen, and the pancreas to the liver before returning to the heart. In this way, the liver first processes all chemicals that are delivered by the GI tract before they can enter the bloodstream, including nutrients, toxins, and infections. Therefore, the liver serves as the body's entrance gatekeeper [4].

Accordingly, the liver has two important blood supplies: the portal vein and the hepatic artery.

It receives blood from the GI tract, spleen, and pancreas through the portal vein [4]. The blood supply through the portal vein accounts for 75% of the total blood volume that reaches the liver and is rich in nutrients but low in oxygen. Next to this, it receives the other 25% of its blood supply from the hepatic artery. The blood from the hepatic artery is oxygen-rich but has a poor nutrient contribution, in contrast to the blood of the portal vein [4].

Liver metabolism can be divided into two main categories: phase I and phase II metabolism [33]. While phase II metabolism predominantly consists of conjugation processes, phase I metabolism also contains hydrolysis, oxidation, and reduction reactions. Phase I reactions are dominated by cytochrome P450 enzymes (CYPs), but phase II reactions are mediated by a number of enzymes, including uridine diphosphate-glucuronosyltransferase (UGT), glutathione S-transferase (GST), and sulfotransferase (ST) [33] (Figure 2.10).

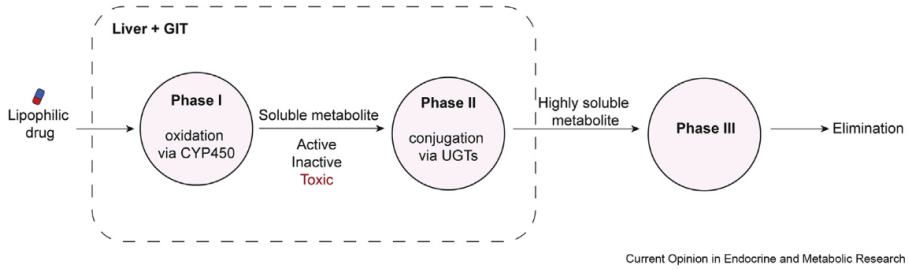

Figure 2.10: Phases of the liver metabolism. Phase I reactions are dominated by cytochrome P450 enzymes (CYPs), but phase II reactions are mediated by a number of different enzymes. Figure adapted from *Lucchetti et al.* [34]

2.2.1. Modeling liver-on-a-chip devices

Because of the complicated microarchitecture of the liver, it is important to carefully determine the most important design criteria to create a liver-on-a-chip device for drug testing purposes.

One of the most important features when designing a liver-on-a-chip device for drug testing purposes is the maintenance of hepatocyte cytochrome P450 inducibility and activity [24]. Cytochromes P450 are an enzyme family, and together they are essential for maintaining homeostasis, cellular metabolism, and the detoxification of xenobiotics [35]. Drug-drug interactions are primarily mediated through the induction or inhibition of CYP enzymes [35]. In order to accomplish this, the continuous perfusion of the chip by means of a fluid flow is of uttermost importance [24]. Hepatocytes situated in a flow system are shown to have an improved ability to metabolize the substrates for specific cytochrome P450 enzymes and to transport the metabolites into the canaliculi compared to non-flow cultures [24].

Another crucial design feature is the *in vitro* simulation of the metabolic gradients that occur in the native liver [24, 26]. This is because the zonation of the hepatic function is assumed to be caused by the gradient of oxygen, growth factors, and hormones that occur along the sinusoid [26]. Nevertheless, some studies contend that metabolic zonation, which is the division of hepatocytes in distinct functional areas, is caused by endothelial-produced Wnt signaling environment for the liver cells [26]. Nevertheless, the hepatic microenvironment is strongly affected by the presence of oxygen, which controls cellular metabolism, differentiation, and growth. *In vivo*, the liver is connected to both the portal circulation and the highly oxygenated arterial circulation, which both

deliver oxygen to the hepatocytes [26]. Consequently, native oxygen levels should be simulated in *in vitro* models to acquire an optimal environment for the liver cells [26]. Finally, the liver cells should have limited exposure to shear forces to perform optimally [26].

In the last decade, multiple liver-on-a-system devices have been developed and used in drug response studies, the most commonly used ones include: liver chips based on 2D planar culture, liver chips based on matrixless 3D spheroid culture, liver chips based on matrix-dependent 3D culture, liver chips based on layer-by-layer deposition, and liver chips based on 3D bioprinting [25].

Despite these advances, similarly to gut-on-a-chip devices, liver-on-a-chip devices perform optimally when the cells that are used in the microfluidic device are cultured in a 3D architecture [24]. In the case of 2D cultures, hepatocytes rapidly lose their distinctive properties and functions. Isolated primary hepatocytes exhibit extremely little proliferative capacity and rapidly lose their differentiated features and liver-specific activities in standard 2D cultures [24, 27]. Although, when isolated hepatocytes are cultivated in 3D, they exhibit up-regulated liver activities, and the preservation of their differentiated characteristics is substantially lengthened [24]. Furthermore, culturing liver cells in a 3D configuration allows for the generation of lobules and tubular structures, thereby mimicking the *in vivo* architecture of the liver more realistically [24].

Therefore, the same microfluidic HFM system as was introduced in Section 2.1.3 can be used for liver cells. Culturing liver cells on an HFM will allow the generation of tubular structures and will lead to increased lobule formation [36]. Unfortunately, the same drawbacks as described in Section 2.1.3 are applicable to the system in this case, and therefore a new and optimized system should be designed to meet the required needs.

A major addition to currently available systems would be the incorporation of two chambers in the model (as is the case in the HFM chip system that is introduced in section 2.1.3) such that the full hepatic clearance process of the liver can be examined. As previously described, hepatic clearance depends both on the metabolization of a drug compound as well as the possible biliary secretion of that same compound [29]. Upon entering the liver, a drug compound can be either metabolized or not, and the compound and its metabolites can be excreted into either the systemic circulation or into the bile [29]. A myriad of liver-on-a-chip devices have been developed, but all of them lack the feature to analyze the biliary secretion of a drug compound. Current systems only induce an external flow passing the liver cells, which allows the examination of the metabolization of a drug compound. However, with these systems, it is not possible to track if these drug metabolites are excreted into the systemic circulation or into the bile. When examining the pharmacokinetics of a drug compound in the liver, it is very important to know where the metabolite of a drug will go to. Suppose the metabolite that is produced is toxic. In the current systems, this drug would immediately be declined for further research. However, the toxicity of this metabolite would be irrelevant if it would be excreted into the bile rather than into the systemic circulation because it would be excreted out of the body in this way. Therefore, a two-chamber model is needed to track where compounds go once they are excreted by the liver cells. One chamber should thus represent the systemic circulation and the other one should represent the bile.

In future research, conventional 2D cell lines could be replaced by human-derived liver organoids. Adult tissue progenitor/stem cells found in the intrahepatic bile ducts are mostly used to create

the liver organoids [36]. These organoids are called intrahepatic cholangiocyte organoids (ICOs). The ICOs can be genetically maintained and grown for several months *in vitro* due to their great proliferative abilities [36]. Additionally, the ICOs have the ability to differentiate into cholangiocyte or hepatocyte lineages after being cultured in specific media compositions [37].

2.3. Connecting liver- and gut-on-a-chip devices

First-pass Metabolism

After ingestion, orally ingested drugs go through a process known as the first-pass metabolism. During this process, drugs are first absorbed in the gut, then they are digested in the liver, and finally, they are circulated throughout the body [2, 3]. Given that many drug candidates fail due to unexpected toxicity or ineffectiveness, which is heavily impacted by the first-pass metabolism, an accurate prediction of the first-pass metabolism is essential for improving the cost and time efficiency of the drug development process [3]. The development of novel MoOc devices is necessary to improve our comprehension of the processes behind this first-pass metabolism. Because of their more complex designs, which enable replication of complex organ-organ interactions and cross-signaling *in vitro*, these systems are more effective at simulating the first-pass metabolism than single OoC devices [3, 4]. As the liver and gut are the two of the most important organs involved in the first-pass metabolism, separate gut- and liver-on-a-chip models should be coupled to provide a more realistic model of the first-pass metabolism [3].

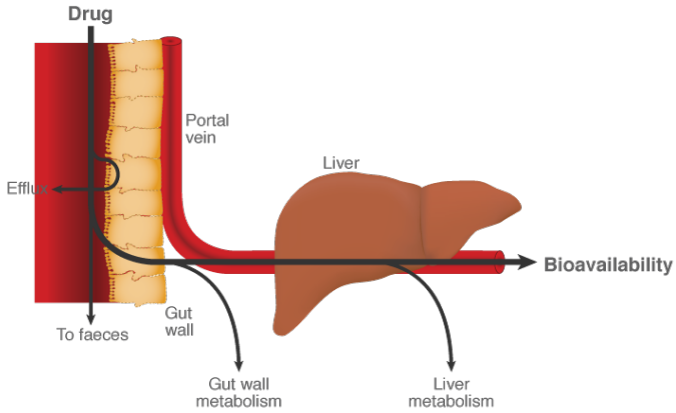

Figure 2.11: Schematic representation of the first-pass metabolism. Orally ingested drugs first enter through the GI tract where they are absorbed after which they enter the liver for digestion [38].

Single Ooc devices lack the complex intercellular and interorgan interactions that occur *in vivo* [3]. Consequently, single OoC systems are unable to accurately mimic the enterohepatic circulation and first-pass metabolism, which are both critical for evaluating the drug and the xenobiotic metabolism.

Therefore, MOoC devices are better suited for gaining a deeper knowledge of the first-pass metabolism because they allow for the analysis of these organ-organ interactions [3]. Also, it has been demonstrated that liver cells perform better physiologically when coupled with gut cells in a microfluidic system, thereby better simulating the native environment. For example, in the intestine-liver chip combination higher metabolite formation was observed compared to a liver-only

device [39, 40, 41]. Additionally, CYP activity in a liver-gut combined system has been observed to be higher when compared to a liver-only system [42, 22]. Furthermore, *Tsamandouras et al.* demonstrated that clearance varied considerably between intestine- or liver only compared to intestine-liver combination [4].

Modeling the Oral Administration Route

In order to model the first-pass metabolism accurately, an analysis of the oral administration route in terms of absorbance and metabolization should be performed. Oral bioavailability (F) is a result of hepatic availability (F_H), gastrointestinal or gut wall availability (F_G), and fraction absorbed (F_{abs}). Consequently, intestinal absorption (F_{abs}) and first-pass elimination (F_G and F_H) can be predicted from *in vitro* data [32].

The following equation describes how orally administered drugs move successively from the GI lumen, via the GI wall, and liver, before reaching the systemic circulation:

$$F_S = F_{abs} F_G F_H \quad (5)$$

With F_S being the percentage of the dosage that, following oral administration, enters the systemic circulation as an unaltered drug; F_G, and F_H, are the fractions of the dosage that escape first-pass elimination in the GI wall and liver respectively [32]. F_{abs} (fraction absorbed) is the fraction of the dose absorbed into the GI wall from the GI lumen [32].

This equation can also be expressed in terms of the hepatic and GI extraction ratios [32]:

$$F_S = F_{abs}(1 - E_G)(1 - E_H) \quad (6)$$

With E_G being the extraction ratio of the gut, and E_H being the extraction ratio of the liver. This concept is visualized in Figure 2.12.

The approach known as in *vitro–in vivo* extrapolation (IVIVE) is the most widely used and validated way to estimate F_G, F_H, and F_{abs} using *in vitro* measurements of drug metabolism [32, 29].

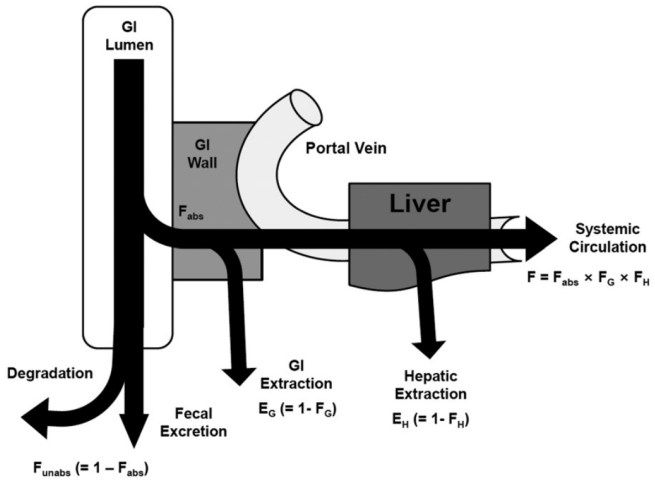

Figure 2.12: Schematic overview of the oral drug absorption process in the first-pass metabolism [32]. Figure adapted from *Cho et al.* [32].

Liver-gut-on-a-chip development

To meet the aforementioned requirements, a new system should be designed that can be easily interlinked and should lend itself to the incorporation of both gut and liver cells in the device. The conceptual and theoretical problems that must be resolved during the system design phase go hand in hand with complexity. The right framing of the physiological problem is essential to develop relevant design requirements. The right design criteria and desires for an OoC and coupled OoCs (MOoCs) might be specified based on the problem of interest. In terms of ease of applicability and device performance, the single OoCs that are to be connected should be produced based on precise, well-defined design criteria. The most important design criteria to be examined for coupling OoC devices comprise coupling method, medium, cell sources and cell culture method, flow rates, fluid circulation method, and materials and production methods.

An elaborate analysis of the possible coupling methods, cell sources, cell culture methods, flow rates and fluid circulation methods and corresponding challenges can be found in Appendix D.

2.3.1. Materials and Production Methods

3D Printing Techniques

3D printing is one of the most suited techniques for the development of OoC prototypes as it can create objects with intricate geometrical elements [43]. Furthermore, 3D printing is a cost-effective and time-efficient technique to produce complicated, precise items with customized designs, particularly for medical applications that require individual care [43].

This technique uses ultraviolet light to progressively print multiple layers to produce 3D objects. Several 3D printing techniques have been developed along with material science and additive manufacturing (AM) technology [43]. The nozzle-based and light-based 3D printing techniques are currently the two most popular types of 3D printing.

Extrusion printing and inkjet printing are both types of nozzle-based 3D printing. In this case, the print materials are extruded or jetted after which they are deposited onto the printing platform [43]. Digital light processing (DLP) printing, laser-assisted printing, selective laser melting (SLM), and selective laser sintering (SLS) are all types of light-based 3D printing [43]. In both DLP and laser-assisted printing, photopolymerization processes are used. In the case of SLM and SLS printing, material particles are melted and molded at a high temperature produced by the laser [43]. These 3D printing techniques vary greatly in terms of the applied methodology, speed, available materials, and resolution [43].

For this project, print resolution, speed, and cell viability (biocompatibility) were the three primary variables to consider. Therefore, an overview is provided of the different printing techniques with their advantages and disadvantages and their applicability for this project (Table 2.1). As the cell viability, print resolution, and speed were all equally important for the purposes of this project, techniques were excluded if the requirements for one of these parameters were not met. Regarding cell viability, there had to be a possibility to use a biocompatible material source for the printing job such that high cell viability could be guaranteed. Therefore, extrusion-based printing was no longer considered as an option for this project. Because very small geometries had to be printed with high accuracy, the print resolution parameter had to be as low as possible in the micrometer (µm) scale. Therefore, inkjet printing and SLS/SLM printing were deemed as not suitable. Finally, the printing speed should be high such that new design iterations could be

implemented as fast as possible. Consequently, laser-assisted printing and DLP were the only remaining candidates. In this case, there was a preference for the DLP printing technique as it was the only technique with a fast printing speed in the range of mm^3/s. In conclusion, DLP printing was chosen as the optimal printing method for the scope of this project.

Name	Material	Process	Speed	Resolution (µm)	Cell viability (%)	Applicable
Nozzle-based						
Inkjet	Thermoplastic Polymer	Serial (drop by drop)	M (mm/s)	50	>85	No
Extrusion	Thermoplastic Polymer	Serial (line by line)	S (µm/s)	50	40-80	No
Light-based						
Laser-assisted	Photosensitive Polymer	Serial (dot by dot)	M (mm/s)	~1	>85	Yes
DLP	Photosensitive Polymer	Continue Plane (layer by layer)	F (mm^3/s)	6	85-95	Yes
SLM/SLS	Metals and alloys powder, ceramic, polymer	Serial (dot by dot)	S (µm/s)	80	/	No

Table 2.1: Overview of different 3D printing techniques and their applicability for this project. Techniques were reviewed based on their speed, resolution, and cell viability. Techniques were excluded if more than one of the parameters did not fit the requirements for this project. Laser-assisted and DLP printing are the two techniques deemed to be suitable for this project. All other techniques were excluded because more than one parameter did not fit the requirements. Table adapted from *Zhang et al.* [43].

DLP 3D Printing

DLP printing utilizes a photopolymer (resin) as a material source. The liquid resin is polymerized and transformed into a solid product by means of projecting light onto the resin by a small beamer. A digital micro-mirror device (DMD), which consists of a collection of programmable mirrors which are micron-sized, is the primary functional component of the device. In order to cure the photosensitive resin at the right place, the mirrors rotate to direct the light to the targeted area on the building plate (Figure 2.13) [43, 44, 45]. Furthermore, when the light is projected onto the resin, an entire contour of the desired part is projected onto the surface of the photopolymer at once, after which this surface hardens and is lifted up one layer thickness. This results in the fact that a whole layer can be printed simultaneously instead of being limited to a specific area like in laser-assisted 3D printing [43, 44]. The employment of this technique results in the high printing speed of DLP printing. The projection plane, which can be modified by adjusting the lens and DMD, determines the resolution. Because the resin can be targeted extremely accurately, the DLP printing technology has a high resolution, which is often at the micron scale [43, 44]. DLP involves working with very thin pillars, also called supports, which support the overhanging parts of the model. These support pillars can be easily removed after printing by post-processing techniques like filing. Additionally, a large number of biocompatible materials are available as a material source for the DLP printing technique [43, 44]. This and the high resolution, size

accuracy, and excellent surface quality make this technique largely suitable for this project with the aim to generate very high precision models.

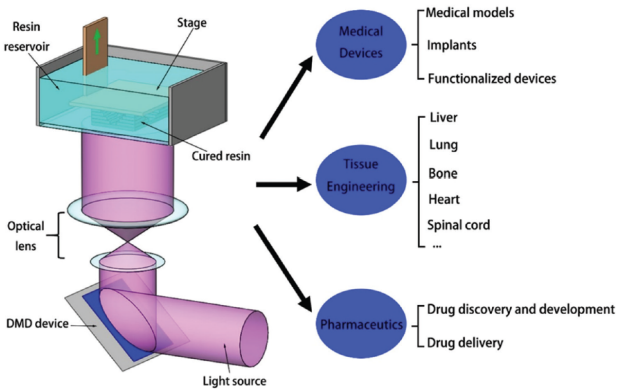

Figure 2.13: Schematic overview of the DLP 3D printing method. The DMD device is the central part of this technology as it allows for the projection of light onto the photopolymer surface and can rotate following the desired direction. After the light hits the surface an entire contour of a part can be cured and the building plate lifts with one layer. This will be repeated until the part is completely generated. Figure adapted from *Zhang et al.* [43]

Material Choice

Polydimethylsiloxane (PDMS) is one of the most popular materials to create OoC devices because of its cost-effectiveness, and researcher- and cell-friendly characteristics [11, 46, 47]. Additionally, PDMS is translucent, which is a crucial quality for the simple optical characterization of cells and tissues [11]. However, PDMS has been shown to absorb metabolites and drug compounds and is therefore not suited as a material for OoCs that serve drug testing purposes [42, 11]. Although some research groups have tried to adapt the surface properties of PDMS, by using for example a plasma treatment, PDMS is still not fit to use in drug development studies, and in particular intestinal absorption studies, because very low concentrations of drugs have to be identified in that case [19]. Especially for drug transport assays where extremely low drug concentrations must be discovered, non-specific adsorption (NSA) of drugs can cause large errors in the eventual analyses [48, 19]. Despite the aforementioned issues with PDMS as chip material, it has been used as the material in the vast majority of gut-liver-on-a-chip devices that have been developed to date [48, 51, 52, 3, 2, 53, 54, 17, 4, 39, 49, 50]. However, recent advancements in 3D printing technology have made it easier to produce chips from other materials than PDMS. Furthermore, the use of 3D printing in OoC technology leads to a larger flexibility in material choice which allows testing various compounds with distinct molecular properties [42, 19].

As 3D printing was selected as the production technique for the HFM chip, a biocompatible photopolymer resin was required for this purpose. The resin that was used to develop the chip in this study is a by TNO developed photosensitive resin [55]. This resin has been used in dental applications and was used to develop the TNO IEBC chip, thereby proving its biocompatibility [19]. Furthermore, the resin has been analyzed and shown to display a low NSA [42, 19]. A description of the resin mixture and contents can be found in Section 4.1.

This Chapter was integrated and adapted from the literature study that was performed for *BME Literature Research (BM51010)* as part of this thesis project.

3

Chip Design Requirements

In Chapter 2, a thorough examination of current systems and their characteristics was performed. Design specifications for the new HFM chip system were created based on the information gathered in the literature analysis. This chapter provides an overview of the design requirements of the new system.

1. **Chip Configuration:**
    - **Two-chamber model:** The chip should consist of two separate compartments. A two-chamber model is required for the intestinal model as well as the hepatic organ model. The chip should contain two completely separable compartments with the possibility to sample in each compartment.
    - **HFM incorporation:** The chip should be designed in such a way that an HFM can be easily incorporated into the device and removed after use.
    - **Straightforward assembly:** The chip should be created in a way that makes it straightforward for everyone to assemble all of the components properly. Design choices should be made such that the simplicity of the assembly of the device is maintained.
    - **Ease of use:** Everyone that has received training in how to use the chip should be able to use it easily. Complexity should be reduced to a minimum to avoid mistakes related to human error in readouts.
    - **Off-chip culturing:** To avoid cells attaching to the walls and bottom of the chip, culturing of cells should be performed outside of the chip environment. Cultured cells should be transferred to the chip at the time of the experiment. The design should lend itself to easy insertion and removal of the cells into the design at any time during an experiment.
    - **Sustainability and re-usability:** The chip should be designed in such a way that (all) parts can be reused for multiple experiments.
2. **Materials:**
    - **Biocompatibility:** The material should not be toxic for the used cell lines and organoids. No harmful particles must be released from the chip material or tubing due to wear in order to guarantee cell viability.

- **Low NSA:** The material should not absorb small (drug) compounds and should therefore not interfere with the readouts. The material should therefore have a proven low NSA.
- **Sterilization:** To prevent microbial contamination and infections, sterilization of chip parts is of utter importance before a chip experiment is conducted. All chip components should thus lend themselves to sterilization and should not deteriorate or release harmful particles because of the sterilization process.
- **Sustainability:** The material should not be harmful to the environment and should be used in a sustainable and responsible manner. No more material than needed should be used to perform the experiments.
- **3D printable:** The material should be suitable for 3D printing purposes as 3D printing is chosen as the production method for this chip. A photosensitive resin is required for the DLP printing process.

3. **Production:**
   - **Sustainability:** The production process should not harm the environment and production time should be shortened to avoid unnecessary energy use.
   - **Cost-effective:** As many design iterations will have to be implemented, the production process should not be too costly.
   - **Time efficient:** The production time should be as short as possible such that new design iterations can be implemented as fast as possible.
   - **High-resolution:** Should be as high as possible as very small geometries need to be printed extremely accurately to develop an OoC device.
4. **Cell Sources, Culturing and Cellular Environment:**
   - **Ability to house Caco-2 and HepaRG cell lines:** The chip should be designed in such a way that optimal survival conditions for the Caco-2, as well as the HepaRG cell line, are created.
   - **Creation of 3D environment for Caco-2 and HepaRG cells:** A scaffold in the form of an HFM should be incorporated into the device to provide optimal growing and differentiation conditions for Caco-2 and HepaRG cells.
   - **Ability to be used in a CO2 incubator:** The chip should provide the possibility to be placed inside a CO2 incubator during experiments and cell culturing.
5. **Medium:**
   - **Universal medium:** A universal medium will have to be developed. This medium should provide both cell types with the necessary elements to survive but should at the same time be kept as simple as possible to prevent interference with one of the two cell types.

6. **Scaling:**
    - **Scalable with computational software:** Scaling will be performed after a chip experiment by use of computational analysis. Therefore, no scaling should be applied in the design phase.
7. **Flow Rates and Fluid Circulation:**
    - **Single perfusion flow through HFM:** A perfusion flow through the HFM is the most important design requirement concerning flow and fluid circulation. This flow is necessary to recreate the native environment of the cells and takes part in the creation of the required two-compartment model.
    - **Peristaltic circulation:** The chip should be designed in such a way that it can be coupled to a peristaltic fluid circulation pump as this is the available fluid circulation system that is available at TNO.
8. **Coupling:**
    - **Plug-and-play configuration:** The chip should be created in a plug-and-play manner, allowing each unit to be quickly connected and uncoupled at any moment. When used independently and in an assembly, each chip should function identically.
    - **Ease of assembly:** Assembling and decoupling chips should be easy and straightforward such that multiple chips can be run at the same time without loss of cell functionality.

4

Chip Design

4.1. Materials and Methods

4.1.1. HFM Chip Fabrication and Design

Based on the findings in Section 2.3.1 DLP 3D printing has been selected as the production technique to create the HFM chip. The resin used for printing is the BI-OC-4 resin, which is a resin that is specifically developed by TNO to ensure the biocompatibility of the chip material. The HFM chip was developed using an iterative design process in which a new design was initially developed, followed by printing, visual testing, validation, and finally improvement and iteration of the process (Figure 4.1). To address any errors or inconsistencies found during testing, the necessary adjustments were included in every new design and in the production process. For greater design process efficiency, multiple potential solutions were produced simultaneously in a single print run and were consequently evaluated. To determine the ideal dimensions of a part, for instance, a variety of sizes were produced in one print iteration. Only one variable was adjusted during every print iteration so it could be clearly assessed which particular adjustment led to an improvement in the system.

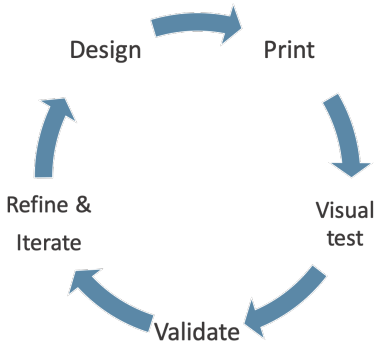

Figure 4.1: Iterative development process of the HFM chip.

All chip parts (holder, insert and cap) were designed in the AutoDesk Fusion 360 CAD modeling software. After designing a part, the CAD files were converted to STL files, which could be imported into the corresponding AutoDesk Netfabb slicing software. After slicing, parts were

printed with the Rapidshape HA30+ DLP resin printer. The average printing time of a print job that included holders, inserts and caps was approximately 30 minutes. Once a printing job was complete, parts were removed from the building plate by scraping them off with a carbon steel hand scraper and supports were removed from the parts with a pair of tweezers. Subsequently, microfluidic channels were flushed with 90% ethanol to ensure proper opening of the channels, and parts were soaked in 90% ethanol for 30 minutes up to one hour, depending on their size. The remainings of supports were removed with a pair of tweezers or filed with a small file to create a smooth surface. Following this, parts were cleaned and dried in the Rapidshape RS-Wash with isopropanol for about 10 minutes. Although parts were dried in the RS-wash system, some parts needed an additional 10 to 30 minutes of drying before they could be cured, depending on their size. Finally, parts were cured in the Rapidshape RS-Cure system with UV-B and UV-A radiation in a vacuum for approximately one hour. After this step, parts were checked for remainings of supports and sometimes some extra filing was needed to ensure an entirely smooth surface.

4.1.2. Resin Preparation

To prepare the 3D printing resin, a mixture of 73.5 wt% ethoxylated (4) bisphenol A methacrylate (Bis-EMA-4, Sartomer Arkema), 24.5 wt% Urethan Dimethacrylate (UDMA, Esstech), 2.0 wt% bis(2,3,6-trimethyl benzoyl)phenyl phosphine oxide (Omnirad 819, IGM Resins), and 0.02 wt% Quinoline Yellow SS (Solvent Yellow 33) was prepared. Thereafter, to ensure a proper resuspension of all compounds, the mixture was magnetically stirred for at least 24 hours (until all compounds were visually completely dissolved in the mixture) [55, 19].

4.2. Final Design HFM Chip

The final design of the HFM chip is the result of an iterative design process and complies with the design specifications as mentioned in Chapter 3. A timeline of the most relevant intermediate chip designs can be found in Appendix B. The chip consists of three parts, from right to left, the HFM chip holder, the HFM chip insert, and the HFM chip cap (Figure 4.2). For assembly, the HFM chip insert can be inserted into the HFM chip holder, whereafter the cap can be put on top of the system to close off the whole configuration. A small rubber O-ring is stretched onto either end of the HFM chip insert to prevent leakage of the inner compartment of the chip. Additionally, a larger O-ring is stretched over the opening of the HFM chip cap to prevent leakage of the outside compartment of the chip.

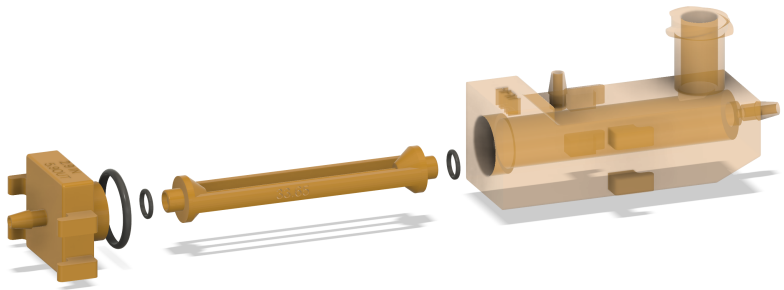

Figure 4.2: HFM chip assembly. The HFM chip consists of three parts, from left to right: the HFM chip cap, the HFM chip insert, and the HFM chip holder.

The primary design requirement for the HFM chip was that it should function as a two-compartment model. To replicate the native environment of the cells, the chip had to consist of one basolateral and one apical compartment. These compartments should be completely isolated from each other during the perfusion of the chip, such that the path of a particular drug compound could be tracked inside the system. Based on the previous HFM chip model (see Section 2.1.3), the basolateral compartment of the chip could serve as the internal environment of the HFM. The fluid flowing through the inside of the HFM thereby mimics the blood flowing in the body. Therefore, the HFM holder should provide the apical compartment of the chip.

As a means to achieve this, the HFM chip insert can be inserted into a larger casing, the HFM chip holder, thereby creating the two-compartment model. The cavity of the HFM holder then serves as the apical compartment of the chip, providing the ability to track all possible pathways of a drug compound and its metabolites. The HFM holder comprises a sampling Luer on top, to provide a way to sample in the apical compartment of the chip (Figure 4.5). This Luer can be closed off with a Luer cap during the perfusion of the chip to prevent leakage. For the outflow of the holder, a TNO connector was chosen to ensure compatibility with other TNO chip equipment, like for example the TNO reservoirs and tubing. Moreover, two hooks are situated on either side of the HFM chip holder that can be used to connect the HFM chip cap.

Another essential design element was that, in order to prevent cell growth inside the chip, the HFM should only be inserted in the chip environment at the onset of an experiment. Since unwanted cell growth was a significant issue in the prior HFM chip system and this unintended cell development compromised the final results, this had to be avoided at all costs. Therefore, an HFM chip insert was developed that allowed for the cultivation of cells on the HFM outside of the chip environment. The insert was designed in such a way as to fit perfectly in both the HFM chip holder and the HFM chip cap during an experiment (Figure 4.4). Before that, the implant can be kept separately for culturing. No cells may therefore grow into the main chip body. To make cell seeding easier, the dimensions of the insert were selected such that it could fit into a two-milliliter (ml) Eppendorf tube.

Furthermore, to facilitate scaling up and to produce the least amount of waste feasible, the dimensions of the insert had to be such that at least two inserts could fit into one well of a six-well culture plate. Subsequently, the ability to easily integrate the HFM into the system was another essential design feature for the insert. Therefore, the insert was made to fit an HFM exactly and the HFM can be fit by pushing it through the aperture like a thread through a needle. To ensure that the HFM can fit into the insert more easily, the aperture has been made a bit larger on one side of the insert. The HFM may then be attached to the implant using dental adhesive, which was selected because of its biocompatible nature. At both ends of the insert, there are two cavities in which the dental glue can be jetted such that the HFM remains at the center of the insert during the experiment and the two compartments of the HFM chip are completely isolated from each other. Next to this, two small O-rings (*Eriks*) of a diameter of two-and-a-half mm should be put on either end of the insert to avoid leakage of the fluid that is running through the fiber to the insert compartment of the chip.

The HFM chip cap consists of a main body with a larger and smaller aperture (Figure 4.3). A seven mm O-ring (*Eriks*) may be stretched over the bigger aperture, which fits precisely within the HFM chip holder. By creating an insertion in the holder in which the cap fits perfectly, this fit

guarantees that the cap is positioned correctly onto the HFM chip holder and was designed to prevent leakage because of a misalignment of the cap and thereby misplacement of the O-ring. Furthermore, the smaller aperture is designed to fit the HFM chip insert exactly. A perfect fit was ensured by printing a myriad of different dimensions and fitting the insert into the cap for every dimension. This was required due to the significant print inaccuracy of the DLP 3D printer when a part is produced at this small scale. A TNO connector serves as the outflow point of the cap. The exact dimensions of all parts can be found in Appendix A.

The system is assembled by attaching the two small O-rings to the ends of the insert and pushing the insert inside of the holder. Subsequently, the larger O-ring should be stretched around the big aperture of the cap, after which the cap can be inserted in the holder as well (Figure 4.6). Thereafter, the cap can be attached to the holder by the use of four small elastic rubber rings (6.5 mm diameter O-ring or 6.5 mm diameter non-stretch rubber elastics) (Figure 4.7 and 4.8). The rubber elastics provide a lateral force on the HFM chip cap and insert and thereby creating a seal by compressing the O-rings in between the touching areas.

The biggest challenge to overcome while designing the HFM chip was the recurring leakage between the apical and basolateral compartments of the chip. As this was one of the most critical design criteria for the chip, the most crucial challenge to overcome in the development of the design was therefore to completely isolate the apical and basolateral compartments. In a previous version of the HFM chip, the dental glue in the cavities of the insert served as a way to isolate the basolateral and apical compartments from each other. However, this version showed leakages of the internal (basolateral) compartment to the external (apical) compartment. Furthermore, fluid leaked out of the chip of the external compartment.

Accordingly, rubber O-rings were introduced to address leaking issues. These O-rings create a strong, moisture-resistant barrier that keeps pressurized liquid inside the system. Many design iterations were required to find the ideal O-ring compression, and various O-ring types, sizes, and thicknesses were evaluated to achieve a tight seal.

However, creating a very tight seal with the O-rings caused air to be trapped in the apical reservoir of the chip when liquid was added by creating a vacuum. Various designs were developed that created a slightly less tight seal, but this resulted again in leakages between the inner and outer compartments of the chip. To solve this issue, an escape route for trapped air was added to the design. A TNO connector was added to the top of the HFM chip holder to serve as an escape route for the air. This connector should not be connected to tubing but exclusively serves as an escape route for the trapped air in the apical reservoir. Alternatively, a sampling Luer can be used, as it can be more easily closed by a Luer screw cap. The alternative final version of the design where the TNO connector is replaced by a sampling Luer can be found in Appendix B.

2D drawings with dimensions of the final design can be found in Appendix A.
An overview of the assembly of the HFM chip can be found in Appendix C.

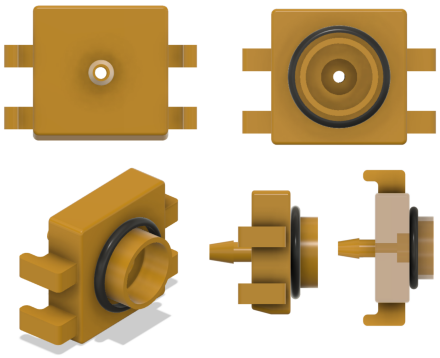

Figure 4.3: HFM chip cap. An O-ring with a diameter of seven mm should be stretched over the opening of the HFM chip cap.

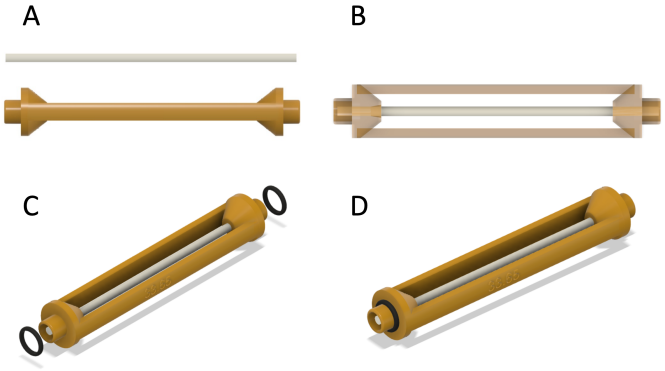

Figure 4.4: **A** HFM (top) and HFM chip insert (bottom) before gluing. **B** Insert with HFM glued inside of it. **C** Two two-and-a-half mm diameter O-rings should be stretched over the HFM chip inserts on both sides. **D** HFM insert with two O-rings in the right configuration.

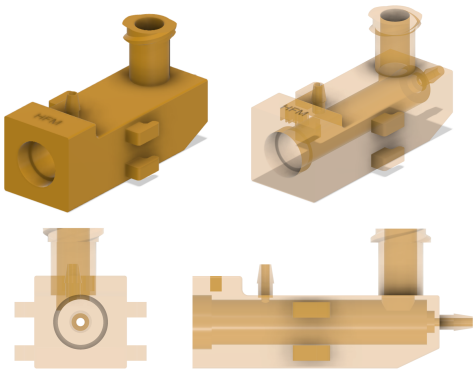

Figure 4.5: HFM chip holder. The holder contains an opening that is tailored to precisely fit the HFM chip insert and HFM chip cap.

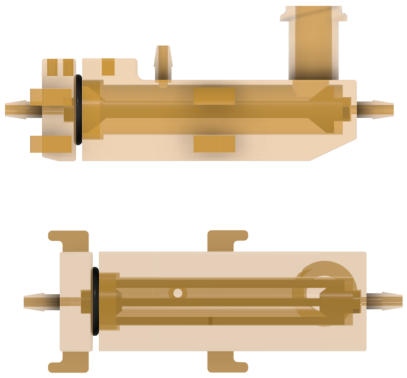

Figure 4.6: HFM chip holder with insert and cap inserted.

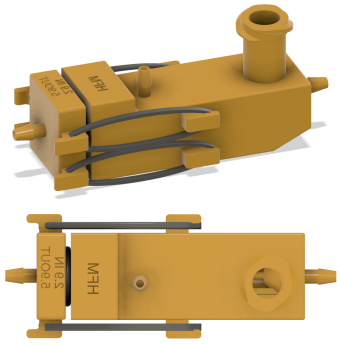

Figure 4.7: HFM complete assembly with elastics or O-rings to exert a lateral force on the HFM cap and thereby ensure the proper forces acting on the HFM insert to avoid leakage.

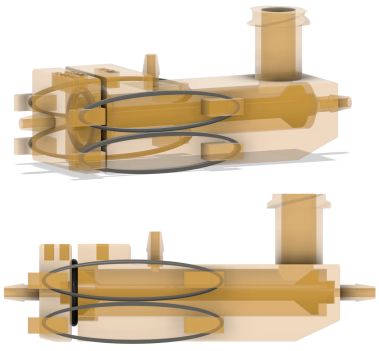

Figure 4.8: Complete assembly with elastics or O-rings (six-and-a-half mm diameter).

4.3. Discussion

According to the literature, DLP 3D printing was the optimal production technique for the production of the HFM chip because of its high speed, high resolution, and the possibility of using a biocompatible resin. Although DLP 3D printers are known for their ability to produce high-resolution and detailed parts, the print inaccuracy of the DLP 3D printer was one of the major challenges to overcome during the development of the HFM chip. This inaccuracy caused the designs to deviate at crucial chip parts as these had to be produced on a very small scale. For instance, the connection between the HFM cap and the HFM insert was particularly prone to deviations because of its small scale, while this part is the most crucial in preventing leakage between the two compartments of the chip. Because of this, multiple scales were evaluated throughout the design phase to find a balance between producing a realistic design and using the best print margins. Parts printed at a larger scale showed higher resolution but often resulted in unrealistic apical and basolateral compartment volumes. As a result, the present scale was selected because it provides a compromise between realistic component size and resolution.

Furthermore, literature research showed that a biocompatible resin with a low NSA was deemed optimal for the purpose of designing an OoC system for drug testing purposes. Therefore, the TNO BIOC-4 resin was chosen as the material to produce the HFM chip. This material has been mostly used for printing larger parts, resulting in sturdy structures. However, for the HFM chip, which consists of smaller parts, the material proved to be brittle, especially under force. When comparing the HFM chip to the IEBC chip, the latter consists of larger parts, leaving the BIOC-4 resin to be an appropriate material for the IEBC chip, but not necessarily for the HFM chip.

End-user feedback on the HFM chip revealed the need for higher user-friendliness. According to end-user reports, using rubber elastics to securely fasten the HFM cap to the holder was challenging, leading to undesired leakage due to misfitting parts. When first using the HFM system, end-users needed multiple efforts to perfectly fit the cap and holder to create a leak-free system. Therefore, taking this feedback into consideration, the final HFM chip was redesigned to create higher user-friendliness. Several cap and holder designs were developed in an effort to resolve this issue. One of the proposed solutions was a screw-cap design, in which the cap could be screwed into the HFM holder (Appendix B). Unfortunately, the screwing motion of the cap into the holder caused a torque on the HFM insert which led to the insert breaking inside the holder. Alternative designs, such as a snap-fit mechanism based on the TNO IEBC chip system, also caused torque and rupture of the insert.

Therefore, a new attachment system based on a clicking mechanism was created, in which the HFM cap could click onto the holder by means of four hooks (Appendix B). This attachment mechanism applied a lateral push to the HFM insert in a manner similar to rubber elastics. However, the attachment in the primary clicking design was too strong, making it impossible to remove the cap from the holder. Because of this, multiple clicking designs were developed to find the balance between exerting force on the insert and allowing easy removal from the holder. Eventually, a design was developed that could easily be removed while also exerting an appropriate force on the insert to create a tight seal. However, after the material was cured, the hooks showed to be very susceptible to breaking. To address this problem, a test was performed in which the HFM caps were not cured. This resulted in higher flexibility of the material, which made the hooks less susceptible to breaking. Unfortunately, the uncured BIOC-4 may contain

remnants of liquid resin, which is toxic to cells. As a result, the design using the elastic rubbers turned out to be the most effective for this phase of the project. To improve the user-friendliness of this design, new hooks were developed to facilitate the stretching of the elastics over the HFM cap and holder.

Taking all this into consideration, I would suggest that for the future development of this chip, a similar approach but with different materials could be used. It would be feasible if the HFM clicking cap could be made of a biocompatible material that exhibits higher flexibility when cured. Alternatively, for later stages of development, molding could be used to overcome the variability between parts and generate completely identical parts. This would also benefit user-friendliness as now every part is different because of the printing process and often remnants of supports need to be filed to ensure a perfect fit for assembly and prevent leakage. Overall, 3D printing was a very good technique to develop a prototype because of its very high speed, but to make a very accurate design, molding would probably be a better technique to generate the HFM chip in the future.

4.4. Chapter Conclusion

A new HFM chip design was developed based on an iterative design process. The final design of the HFM chip comprises the HFM chip holder, HFM chip insert, and HFM chip cap. The system is assembled by inserting the HFM chip insert into the holder and close it with the HFM cap. O-rings prevent leakage between the different compartments of the HFM chip and prevent leakage of the liquid through the gap between the HFM holder and cap. The HFM cap is attached to the HFM holder by stretching four rubber rings over the connections on the HFM cap and holder. By means of this attachment, a tight seal between all compartments is created due to the lateral force that is exerted on the HFM insert and holder.

5

Technical Validation Chip Design

5.1. Materials and Methods

5.1.1. General Design Evaluation

The first step in the validation of a new design was to visually check the fit of all chip parts. All individual parts were checked for structural integrity and sufficient rigidity. By performing the assembly multiple times and checking for improper part connections, a proper fit of all chip components was ensured. Furthermore, the printing process was reviewed. The process was reviewed for easiness of the removal of parts from the build plate, build time of the parts, and lengthiness of the post-processing steps for individual parts.

5.1.2. Visual Leakage Validation Chip Design

The seal between the different chip compartments was first evaluated by a visual test with either water or coffee. The chip was first assembled, after which tubing was attached to the TNO connector of either the holder or the cap. By the use of a syringe, water or coffee was pushed through the basolateral compartment of the system (through the HFM) under high pressure (Figure 5.1). This was a quick and effective method to evaluate the leakiness of the different compartments of the chip. In the ideal situation, no liquid should leak from the basolateral to the apical compartment. In that case, the apical compartment should have stayed completely dry. In the case of an improper seal between the basolateral and apical compartments, the apical compartment was filled with liquid because the fluid could escape to that compartment through the parts where the seal was insufficient. This could be visually checked as the chip material was somewhat translucent. The leakage of the apical compartment to the outside (through the gap between the HFM chip holder and cap) could be checked at the same time. In the case of an improper seal between the cap and holder, fluid leaked out of the system to the outside. Any visual evidence of leakage resulted in a new design iteration being generated and printed right away and no further evaluation was performed.

Figure 5.1: Visual test for leakage of the chip compartments. Coffee or water was pushed through the basolateral compartment of the system (through the HFM) by the use of a syringe to test the effectiveness of the seal between the compartments.

5.1.3. Microfluidic Set-up

Figure 5.2 provides a schematic overview of the microfluidic set-up of the HFM chip. The chip is connected through tubing to a basolateral 3D printed reservoir on the one end, and a peristaltic pump on the other end. Pictures of the real-life set-up of the system can be found in Appendix A.

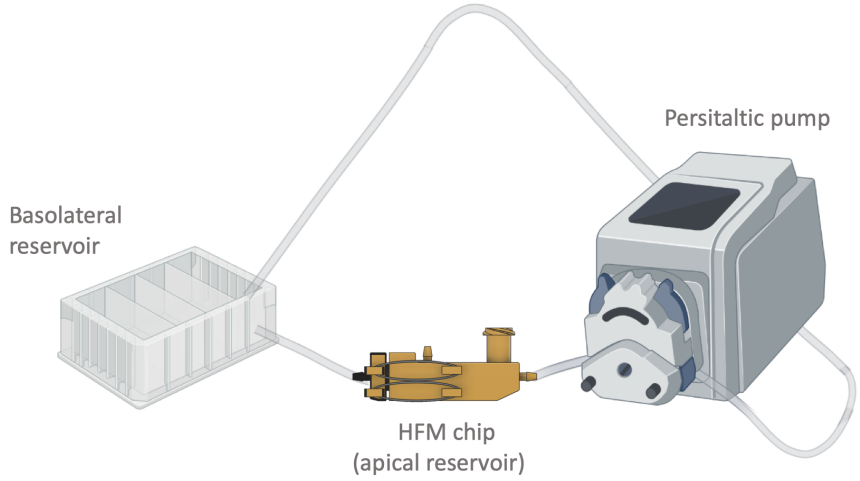

Figure 5.2: Microfluidic set-up. The HFM chip is connected to the tubing on either side. The peristaltic pump is attached to one end. The basolateral reservoir is on the other end.

5.1.4. FD4 Leakage Assay

If a design passed the visual leakage test, a FITC-Dextran 4 (FD4) leakage assay was performed as a second technical test in order to check if there were any leakages between the basolateral and apical compartments of the chip system. FD4 is a small inert molecule that can be used as a barrier integrity indicator [56]. When a cell barrier is intact, FD4 cannot pass through the barrier. Measuring the FD4 concentration on either side of a barrier can therefore reveal if the barrier is still intact. For this test, a cell barrier was mimicked by adding a layer of nail polish on the HFM in the insert. In this way, in theory, FD4 could not pass this barrier, and when FD4 was added to the basolateral compartment, it should not be found in the apical compartment. This is only the case if there are no internal leakages between the basolateral and apical compartments (Figure 5.3).

Thus, by measuring the FD4 concentration on either side of the barrier (both in the apical and basolateral compartments), technical leakages between the two compartments can be detected. An uncoated (empty) HFM served as the negative control in each experiment.

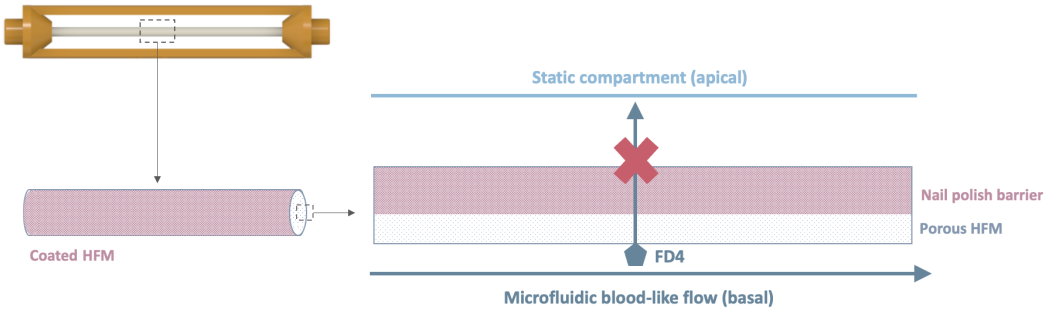

Figure 5.3: Schematic overview of the FD4 assay test to test for leakages in the HFM chip system. A cell monolayer was mimicked by adding a layer of nail polish on the HFM. FD4 was added to the basolateral compartment of the HFM chip. When a tight seal was created and there were no leakages in the system, no FD4 should be found in the apical compartment of the system. Samples were taken from the apical compartment through the sampling Luer.

Hence, two milliliters (ml) of a dosage mixture consisting of FD4 and Hanks' Balanced Salt Solution (HBSS) or cell medium were introduced to the basolateral reservoir of the chip system to assess the efficacy of the seal created between the two compartments. 50µl 10mM FD4 was dissolved in 10ml of medium or HBSS for a working solution of 50µM. In the apical reservoir, 710µl of a blank solution (HBSS or medium) was added. Thereafter, the chip was perfused by a basolateral flow of 0.2 ml/min for one hour with samples being taken from the apical reservoir every 10 minutes. This flow rate was previously determined and was the highest flow rate that can be used with the HFM without rupturing the fiber [23]. 100 µl apical sample was pipetted into a black Thermo Scientific™ Nunc MicroWell 96-Well Optical-Bottom Plates, as well as 100 µl of the blank and the dose solution. After a perfusion experiment, the concentration of FD4 could be examined by measuring the fluorescence intensity of FD4 with a spectrophotometric plate reader at an excitation wavelength of 485 nm and an emission wavelength of 528 nm. The protocol for the FD4 perfusion experiment with a detailed overview of all steps for this experiment can be found in Appendix C.

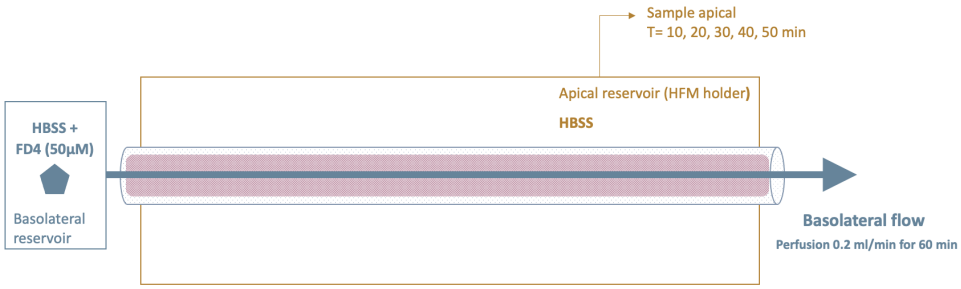

Figure 5.4: FD4 perfusion experiment. The FD4 dose mixture was added to the basolateral reservoir and pushed through the fiber by the introduction of a basolateral flow (0.2 ml/min) for one hour. Every 10 minutes, samples were taken from the apical reservoir.

5.1.5. FD4 Data Analysis

To get an idea about the absolute leakage between the compartments of the chip, the raw FD4 measurement data were converted into apparent permeability (P_{app}) values. The P_{app} value of a compound shows how quickly a compound permeates a specified surface area [57]. It is based on the flux or outflow of a molecule of known molecular weight across a barrier. In this experiment, the P_{app} values represent the basolateral to apical permeability of FD4. This is defined as the rate of transport across the monolayer normalized to the cell surface area.

The apparent permeability of a compound was calculated based on the following formula:

$$P_{\text{app}} = \frac{dQ/dt}{AC_0} \quad (13)$$

With P_{app} [cm/s] indicating the apparent permeability coefficient, dQ/dt denoting the rate of appearance of FD4 at the acceptor side (=apical compartment) over time, A being the surface area of the HFM and C_0 indicating the initial dose concentration of FD4. By comparing the quantity of FD4 still present in the donor (=basolateral) compartment to the amount that was initially present in the apical and basolateral compartments, the recovery of FD4 could be calculated at the end of the experiment.

All data samples were converted using a Microsoft Excel calculation sheet to determine the complementary P_{app} values. The resulting P_{app} values could thereafter be compared to validated P_{app} values of the TNO IEBC chip system and the previous version of the HFM chip system. The FD4 leakage results are provided over time, but the statistical analysis was performed for single time frames.

5.2. Statistical Analysis

GraphPad Prism (Version 8.0.1, GraphPad Software) was used to perform statistical Analyses. Graphs were plotted with their mean and standard deviation (SD). An unpaired t-test was used to determine the significance of the results between the chips containing a coated and an uncoated HFM. In all tests, a p-value of < 0.05 was considered significant.

5.3. Results

The perfusion experiment for the final design of the HFM chip was repeated three times, in which three to four HFM chips were perfused simultaneously for every experiment. A chip containing an uncoated HFM within the HFM chip insert served as the control in each experiment. All chips were perfused for a duration of 50-60 min, of which the first ten minutes were not displayed in the results as this was considered as the time for the system to start up. The P_{app} values were calculated for all experiments.

The P_{app} values resulting from the first experiment are shown in Figure 5.5A. During the first experiment, the chips were perfused for a duration of 60 minutes (Figure 5.5A). Here, the uncoated HFM chip (control), showed a gradual increase in P_{app} value over time, with a maximum of approximately 500 x 10^{-6} cm/s at the final time interval of 40-50 min. The chips containing a coated HFM showed very low P_{app} values (around zero) for the whole duration of the experiment.

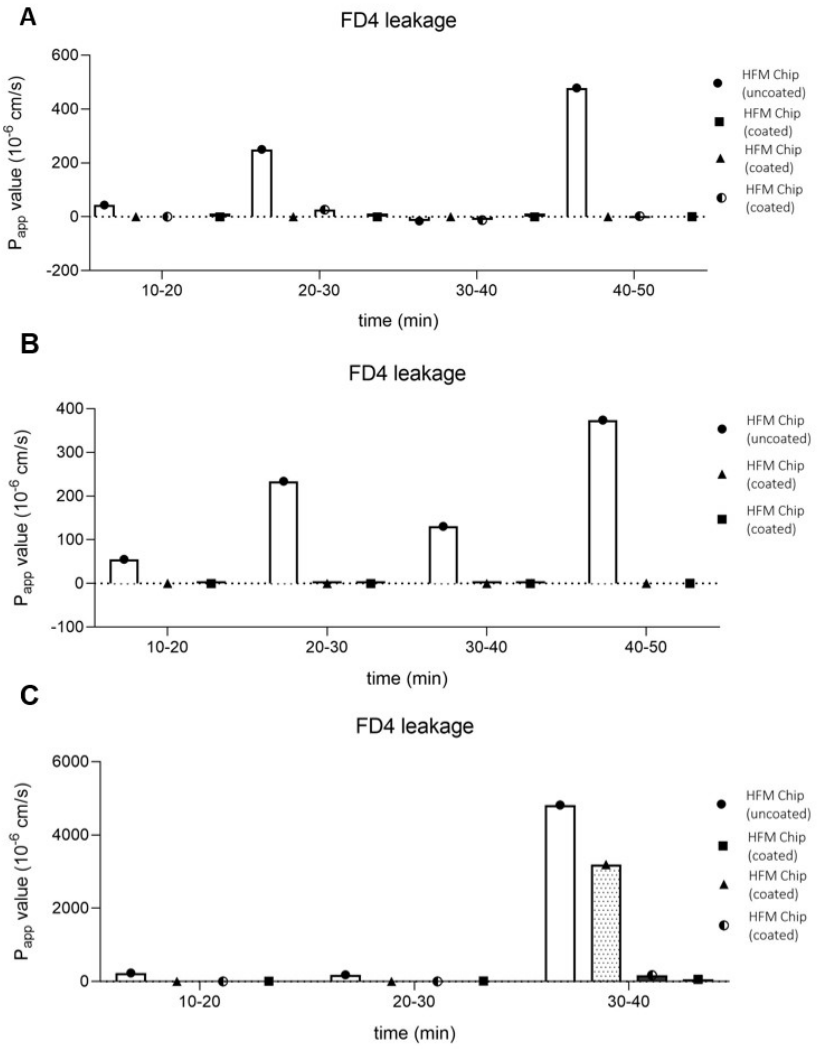

Figure 5.5: P_{app} values for a FITC-dextran-4000 (FD4, 50 µM) assay of the final design of the HFM chip. **(A)** The P_{app} value of the control shows a gradual increase over time, while the P_{app} values of the coated fiber chips remain close to zero. **(B)** Again, the P_{app} value of the control shows a gradual increase over time, while the coated fiber chips show values around zero. **(C)** P_{app} values of the chips containing coated fibers remained around zero for the entire experiment, except for one that showed a higher P_{app} value at the final time interval. The P_{app} value of the uncoated fiber chip (control) shows a very high leakage for the final interval, which may indicate a technical issue with the chip, for instance, the detachment of the HFM after a certain period of time due to inaccurate attachment inside the system.

Secondly, figure 5.5B displays the P_{app} values for the second iteration of the experiment, where the chips were again perfused for 60 minutes. Again, the control displays a gradual increase in P_{app} value over time, with a maximum value of approximately 400 x 10^{-6} cm/s at the final interval. Similar to the previous experiments, the P_{app} values of the chips with a coated HFM remained very low throughout the whole experiment (around zero).

Finally, Figure 5.5C shows the P_{app} values resulting from the third and last iteration of the experiment. In this case, the chips were only perfused for a total of 50 minutes. The control, as seen in the figure, exhibits a very high P_{app} value at the interval of 30 to 40 minutes (about 6000

x 10 $^{-6}$ cm/s). This could indicate that at this point, a technical failure in the system appeared. For instance, the HFM could have detached after a certain period of time due to inaccurate attachment inside the system. One of the coated HFM chips displayed a P_{app} of around 4000 x 10 $^{-6}$ cm/s during the time period of 30 to 40 minutes, which might also possibly be due to a technical leakage at this time.

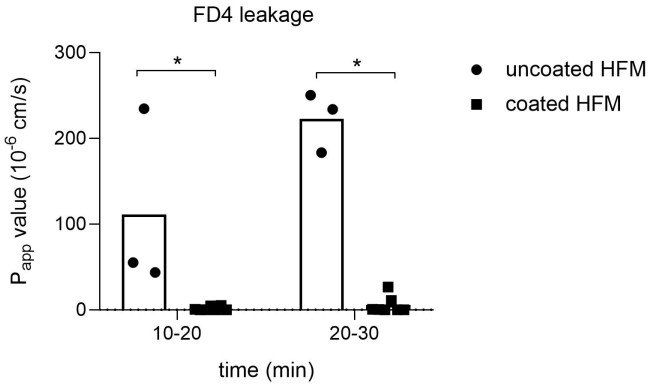

Figure 5.6: FITC-Dextran-4000 (FD4) leakage for all three (independent) experiments mentioned above for the intervals 10-20 min and 20-30 min, comparison of uncoated (control) and coated HFM chips. The comparison was deemed significant for both time intervals using a t-test comparison ($p < 0.05$).

Consequently, Figure 5.6 shows the comparison for all three experiments between the chips with uncoated HFM (control) and coated HFM for the time intervals 10-20 min and 20-30 min. From the comparison, it is clear that the chips with coated fibers comprise a significantly lower P_{app} value than the ones with uncoated fiber for both time intervals, which indicates that the FD4 leakage is relatively significantly lower in the chips with coated fiber than the ones containing an uncoated fiber. These findings suggest that a tight seal is produced between the two compartments of the chip and that there is little leakage between the apical and basolateral compartments of the HFM chip.

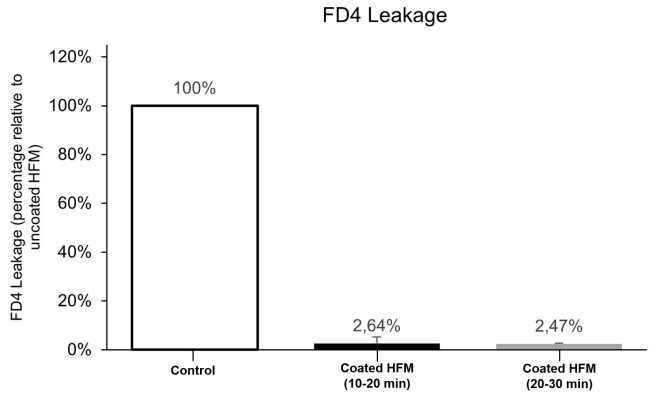

Figure 5.7: FITC-Dextran-4000 (FD4) leakage as a percentage relative to an uncoated fiber (control) for all three experiments mentioned above for the intervals 10-20 min and 20-30 min. The coated HFM chips show a significantly lower leakage when compared to the control. This is true for both the 10-20 min and the 20-30 min time intervals.

Additionally, a comparison based on the leakage percentage of the chips with coated HFM relative to the control (uncoated HFM) was generated for all three experiments (Figure 5.7). Here, it becomes very clear that there the leakage in the coated HFM chips is significantly lower relative to the control situation. For the 10-20 min time interval, an average leakage percentage of 2.46% could be found and for the 20-30 min interval, the average leakage percentage comprised 2.47%.

Finally, the FD4 leakage data for the HFM version 4.8 are provided by Figure 5.8. When comparing the leakage data of the final design of the HFM to these data, a significant reduction in leakage can be perceived for the final design. The data for version 4.8 of the HFM chip system are provided as this version of the system was used for the biological validation in Chapter 7 because new versions of the final version of the HFM chip design could not be printed and therefore used because of printing issues with the 3D printer in the last part of this thesis.

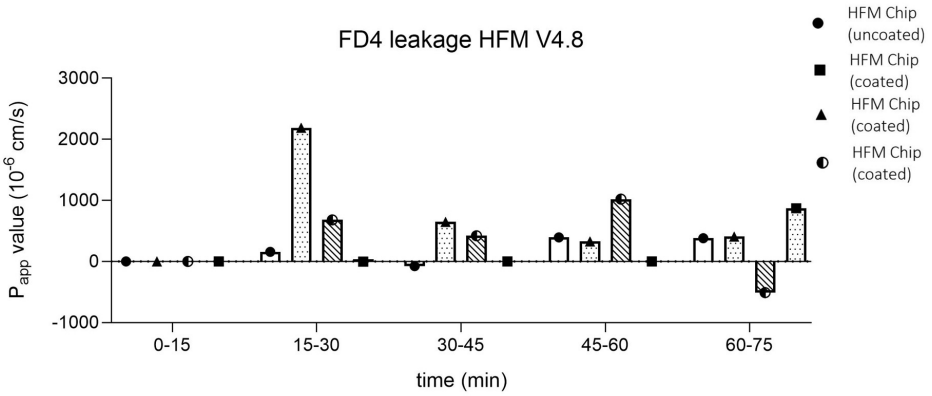

Figure 5.8: FITC-Dextran-4000 (FD4) leakage for version 4.8 of the HFM chip system.

5.4. Discussion

In order to obtain reliable results, a cut-off value for the leakage of the HFM chip system had to be determined. However, determining a cut-off value for the leakage of this system was challenging as there were no clear guidelines or specific thresholds that specified the ideal cut-off value for this scenario. To determine a cut-off value, factors such as the complexity of the problem, the input data, and the desired level of accuracy should be considered. Since the HFM chip OoC system is a completely novel system, there are no established cut-off values for leakiness in the literature.

Therefore, the most relevant system to compare the final version of the HFM chip to was a previous version of the HFM chip (see Section 2.1.3) by *Langerak et al.*, where a SENUOfil HFM was glued inside of a chip system with an open culture chamber. In a previous publication by *Jochems et al.*, Inulin-FITC leakage for the SENUOfil HFM was performed. Figures 5.9A and 5.9B show that the FD4 leakage of the coated SENUOfil HFM relative to an uncoated HFM (control) was determined to be approximately 25%. For the Inulin-FITC measurements with a SENUOfil HFM in the system of *Jochems et al.*, the system was connected to a basolateral reservoir containing Inulin-FITC (0.1 mg/ml). Subsequently, the basolateral flow was pushed through the fiber with a flow rate of 0.1ml/min for ten minutes via a peristaltic pump, and samples

were taken from the apical compartment [23].

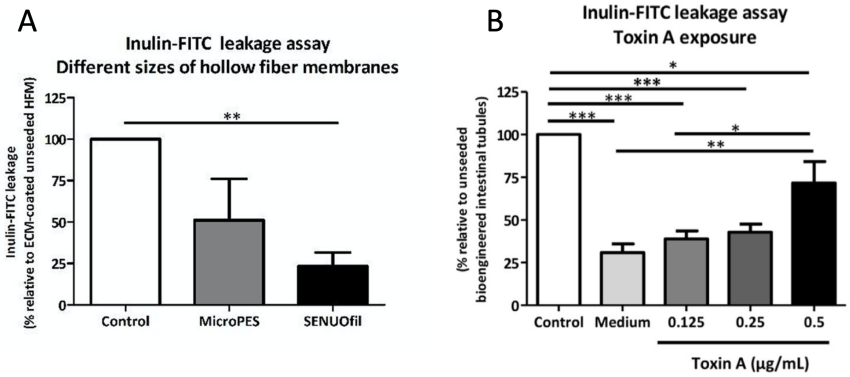

Figure 5.9: (A) Inulin-FITC leakage for different sizes of coated HFMs, expressed as a percentage relative to an uncoated HFM (control). The SENUOfil HFM was used in this thesis. The leakage percentage of a coated SENUOfil HFM was shown to be approximately 25% relative to the uncoated control. **(B)** Inulin-FITC leakage for the SENUOfil HFM with medium relative to an uncoated control. Again, a leakage percentage of 25% was found relative to the control. Figure adapted from *Jochems et al.* [18].

When comparing the leakage percentages of the HFM chips with coated fibers to a control (uncoated HFM) in this study, the leakage percentage for the final version of the HFM chip showed to be significantly lower than the 25% for perfusion of ten minutes. For the time period of 10–20 minutes, an average leakage rate of 2.46% was discovered for the final version of the HFM chip (Figure 5.7). This percentage is considerably less than the 25% discovered by *Jochems et al.* for a previous version of the HFM chip system. One thing to note is that *Jochems et al.* used Caco-2 coated HFMs, while in this experiment, HFMs were coated with a nail polish layer to mimic the monolayer on the HFM. The difference in leakage percentage may thus be a result of the nail polish layer being tighter than a cell monolayer on the HFM. More experiments with HFMs coated with Caco-2 monolayers should be performed to further compare these results.

Furthermore, for the system by *Langerak et al.*, the Inulin-FITC leakage was measured for chips with SENUOfil HFM that were treated with and without the test compound p-cresol. P-cresol was added in different concentrations to the coated fibers to assess its effect on monolayer tightness [23]. P_{app} values were determined for all concentrations (Figure 5.10A). Exposure to p-cresol resulted in a strongly compromised barrier function of the monolayer on the HFM. The value that is of particular importance for this research is the one without p-cresol as this one can be compared to the HFM chip system with a coated HFM in this study.

When comparing the P_{app} value of the system of *Langerak et al.* without p-cresol and the one of the final version of the HFM for the time interval of 10-20 minutes (Figure 5.6B), a similar P_{app} value can be found for both conditions. This shows that the final version of the HFM chip system as presented in this research shows a similar functionality as the one by *Langerak et al.*. Furthermore, a similar P_{app} value could be perceived in Figure 5.10B, where the influence on the seeding method of cells on the SENUOfil HFMs inside the chip system was examined. The difference between cell seeding and consequently barrier integrity with the gravity-driven flow

(GDFS) (for 21 days) and pump-driven flow (PDFS) (for 10 days) was examined. Since the new HFM chip system made use of the GDFS method for 21 days, corresponding P_{app} values of the first condition (GDFS - p-cresol) and the 10-20 minutes condition for the final version of the HFM (Figure 5.6B) can be compared. Again, a similar P_{app} has been obtained for the new HFM chip system when compared to the one of *Langerak et al.*.

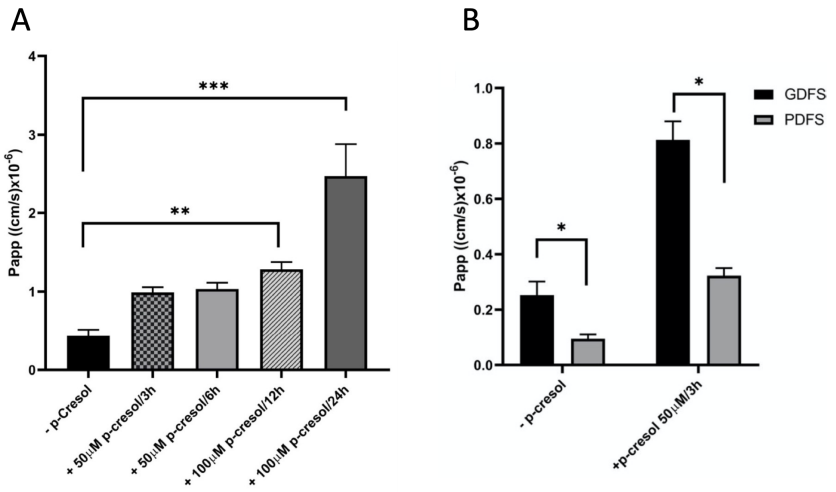

Figure 5.10: Inulin-FITC leakage for **(A)** SENUOfil HFMs treated with increasing concentrations of the compound p-cresol. The first condition (-p-cresol) is of particular importance for this research as the resulting P_{app} can be compared to the P_{app} values of HFM chips containing coated HFMs. **(B)** SENUOfil HFMs that were seeded with Caco-2 cells with either gravity-driven flow (GDFS) or pump-driven flow (PDFS). The figure shows the influence of the seeding method on the P_{app} value of the barriers. Again, the first condition is most important for this research (GDFS - p-cresol) as this value can be compared to the ones in this study. Figure adapted from *Langerak et al.* [23].

In comparison to the ten-minute perfusion described by *Langerak et al.*, the novel HFM chip system may be perfused for up to an hour and exhibits minimal leakage values during the whole experiment. This is a significant improvement compared to the existing HFM chip system. Visual tests that were conducted for a longer time indicated promise for leak-free perfusion for longer durations, but more tests are required to confirm that similar findings can be obtained in longer duration studies using the final version of the new HFM chip.

To establish a standard cut-off value for the HFM chip system for longer-duration trials, further tests that assess leakage over longer time periods are necessary. Since the experiments in this thesis lasted at most one hour, they were not conducted inside the CO_2-incubator. For longer-duration experiments, the HFM chip experiments should be performed inside the incubator. Therefore, future work should include incubator tests and design optimization considering the changing properties of the HFM chip at higher temperatures.

It is crucial to consider that when gluing the HFM inside the insert, the dental adhesive must completely cover the interior of the insert in order to avoid leakage discrepancies across systems. Human error is possible at this stage since various people may apply the glue in different ways. If this step is done incorrectly, the HFM could move or detach during a perfusion experiment due

to the pressure of the fluid going through it. Additionally, the movement or detachment of the HFM might result in leakage, which thus results in very high P_{app} values as displayed in Figure 5.6C. Here, in two of the chips, the HFM was not glued properly inside the system and high leakage occurred over time as the fiber detached from the insert after a certain period of time. This resulted in deviating leakage results that had nothing to do with technical leakage problems of the system. Because of this, the gluing step should be closely monitored during the set-up of the system.

5.5. Chapter Conclusion

In this chapter, a visual leakage test was first performed to validate new versions of the HFM chip system. After a new design passed the visual leakage test, an FD4 leakage test was used to carry out the technical validation of the HFM chip system. The usability of the novel system was demonstrated by the fact that it exhibited similar P_{app} values to those of the previously published HFM chip system by *Langerak et al.*. When compared to the system developed by *Langerak et al.*, one major improvement of the novel system is the increased perfusion time. This leads to more realistic results compared to the native situation in the body. After conducting leakage research and analysis, it can be concluded that the novel system has proven its usability for further development and validation through biological techniques. The results of this research provide a foundation for further investigation and experimentation, allowing for a deeper understanding of the capabilities and limitations of the system.

6

Cell Studies

6.1. Materials and Methods

6.1.1. Starting Up Cell Line Cultures and Cell Culturing

HepaRG Cell Line

Human hepatic progenitor cells were cultured in sterile culture flasks with filter caps from e.g. Corning with a culture area of 25 cm^2 (T25), 75 cm^2 (T75) or 100 cm^2 (T100), containing 5 ml, 10 ml or 25 ml of growth medium respectively, depending on the number of cells that were needed for a specific experiment. The growth medium for HepaRG cells consisted of 500 ml William's E without phenolred, 5.7 ml of 100 IU/ml penicillin, and 100 µl/ml Streptomycin (100x concentrated in saline solution), 57 ml of 10% fetal bovine serum (FBS), 1885 µl if 50 µM hydrocortisone 21-hemisuccinate, 486 µl of 5 µg/ml insulin (1mM in acidified distilled water), and 5.7 ml L-glutamine (200mM). When a cell line was not in use, cells were preserved inside a cryo vial in a nitrogen vessel. To start up the cell culture of HepaRG cells (day one), a cryo vial with HepaRG cells was taken from the nitrogen vessel and was thawed inside a water bad. Subsequently, 10 or 25 ml of heated (37 °C) culture medium was transferred into a T25 or T75 flask, respectively. Then, 1 ml of culture medium was transferred with a pipette into the vial with cells to mix the cells with the medium. Consequently, the mixture was transferred to the culture flask containing the remaining medium. Next, the flask was laid flat and shaken briefly to evenly distribute the cells across the bottom and was placed inside a CO_2 incubator at a temperature of 37 °C. On day two, the medium was removed from the cells with a sterile suction pipette and 5 ml or 10 ml was added to a T25 or T75 flask, respectively. This is done in order to get rid of the DMSO in the medium of the started cell culture. Afterwards, cells were placed back in the CO_2 incubator for further incubation. After approximately three to four days, a confluency of 90% was reached and passaging was required.

For cell passaging, PBS, trypsin solution 0.25%/EDTA (Gibco™ 25300054), and culture medium were heated in a water bad. The culture flasks were removed from the CO_2 incubator and the old culture medium was removed with a sterile suction pipette. The cells were washed one time with 5 ml (T25) or 10 ml (T75) PBS. Next, 0.5 ml (T25) or 1 ml (T75) of trypsin solution was transferred and spread over the bottom of the flask, whereafter the flask was placed back in the incubator for about six to ten minutes (until the cells detach from the bottom). If necessary, the cells were

knocked loose by tapping the bottle. Afterwards, 4 (T25) or 9 (T75) ml of culture medium was added to the flask, and cells were resuspended in the medium by a suction pipette until they were homogeneously suspended. Subsequently, the mixture was collected and spun down for five minutes at 300 rcf in a sterile 15 ml tube (e.g. from Costar). Then, the supernatant was removed and the cell pellet was resuspended in growth medium in a ratio of 1:2 to 1:25 depending on e.g. their growth rate, the research planning, etc. For HepaRG cells, passaging was performed up to two times a week. After the first passaging, cells could also be transferred to a bigger T100 flask if needed, which contains 25 ml of culture medium and for which 2 ml of trypsin is added for trypsinization.

Caco-2 Cell Line

For culturing of Caco-2 cell lines, the same principles hold as for HepaRG cell lines except for a few differences such as the required cell medium and trypsin concentration for passaging. For Caco-2 cells, the culture medium comprises 500 ml of DMEM with Glutamax™, 50 ml FCS, 5 ml L-glutamine (100x), 5 ml NEAA, 0.5 ml gentamycin (50mg/ml), and 5 ml Pen/Strep. For trypsinization, 0.05% trypsin solution is used.

6.1.2. HFM Preparation and Cell Seeding on HFM

For cells to grow on the HFM, the fiber should be prepared and coated prior to cell seeding.

6.1.3. HFM Preparation and Coating

L-DOPA was dissolved in 10mM Tris p 8.5 (2 mg/ml) and was incubated overnight at 37 °C in the CO_2 incubator. The following day, the mixture was filter sterilized using a 0.22 µm syringe filter. Furthermore, the SENUOfil HFMs were cut into pieces of 35 mm and were sterilized in 70% ethanol in a sterile 15 ml tube for 30 minutes at room temperature. Afterwards, the fibers were washed with 5 ml of PBS three times. Subsequently, the fibers were added to the L-DOPA solution and were incubated at 37 °C in the CO_2 incubator for four hours on a carrousel or rocker. After this step, the fibers were washed again with 5 ml of PBS three times. Subsequently, an ECM mixture was prepared by adding collagen I/IV (25 µg/ml) in PBS (25 µl collagen I/5 ml PBS) and the fibers were incubated with this ECM solution for two hours at 37 °C on a carrousel or rocker. After two hours, the ECM solution was removed and the fibers were dried for 45 minutes at room temperature with an open lid, in a sterile environment. Finally, the fibers were washed one time with 5 ml of PBS and ready for immediate use. If the fibers were not used immediately, they could be stored in the fridge in 5-10 ml PBS for up to seven days.

HFM Gluing in Insert

Firstly, the HFM chip inserts were sterilized in 70% ethanol for 30 minutes in a sterile environment. Afterwards, they were washed with PBS three times and sterilized with UV for 15 minutes. Then, the coated HFMs were inserted into the inserts by using a pair of tweezers, like a thread inserted in a needle. Consequently, the HFM was glued into the insert by depositing dental glue in the openings on both sides of the insert, thereby making sure that the HFM is located in the center of the opening. For the deposition of the dental glue, a sterile 5 ml syringe and a blunt-end syringe needle were used. The blunt-end syringe needles were created by shortening a normal BD Microlance™ 3 (21Gx2”, 0.8x50mm) needle with dressing forceps (from e.g. Maier). The plunger was removed from the syringe, and dental glue was deposited into the syringe, which

was subsequently mixed with a 200 µpipette tip. The plunger was put back on the syringe and the glue was pushed through the opening of the HFM chip insert. After this, the glue was left to harden for five minutes. Finally, the excess glue that was sticking out of the opening was cut off with a sterile scalpel blade, while making sure that the fiber was not closed because of the cutting.

HFM Cell Seeding

Upon seeding, Caco-2 or HepaRG cells were harvested by removing the cell culture medium in the flask, adding 0.05% or 0.25% trypsin respectively, incubating the flask for 6-10 min, adding new culture medium in the required volume, and spinning off and resuspending the cell pellet in the required volume of medium (as described in section 6.1.1). For a dense seeding of the HFM, 300k-500k cells per ml were harvested. The number of cells in one milliliter of the medium was counted using a Scepter™ 3.0 Cell Counter. The insert with glued HFM was placed inside a sterile Eppendorf tube of 2 ml and a volume of approximately 1.9 ml of the cells with culture medium was added to the tube. The tube has to be filled completely to minimize the risk of air bubbles in the tube, which could complicate the seeding process. Consequently, the tube was incubated for a total of four hours, while rotating the tube every 45 minutes by 90 degrees to ensure complete coverage of the HFM on every side. Next, the insert was removed from the 2 ml Eppendorf tube and was placed in a well of a 6-well plate with 6 ml of culture medium. One 6-well plate well could hold up to three holders. The cell culture medium was refreshed every other day. For Caco-2 cell lines, a tight monolayer was seen after 12 days, after which they were placed on a rocker to enhance the differentiation, and full maturity was reached after 21 days. In the case of HepaRG cells, a tight monolayer was formed after 10 days, after which a differentiation medium was added. This medium consists of the HepaRG cell culture medium with 1% DMSO added to it. Full maturity was reached after 20 days.

6.2. Results

6.2.1. Caco-2 and HepaRG cell culturing

Both liver (HepaRG) cells and intestinal (Caco-2) cells were used in this study. Both cell lines were cultured inside culture flasks in between experiments. Figure 6.1 displays their 2D configuration on the bottom of a culture flask.

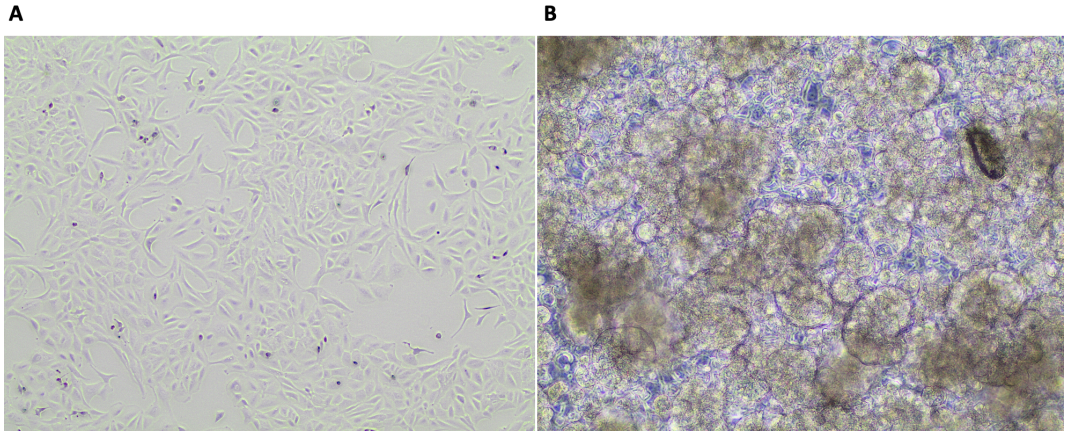

Figure 6.1: Microscopy images of the 2D configuration of **(A)** HepaRG cells and **(B)** Caco-2 cells.

6.2.2. Caco-2 and HepaRG on HFM

For the seeding of cells, only an HFM and an HFM insert are required (Figure 6.2 A, B, C). After seeding, inserts could be kept in a six-well plate in a CO_2-incubator for the entire culturing process (Figure 6.2 D).

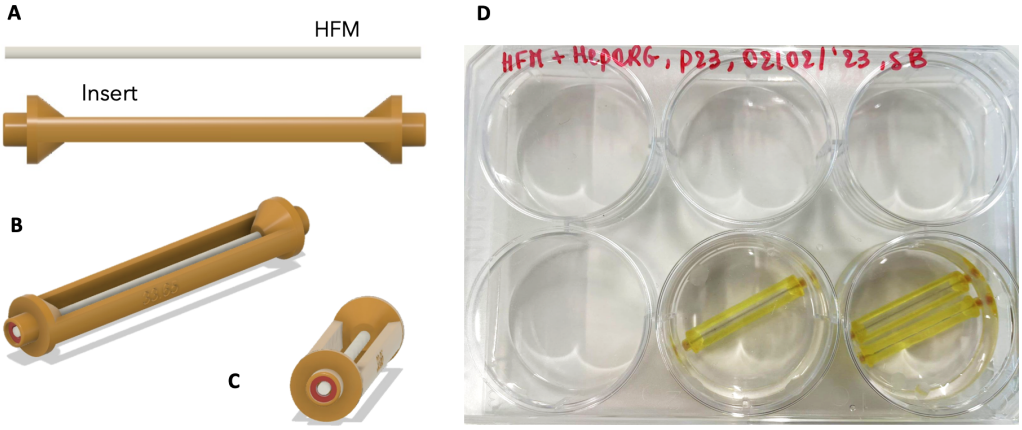

Figure 6.2: (A) The two components necessary for seeding cells are an HFM and an HFM chip insert. **(B, C)** The HFM is glued into the insert by means of a biocompatible dental glue (red). The inner compartment of the insert should be completely filled with dental glue. **(D)** After gluing and seeding of cells, inserts could be kept in a six-well plate in the incubator for culturing.

In this study, the growth of confluent Caco-2 and HepaRG cell layers on HFMs attached inside the chip inserts was investigated. Results show that confluent Caco-2 and HepaRG cell layers could be grown on HFMs attached inside the chip inserts within just one week, and complete maturity was attained after approximately 20 days for HepaRG cells, and 21 days for Caco-2 cells. These findings suggest that the HFM chip insert is a promising platform for the development of 3D cell culture models. Moreover, the HFMs seeded with Caco-2 cells were put on a rocker after 12 days of culture to promote maturation by applying shear stress to the cell surface. The maturation from day 12 onwards is clearly visible in Figure 6.4, as more pronounced villi structures develop from that moment on. This indicates the successful cultivation of 3D Caco-2 monolayers on the HFM. HepaRG cells seeded on the HFM showed a visibly tight monolayer after 10 days, and the formation of small lobules was visible after the addition of the differentiation medium on day 10 (Figure 6.3). These results demonstrate the suitability of the HFM chip insert for culturing 3D cell monolayers and suggest that it could be employed in perfusion experiments, paving the way for further advancements in the field of tissue engineering and drug discovery.

In order to sustain adherence of cells onto the fiber, the fibers were suspended in a medium that contained cells and rotated regularly during the seeding process (see Section 6.1.3 for details). This rotation allowed the cells to adhere to the fiber by resuspending them from the bottom. While various rotational patterns were attempted, no appreciable variations in the production of Caco-2 or HepaRG monolayers were found when changing the rotational pattern. Concerning the seeding densities, varying densities led to variations in monolayer thickness and development rate of the monolayers.

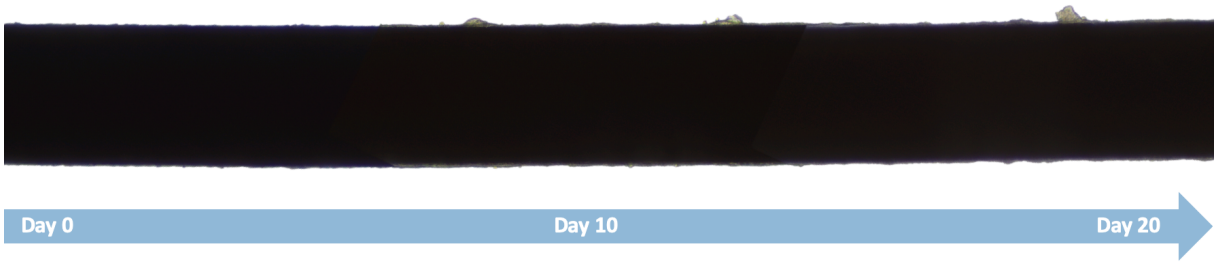

Figure 6.3: HepaRG cell monolayer developing on the HFM over time. A tight monolayer could be seen after 10 days, and full maturity was reached after 20 days.

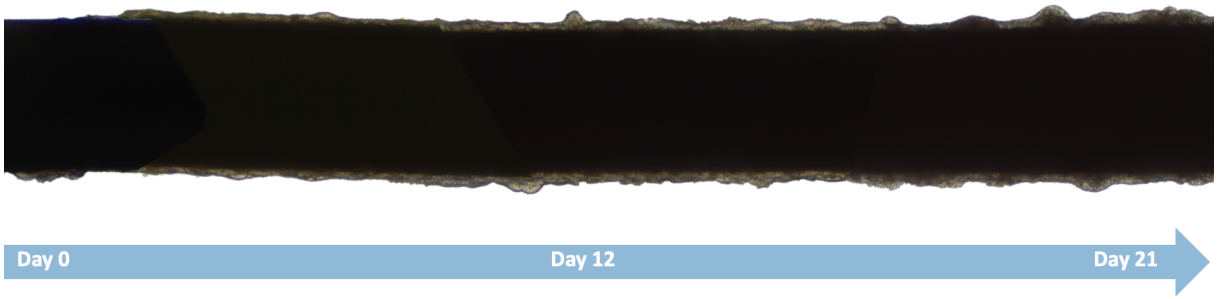

Figure 6.4: Caco-2 cell monolayer developing on the HFM over time. A tight monolayer was developed after 12 days, after which the plate was placed on a rocker for an upcoming 9 days to induce Caco-2 differentiation and maturation (leading to villi formation).

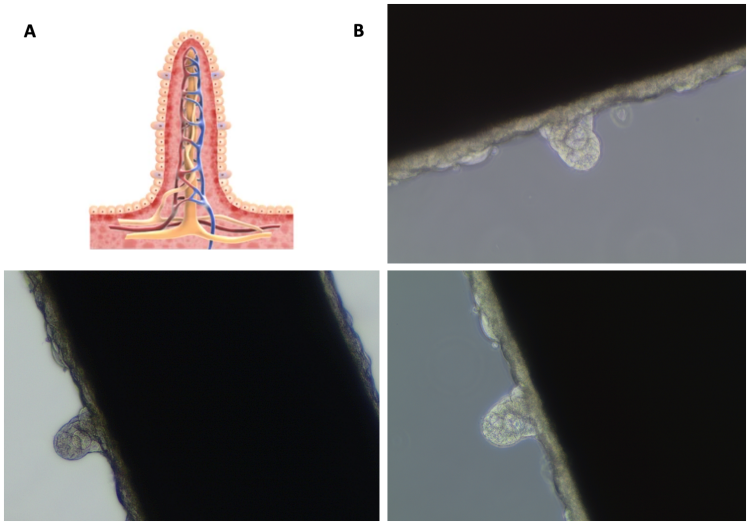

Figure 6.5: **(A)** Schematic representation of intestinal villi. **(B)** Microscopy pictures of Caco-2 cells developing intestinal villi on the HFM, proving the possibility of Caco-2 cells to grow in a 3D configuration on the HFM while in the HFM chip insert.

An optimal seeding density of approximately 400k cells per ml was identified to create a tight and

functional cell monolayer. Significantly lower seeding densities led to incomplete fiber confluence, which could lead to read-out errors due to incomplete monolayer functionality and escape drug components through the fiber. On the other hand, seeding densities that were substantially above this amount caused unintended cell attachment and growth to the walls of the insert, which can lead to inaccuracies in the read-outs caused by the unwanted uptake of drug compounds by those cells. Therefore, a balance between excessive cell proliferation and imperfect fiber confluence had to be established. This resulted in an ideal seeding density of 400k cells per milliliter (ml).

6.3. Discussion

The results of this study are consistent with those previously reported in the literature. *Wang et al.* and *Jochems et al.* have reported that using an HFM as a scaffold results in more pronounced 3D structures for both intestinal and liver cells [36, 18]. The use of an HFM allows for the clear visualization of the 3D configuration of Caco-2 cells, which develop villi structures that are not present when Caco-2 cells are cultured in a 2D configuration (e.g. on a Transwell) (Figure 6.5). The development of these villi shows the importance of a 3D scaffold to support Caco-2 cell differentiation and promote the development of 3D tubules, resulting in a more realistic representation of the native intestinal environment. These findings are in line with those of *Jochems et al.*, who also observed improved Caco-2 cell morphology due to the appearance of villi-like structures, thereby showing the applicability of the HFM as a 3D scaffold for Caco-2 cells.

As for liver cells, *Wang et al.* showed that culturing liver organoids on an HFM resulted in the formation of tubular structures and increase lobule formation. In the field of tissue engineering, liver organoids have emerged as a promising tool for studying liver biology and disease modeling. The use of hydrogel-based matrices such as hyaluronic acid and collagen has enabled the creation of a 3D microenvironment conducive to the growth and differentiation of liver cells [36]. Research conducted by *Wang et al.* has shown that culturing liver organoids on an HFM resulted in the formation of tubular structures and increased lobule formation, mimicking the microarchitecture of the liver [36]. Here, the potential of using the HepaRG liver cell line instead of liver organoids on the HFM to create a functional 3D liver tissue model was investigated. While the use of a cell line resulted in a less bulky 3D configuration of the liver cells, the formation of tubular structures and lobules was still observed on top of the formation of a tight monolayer, indicating that the HFM is a suitable scaffold for the growth and differentiation of liver cells.

During the culturing process, attachment of both Caco-2 cells as well as HepaRG cells was observed to the plastic walls of the HFM chip insert. In cell culture experiments, unwanted cell adhesion and proliferation to plastic surfaces can be challenging. The surface topography and chemistry of the plastic might affect the process of cell adhesion, which can result in unexpected cell attachment and growth [58]. Previous research has shown that attachment and proliferation of undesirable cells can be reduced by using anti-adhesion products such as the Stemcell™ Anti-Adherence Rinsing Solution 07010 [59, 60]. One potential solution to unwanted cell attachment is therefore to immerse the HFM chip inserts in a Stemcell™ Anti-Adherence Rinsing Solution 07010 for up to 30 minutes, which can prevent cell growth on the walls of the HFM chip insert.

As previously stated, an important remark regarding the gluing of the HFM into the insert is that the inner compartment of the insert must be completely filled with dental glue. This step is prone to human error, as each individual may conduct the gluing process differently. Therefore, it is crucial

to ensure that when gluing the fiber in the insert, the inner compartment is thoroughly checked to ensure that it's entirely filled with dental glue and that the fiber is completely surrounded by the glue. If not, the pressure of the fluid passing through the fiber during a perfusion experiment may cause it to shift or detach. Moreover, the detachment or movement of the fiber could cause leakage, leading to errors in the readouts. As a result, the glue stage of the HFM chip processing is the one that requires the most monitoring to avoid human mistakes.

6.4. Chapter Conclusion

Caco-2 cells and HepaRG cell lines were seeded onto the HFM inside the HFM chip insert. Both cell lines showed a tight monolayer after approximately 20 days. These results demonstrate that the HFM chip insert was suitable to develop 3D cell monolayers and could therefore be used in perfusion studies. Caco-2 cells that were seeded on the HFM also developed villi structures, which cannot be seen in their 2D configuration. The formation of these villi illustrates the importance of a 3D scaffold for the Caco-2 cells to more closely resemble their native environment and display the applicability of the HFM insert to be used as this 3D scaffold.

Concludingly, the HFM chip insert provides a promising platform for the development of 3D cell culture models. These findings suggest that the development of 3D cell monolayers that more closely resemble *in vivo* conditions may help to improve the fields of tissue engineering and drug discovery.

7

Biological Validation Chip Design

7.1. Materials and Methods

7.1.1. FD4 Assay

Next to being used as a technical leakage indicator for the chip system, FD4 was also used to determine the integrity of the cell barrier on the HFM in the chip. To determine if the cell barrier function on the HFM is still intact, the FD4 permeability had to be measured, and the accompanying P_{app} value of the FD4 measurement was determined (see Section 5.1.5). A similar set-up as in Section 5.1.3 was used to perform the perfusion experiment.

To test the barrier integrity of the monolayer on the HFM, 710µl of dose mixture, consisting of FD4 and Hanks' Balanced Salt Solution (HBSS) or cell medium, was added to the apical reservoir of the chip system. 50µl 10mM FD4 was dissolved in 10ml of medium or HBSS for a working solution of 50µM. In the basolateral reservoir, 2ml of a blank solution (HBSS or medium) was added. Thereafter, the chip was perfused by a basolateral flow of 0.2 ml/min for one hour with samples being taken from the basolateral reservoir every 10 minutes. 100 µl basolateral sample was pipetted into a black Thermo Scientific™ Nunc MicroWell 96-Well Optical-Bottom Plates, as well as 100 µl of the blank and the dose solution. After a perfusion experiment, the concentration of FD4 could be examined by measuring the fluorescence intensity of FD4 with a spectrophotometric plate reader at an excitation wavelength of 485 nm and an emission wavelength of 528 nm.

It is important to note that the perfusion experiment was performed with an older version of the HFM chip (V4.8). Unfortunately, due to technical issues with the 3D printer throughout this thesis, there is no biological validation data available for the final version of the HFM chip system.

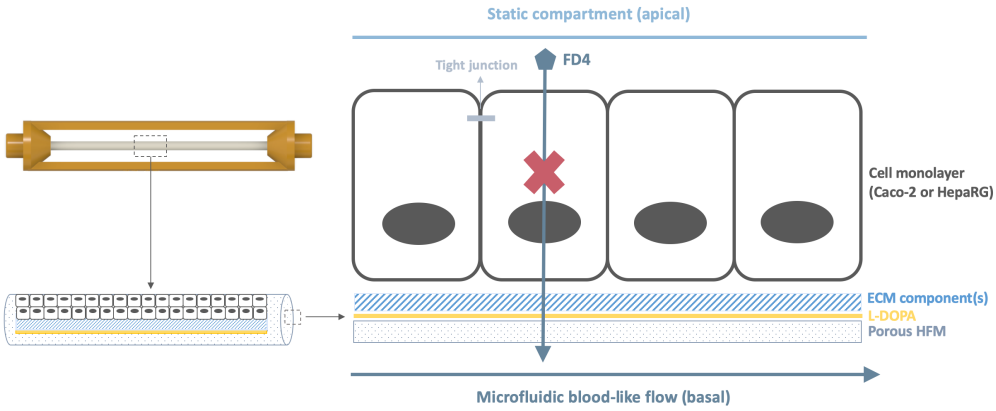

Figure 7.1: Schematic overview of the FD4 assay test to test for leakages and barrier integrity in the HFM chip system. FD4 was added to the apical compartment of the HFM chip. When there were no leakages in the system and the barrier of the monolayer remained intact during the experiment, no FD4 should leak from the apical to the basolateral compartment of the system. Samples were taken from the basolateral compartment.

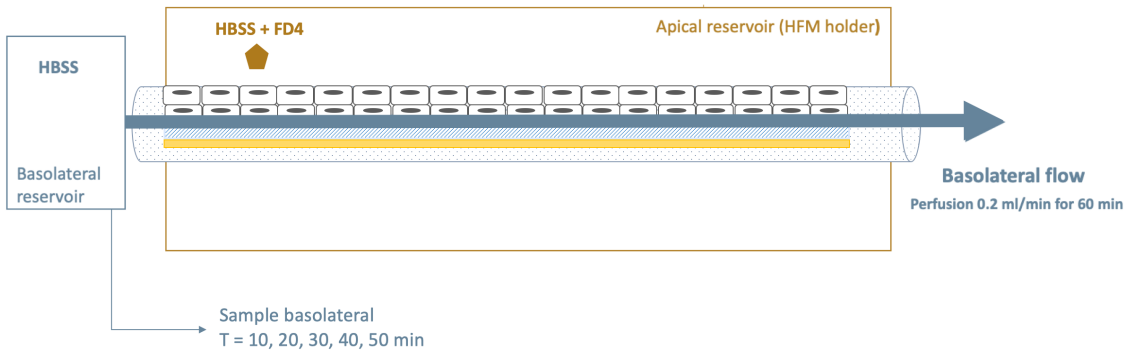

Figure 7.2: Schematic overview of the perfusion FD4 assay to test for barrier integrity of the cell monolayer on the HFM in the chip system. FD4 was added to the apical reservoir of the HFM chip. Samples were taken from the basolateral compartment every 10 minutes for a duration of one hour.

7.1.2. MTT Assay

An MTT assay was used as a colorimetric assay used to measure cell metabolic activity after a perfusion experiment. This assay is based on the conversion of MTT (3-(4,5-dimethylthiazol-2-yl)-2,5-diphenyltetrazolium bromide) to formazan by mitochondrial dehydrogenase in living cells. After a perfusion experiment, 0.5 mg/ml MTT was dissolved in Caco-2 or HepaRG cell medium. The HFM with cell monolayer (Caco-2 or HepaRG) was submerged in the MTT mixture in a 96-well plate for one hour. Afterwards, a visual inspection of the conversion was performed to detect the number of living cells on the HFM after a perfusion experiment.

7.1.3. Confocal Microscopy

Confocal microscopy was used to validate the viability of the monolayers on the HFM after a perfusion experiment. Through confocal microscopy, it could be determined if the cells survived the applied flow during an experiment and if the cell monolayer was still intact. To fix the HFM, the HFM was added 4% Paraformaldehyde (PFA) for 45 min at 4 °C, after which it was washed with PBS three times. Consequently, the HFM could be stored in PBS at 4 °C until use. For blocking, the HFM was added to a solution of PBS, 0.1% Tween, 1% Bovine Serum Albumin (BSA), and 10% goat serum for one hour. Thereafter, the primary antibodies could be added overnight in a solution with PBS, 0.1% Tween, and 1% BSA (concentration 1:500). Consequently, the HFM could be washed three times for 10 minutes and one time for 5 minutes, after which it was rinsed with H_2O and was ready to mount. DAPI was used as an antibody to stain the nucleus of the cells. Zonula occludens-1 (ZO-1) was used for the visualization of the tight junctions.

7.2. Results

7.2.1. FD4 Assay

Figure 7.3 shows the results of an FD4 perfusion experiment (HFM chip V4.8) for a nail-polish-coated HFM, an HFM coated with Caco-2 cells, and an HFM coated with HepaRG cells where the FD4 dose was added apically. The control is again an uncoated HFM. The P_{app} values for all conditions are provided by the figure. Very high leakage values can be seen for this system for all conditions but the coated one. This is most likely the result of an insufficient seal between the apical and basolateral compartments of the chip during the experiment.

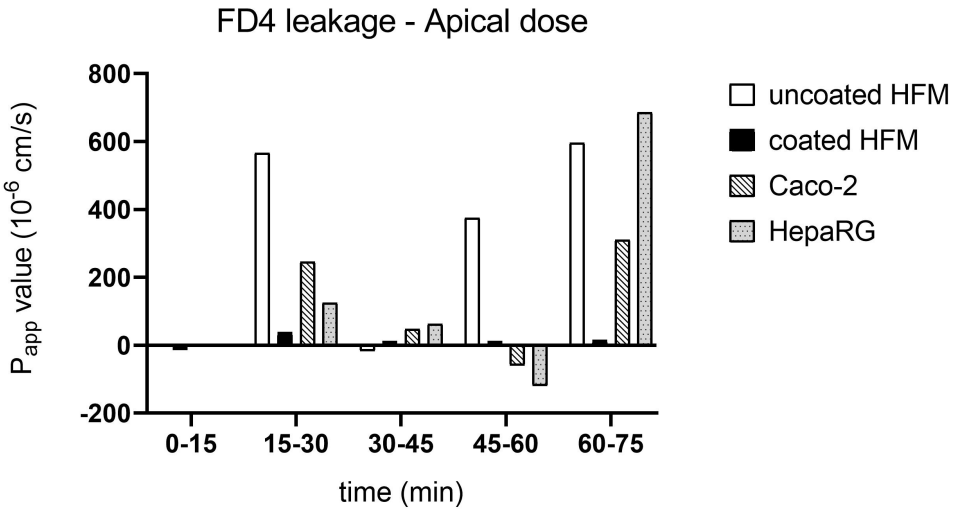

Figure 7.3: P_{app} values of FITC-dextran-4000 (FD4, 50 µM) of the HFM (V4.8) chip. P_{app} values are shown for an empty HFM (control), a nail polish-coated HFM, an HFM coated with Caco-2 cells, and an HFM coated with HepaRG cells.

For the initial time span of 0–15 min, the P_{app} values are still low and exhibit a logical tendency. The uncoated fiber has the greatest P_{app} value, whereas the coated fibers have values that are comparable. However, because this period is thought of as the startup time of the system to cycle the fluid through the tubing, it is typically not taken into account in the results.

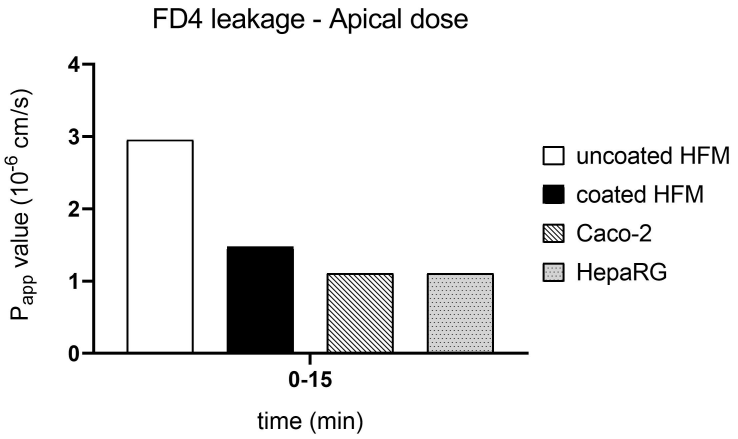

Figure 7.4: P_{app} values of FITC-dextran-4000 (FD4, 50 µM) of the HFM (V4.8) chip for the time interval 0-15 min.

Figure 7.5 shows the results for the time interval 15-30 min. A high P_{app} value of around 800 x 10^{-6} cm/s can be seen for the control condition, which is most probably the result of a technical leakage in the chip. For the closed fiber, the P_{app} value is approximately 50 x 10^{-6} cm/s, while the one for the Caco-2 cells shows a value of approximately 400 x 10^{-6} cm/s, and the one for the HepaRG monolayer 200 x 10^{-6} cm/s. The less tightly packed cell monolayers may account for the greater leakage values for cell-coated HFM chip systems compared to nail polish-coated HFM.

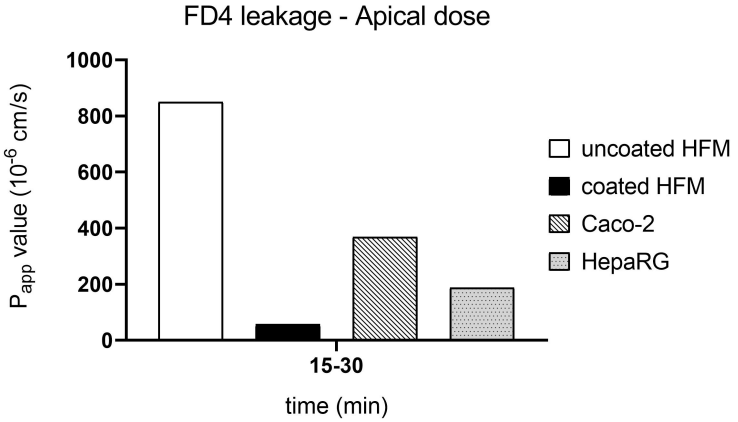

Figure 7.5: P_{app} values of FITC-dextran-4000 (FD4, 50 µM) of the HFM (V4.8) chip. Results are provided for the time interval 15-30 min.

Finally, one experiment with the HFM V4.8 was performed with cells where the FD4 dose was added to the basolateral reservoir, as was the case in the technical validation in Chapter 5. The HepaRG coated chip showed a gradual increase in P_{app} value over time. However, the HFM chip that was coated with Caco-2 cells showed a decrease in P_{app} value. This is most probably the result of a defect within the chip or tubing system, where FD4 could escape the system e.g. by leaking out of damaged tubing. The negative values at the time interval 60-75 might be a result of a read-out error or inconsistency of the plate reader.

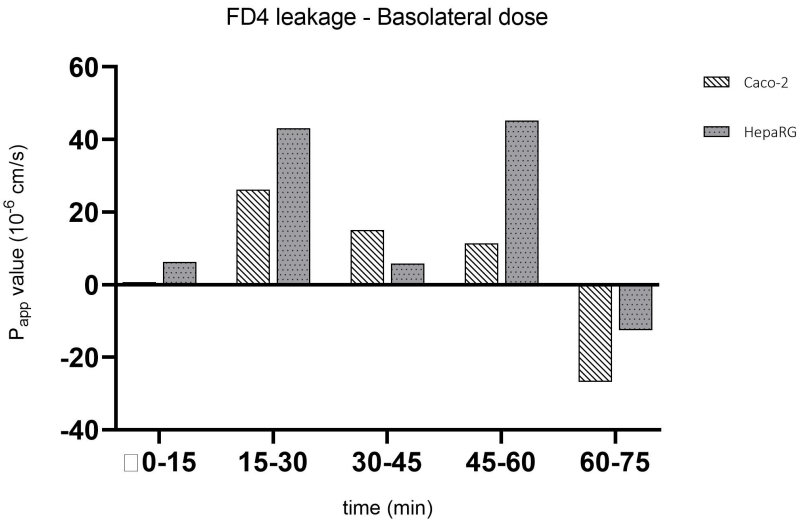

Figure 7.6: P_{app} values of FITC-dextran-4000 (FD4, 50 µM) of the HFM (V4.8) chip. P_{app} values are shown for an empty HFM (control), a nail polish-coated HFM, an HFM coated with Caco-2 cells, and an HFM coated with HepaRG cells. Results are provided for the time interval 20-30 min.

7.2.2. MTT Assay

Following a perfusion experiment, the metabolic activity of the cell monolayer was observed using a MTT assay. Cell viability is presented by the purple regions. Nearly the whole HFM was purple, demonstrating that a high level of cell viability could still be discovered following a perfusion experiment. This indicates that the cell monolayer remained intact for the whole duration of the experiment, suggesting that the pressure inside the system and the flow rate being used enable the cells to continue to function.

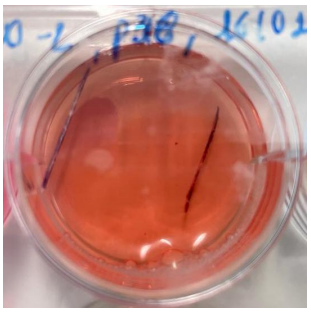

Figure 7.7: An MTT assay was used to visualize the cell metabolic activity of the cell monolayer after a perfusion experiment. The purple areas indicate cell viability. Allmost the whole HFM showed to be purple, which indicated a high cell viability could still be found after a perfusion experiment.

7.2.3. Confocal Microscopy

As a second validation method for cell viability, HFMs were fixed and stained with the fluorescent probes DAPI (nucleus or DNA content) and ZO-1 (tight junctions). Figure 7.8 shows the resulting confocal microscopy images for both an HFM coated with Caco-2 cells (Figure 7.8A) and an HFM coated with HepaRG cells (Figure 7.8B). For both the HFM stained with Caco-2 cells and

HepaRG cells, it is clear that both nuclei and tight junctions are still present after the perfusion experiment, which shows the applied flow and pressure allow the cells to stay viable for the whole duration of the experiment.

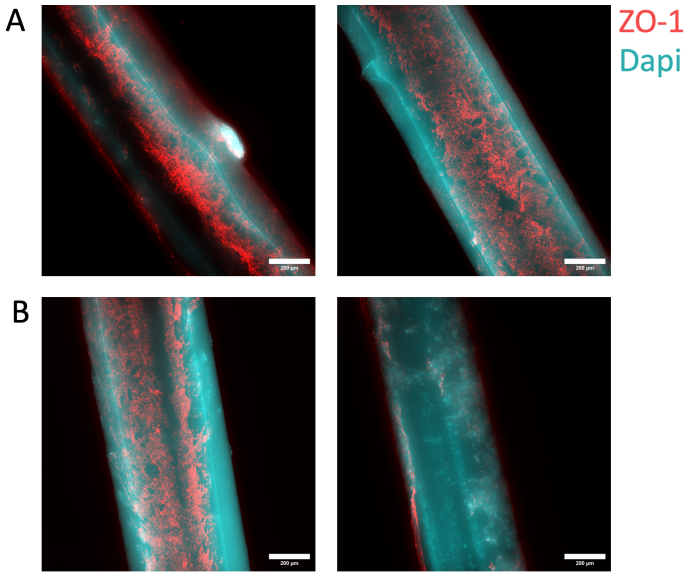

Figure 7.8: Confocal microscopy images of the HFM seeded with (**A**) Caco-2 cells, and (**B**) HepaRG cells show that both cell monolayers remained intact after the perfusion experiment. This demonstrates the usability of the HFM chip for perfusion experiments.

7.3. Discussion

In the perfusion experiment that was performed in this chapter, adding FD4 in the apical compartment was the most logical in terms of cell barrier integrity as this is the compartment where the cells are situated and thus can be exposed to compounds. Unfortunately, an apical dose of FD4 in the HFM chip system has not yet been reported in the literature. Therefore, results will be compared to the IEBC chip system of TNO (see Section 2.1.3), a gut-on-a-chip system that also contains an apical and basolateral compartment. However, it is important to note that while the HFM chip system only has one flow through the basolateral compartment, the IEBC chip comprises a double flow, allowing it to be perfused from both the apical and basolateral sides. Furthermore, the IEBC results were based on the incorporation of a tissue insert into the device instead of cell sources. This results in increased complexity when comparing both systems. Figure 7.9 shows the results of a barrier integrity analysis with FD4 in the IEBC. The first condition with a perfusion flow of 2 ml/h is most relevant to this research as this condition most closely resembles the conditions in the HFM chip system. For the IEBC, a P_{app} value of around one could be found for this condition (Figure 7.9). Comparing these outcomes to the ones for all situations in the HFM chip (Figure 7.3), the P_{app} values are significantly higher.

The significantly higher leakage values observed in this experiment are most likely the consequence of technical issues with the HFM chip system rather than compromised barrier integrity. When looking at the coated fiber condition in both Figure 5.6A (FD4 added basolaterally), and Figure 7.3 (FD4 added apically), in theory, both P_{app} values should be in the same order as the compartment in which the compound is added should give no significant differences in the results

for the P_{app} value. However, it is important to note that a previous version (V4.8) of the HFM chip system was used for the experiments in this chapter, which showed higher leakage values than the final version because of an insufficient seal between the apical and basolateral compartments. Therefore, P_{app} values were expected to be higher when compared to the results of the final version of the HFM chip system. One possible explanation for the significantly higher P_{app} values compared to the basolateral addition of the compound, could be the fact that the chips were connected to the peristaltic pump in such a way that the fluid was sucked through the chip system. Because of this, liquid from the apical compartment could be sucked into the fiber, and thus in the basolateral compartment, at the extremities of the fiber because of the flow. However, more experiments should be conducted to draw clear conclusions concerning this possibility as the results might also be misleading because of individual deviations between the chip systems in the experiments.

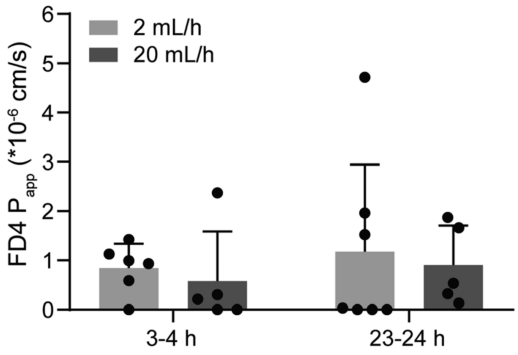

Figure 7.9: Integrity and functionality of the tissue explant in the IEBC. P_{app} of FITC-dextran-4000 (FD4, 50 µM). Figure adapted from *Eslami Amirabadi et al.* [19].

Next to adding the FD4 dose apically, one experiment with cell monolayers was performed in which the FD4 dose was added basolaterally, similarly to Chapter 5 (Figure 7.6). Here, the P_{app} values of the chips were significantly lower than those where the dose was added apically. When comparing these results to those of *Langerak et al.*, similar P_{app} values can be found for the 0-15 time interval. However, for the HepaRG coated HFM system, the P_{app} values significantly increased after this time interval, which most probably was the result of an insufficient seal between the apical and statical compartments. The P_{app} values of the Caco-2 cells remarkably decreased over time, which might be explained by a technical issue with e.g. the tubing, leading to liquid leaking being able to leak out of the perfusion system.

Furthermore, it is crucial to note that the experiments in this chapter were repeated only once, which might result in misleading data and faulty conclusions due to individual deviations of the chip systems and research equipment. Therefore, because a previous version of the HFM chip system design (V4.8) was used and the repetition of the experiments was very low, no clear conclusions can be drawn from the results of the experiments in this chapter, and far more biological validation studies for the final version of the HFM chip are necessary. Next to this, validation with antipyrine and atenolol would also be advised for further biological validation of the HFM chip device. These are two small molecules that are frequently used as model drugs to examine the permeability and functionality of intestinal tissue [19]. This assay can be used to discover more about the functionality of the cell monolayers on the HFM inside the HFM chip.

However, one thing that is noteworthy is that the cell monolayers (both HepaRG and Caco-2) stayed viable for the whole duration of the experiment (75 minutes). This was validated by means of an MTT assay and by visualizing cell nuclei and tight junctions with confocal microscopy. This is a significant improvement when compared to the system of *Langerak et al.*, where the system could be only perfused for ten minutes because of compromised barrier integrity after this period. The improvement is the result of a decreased pressure difference between the apical and basolateral compartments because of the closed nature of the apical compartment in the HFM chip system. In the system of *Langerak et al.*, the apical compartment was open, resulting in the fluid wanting to escape from the HFM to the lower-pressure apical compartment. By closing the apical compartment, the pressure difference between the inside of the HFM and the outside compartment is minimized, leaving the barrier integrity to be uncompromised for the whole duration of the experiment. In the future, this pressure difference can be further optimized by finetuning the dimensions of the apical compartment with flow studies combined with biological validation.

7.4. Chapter Conclusion

In this chapter, a biological validation for the HFM chip (V4.8) system was performed. Results from an MTT assay and confocal microscopy images showed that the cell monolayer remained intact over a perfusion experiment of 75 minutes. This displays that the applied perfusion flow allows the cells to remain viable over the entire span of the perfusion experiment. An FD4 assay was performed to discover more about the barrier integrity of the cell monolayers on the HFM inside the chip system. Unfortunately, no conclusions can be drawn from the data in this chapter as a previous version (V4.8) of the HFM chip device was used for the experiments and the repetition of the experiments was too low. Therefore, before any conclusions can be drawn about the biological validity of the HFM chip device, many experiments with the final version of the HFM chip system have to be performed to acquire reliable data in the future.

8

Discussion

To establish a universal cut-off value for the allowed chip leakage across chip compartments, far more investigation is required before the final version of the HFM chip system can be used for further studies. As the chip is part of a larger consortium effort, researchers at Utrecht University will carry on the research and use the final design of the HFM chips to conduct experiments with liver, intestinal, and renal cell sources. The first steps that should be conducted are to refine the validation and repeat the validation experiments, particularly the biological validation using atenolol and antipyrine, as well as biological validation by adding FD4 to the chip's apical component.

Furthermore, the single flow system creates a highly relevant environment for both liver and renal cell sources. However, the intestinal cells require a double-flow perfusion system to generate a microfluidic environment that resembles their native environment. Therefore, the design and development of a double-flow HFM chip system should be one of the next steps before multiple systems can be coupled to create a MOoC device. As the final version of the HFM chip already contains two compartments, as is required for an intestine-on-a-chip, this double flow can be easily generated by creating a second flow through the apical compartment of the chip. Alternatively, the TNO IEBC chip system, which has been developed and completely validated already, can be used as the intestine-on-a-chip and can therefore be directly coupled to the HFM system containing liver or renal cell sources. If this would to be realized, flow rates of the individual devices should be optimized and adjusted such that the system can function as a whole when all components are connected.

After further validation and optimization of the HFM chip design, a MoOC device can be created by coupling individual OoC devices in a plug-and-play manner by the means of tubing. For further information, an elaborate literature analysis about coupling methods, accompanying flow rates, and scaling can be found in Appendix D. Based on the literature, a single-chip system in which all chip components are integrated into a single chip body is the most ideal method to couple individual chip components to generate the most accurate results for the first-pass metabolism. However, as the individual chip designs for this consortium project are developed at different laboratories, a plug-and-play system in which all individual components can be easily interconnected and removed by tubing was the most feasible option for this project. When employing a direct or physical connection, the separate organ models are coupled via connecting

channels or tubing systems, and off-chip pumping systems are used to accomplish circulatory perfusion. The high degree of modularity of such a configuration, which enables individual organ modules to be created and enhanced before being integrated into the system, is a key benefit of such a ”plug-and-play” platform arrangement and is best suited for the scope of this project. Other advantages comprise the facilitation of decoupling of malfunctioning organ modules and facile coupling of newly developed organ modules. Unfortunately, this type of arrangement has a few drawbacks as well. These comprise a high dead volume, the risk of bacterial contamination, failure, and skewed results because of re-use of tubing, difficulty to reproduce the desired circulation of medium to reproduce organ-specific flow rates, difficulties in reducing metabolic waste to the next organ and scaling issues. Designing and developing each OoC in close collaboration with all stakeholders is the best method for tackling these challenges, making this the main suggestion for the future development of the MOoC system.

9

Conclusion

The presented work is part of the first step toward developing a modular MOoC drug-deposition-on-a-chip system to predict human pharmacokinetics *in vitro*. The purpose of this thesis was to develop a new OoC model that lends itself to accommodate both intestinal and hepatic cell sources, along with the ability to interconnect quickly and easily, enabling the ultimate realization of the required organ-organ interactions in the envisioned MOoC device. The two main design requirements for the new system were the inclusion of a hollow fiber membrane (HFM) as a scaffold for the cells to generate a 3D structure that more closely reflects their *in vivo* architecture, along with the incorporation of a two-compartment model. The inclusion of a two-compartment model represents a significant improvement compared to the previous OoC models as it allows for precise tracking of the pathway of a drug and its metabolites after they leave the hepatic circulation. Consequently, drugs that would have been immediately rejected in the first phase of development can now be tested, allowing for a higher throughput of drugs in the first phases of the development process. A new HFM chip system was developed, optimized, and validated in order to pave the way to a modular MOoC system. The HFM insert system allows for the off-chip culturing of Caco-2 and HepaRG cells and was proven effective in this study. Furthermore, leakage analyses were performed that showed promising results for the further use of the HFM chip system. However, before the system can be used for drug research purposes, more validation studies need to be performed to generate standard cut-off values and validate the full functionality of the system. In conclusion, the design and development of accurate organ models through OoC is ultimately a complex process that requires a bottom-up, step-by-step methodology. To accurately model the first-pass metabolism, it is crucial to develop well-defined control conditions in which every variable is thoroughly documented. More steps are required to develop an accurate MOoC device for the first-pass metabolism and, therefore, reach the ultimate goal of the consortium project. However, this approach has great potential and might significantly reduce the time and costs associated with drug development, ultimately leading to more effective drugs and improved patient outcomes.

References

[1] JR Coppeta et al. “A portable and reconfigurable multi-organ platform for drug development with onboard microfluidic flow control”. In: *Lab on a Chip* 17.1 (2017), pp. 134–144.

[2] Aerim Choe et al. “Microfluidic Gut-liver chip for reproducing the first pass metabolism”. In: *Biomedical microdevices* 19.1 (2017), pp. 1–11.

[3] Dong Wook Lee et al. “3D gut-liver chip with a PK model for prediction of first-pass metabolism”. In: *Biomedical microdevices* 19.4 (2017), pp. 1–13.

[4] Nikolaos Tsamandouras et al. “Integrated gut and liver microphysiological systems for quantitative in vitro pharmacokinetic studies”. In: *The AAPS journal* 19.5 (2017), pp. 1499–1512.

[5] United Nations. *The17goals|sustainabledevelopment*. 2023. URL: `https://sdgs.un.org/goals`.

[6] van den Eijnden-van Raaij, van Meer, B., Mummery, C., van de Graaf, A. *Towards new research models for studying disease and finding treatments: mini organs-on-chips*. Dutch Foundation BMW. 2020.

[7] Amir Bein et al. “Microfluidic organ-on-a-chip models of human intestine”. In: *Cellular and molecular gastroenterology and hepatology* 5.4 (2018), pp. 659–668.

[8] Mark Lyte. “Microbial endocrinology in the microbiome-gut-brain axis: how bacterial production and utilization of neurochemicals influence behavior”. In: *PLoS Pathog* 9.11 (2013), e1003726.

[9] Gabriele Moser et al. “Intestinal microbiome-gut-brain axis and irritable bowel syndrome”. In: *Wiener Medizinische Wochenschrift* 168.3 (2018), pp. 62–66.

[10] Thomas C Fung et al. “Interactions between the microbiota, immune and nervous systems in health and disease”. In: *Nature neuroscience* 20.2 (2017), p. 145.

[11] Nureddin Ashammakhi et al. “Gut-on-a-chip: Current progress and future opportunities”. In: *Biomaterials* (2020), p. 120196.

[12] Debby Laukens et al. “Heterogeneity of the gut microbiome in mice: guidelines for optimizing experimental design”. In: *FEMS microbiology reviews* 40.1 (2016), pp. 117–132.

[13] Katja Hoehn Elaine N. Marieb. *Human Anatomy Physiology, Global Edition (10th edition)*. 2016.

[14] Margaret E Smith et al. *The digestive system*. Elsevier health sciences, 2001.

[15] Sebastiaan J Trietsch et al. “Membrane-free culture and real-time barrier integrity assessment of perfused intestinal epithelium tubes”. In: *Nature communications* 8.1 (2017), pp. 1–8.

[16] Seung Hwan Lee et al. “Organ-on-a-chip technology for reproducing multiorgan physiology”. In: *Advanced healthcare materials* 7.2 (2018), p. 1700419.

[17] Seung Yeon Lee et al. “Gut-liver on a chip toward an in vitro model of hepatic steatosis”. In: *Biotechnology and bioengineering* 115.11 (2018), pp. 2817–2827.

[18] Paulus GM Jochems et al. “Development and validation of bioengineered intestinal tubules for translational research aimed at safety and efficacy testing of drugs and nutrients”. In: *Toxicology in Vitro* 60 (2019), pp. 1–11.

[19] Hossein Eslami Amirabadi et al. “Intestinal Explant Barrier Chip: Long-term intestinal absorption screening in a novel microphysiological system using tissue explants”. In: *Lab on a Chip* 22.2 (2022), pp. 326–342.

[20] Amy Dawson et al. “A microfluidic chip based model for the study of full thickness human intestinal tissue using dual flow”. In: *Biomicrofluidics* 10.6 (2016), p. 064101.

[21] Alexandre Grassart et al. “Bioengineered human organ-on-chip reveals intestinal microenvironment and mechanical forces impacting Shigella infection”. In: *Cell host & microbe* 26.3 (2019), pp. 435–444.

[22] Huanhuan Joyce Chen et al. “A pumpless body-on-a-chip model using a primary culture of human intestinal cells and a 3D culture of liver cells”. In: *Lab on a Chip* 18.14 (2018), pp. 2036–2046.

[23] Nicky Langerak et al. “A theoretical and experimental study to optimize cell differentiation in a novel intestinal chip”. In: *Frontiers in Bioengineering and Biotechnology* 8 (2020), p. 763.

[24] Kwang-Ho Lee et al. “3D liver models on a microplatform: well-defined culture, engineering of liver tissue and liver-on-a-chip”. In: *Lab on a Chip* 15.19 (2015), pp. 3822–3837.

[25] Jiu Deng et al. “Engineered liver-on-a-chip platform to mimic liver functions and its biomedical applications: A review”. In: *Micromachines* 10.10 (2019), p. 676.

[26] Ye Cong et al. “Drug toxicity evaluation based on organ-on-a-chip technology: a review”. In: *Micromachines* 11.4 (2020), p. 381.

[27] Volker M Lauschke et al. “Novel 3D culture systems for studies of human liver function and assessments of the hepatotoxicity of drugs and drug candidates”. In: *Chemical research in toxicology* 29.12 (2016), pp. 1936–1955.

[28] Nikolaos Tsamandouras et al. “Quantitative assessment of population variability in hepatic drug metabolism using a perfused three-dimensional human liver microphysiological system”. In: *Journal of Pharmacology and Experimental Therapeutics* 360.1 (2017), pp. 95–105.

[29] Jasleen K Sodhi et al. “Successful and unsuccessful prediction of human hepatic clearance for lead optimization”. In: *Journal of medicinal chemistry* 64.7 (2021), pp. 3546–3559.

[30] M Rowland et al. “Clinical Pharmacokinetics: Concepts and Applications, Lippincott Williams & Wilkins, Baltimore”. In: (1995).

[31] AJ Atkinson Jr et al. “Clinical pharmacokinetics”. In: *Annual review of pharmacology and toxicology* 19.1 (1979), pp. 105–127.

[32] Hyun-Jong Cho et al. “In vitro–in vivo extrapolation (IVIVE) for predicting human intestinal absorption and first-pass elimination of drugs: principles and applications”. In: *Drug development and industrial pharmacy* 40.8 (2014), pp. 989–998.

[33] Jong H Sung et al. “Microfabricated mammalian organ systems and their integration into models of whole animals and humans”. In: *Lab on a Chip* 13.7 (2013), pp. 1201–1212.

[34] Mara Lucchetti et al. “Emulating the gut–liver axis: Dissecting the microbiome’s effect on drug metabolism using multiorgan-on-chip models”. In: *Current Opinion in Endocrine and Metabolic Research* 18 (2021), pp. 94–101.

[35] Palrasu Manikandan et al. “Cytochrome P450 structure, function and clinical significance: a review”. In: *Current drug targets* 19.1 (2018), pp. 38–54.

[36] Zhenguo Wang et al. “Human cholangiocytes form a polarized and functional bile duct on hollow fiber membranes”. In: *Frontiers in bioengineering and biotechnology* (2022), p. 922.

[37] Nathalie Picollet-D’hahan et al. “Multiorgan-on-a-chip: a systemic approach to model and decipher inter-organ communication”. In: *Trends in biotechnology* 39.8 (2021), pp. 788–810.

[38] Cryptotex. *ADME guide - First pass metabolism*. 2023. URL: `https://www.cyprotex.com/admepk`.

[39] Jean Matthieu Prot et al. “First pass intestinal and liver metabolism of paracetamol in a microfluidic platform coupled with a mathematical modeling as a means of evaluating ADME processes in humans”. In: *Biotechnology and bioengineering* 111.10 (2014), pp. 2027–2040.

[40] Talita Miguel Marin et al. “Acetaminophen absorption and metabolism in an intestine/liver microphysiological system”. In: *Chemico-biological interactions* 299 (2019), pp. 59–76.

[41] Hiroshi Arakawa et al. “Kinetic analysis of sequential metabolism of triazolam and its extrapolation to humans using an entero-hepatic two-organ microphysiological system”. In: *Lab on a Chip* 20.3 (2020), pp. 537–547.

[42] Mandy B Esch et al. “Modular, pumpless body-on-a-chip platform for the co-culture of GI tract epithelium and 3D primary liver tissue”. In: *Lab on a Chip* 16.14 (2016), pp. 2719–2729.

[43] Jiumeng Zhang et al. “Digital light processing based three-dimensional printing for medical applications”. In: *International journal of bioprinting* 6.1 (2020).

[44] Yinyin Bao et al. “Challenges and opportunities in 3D printing of biodegradable medical devices by emerging photopolymerization techniques”. In: *Advanced Functional Materials* 32.15 (2022), p. 2109864.

[45] Yan Yang et al. “Printability of external and internal structures based on digital light processing 3D printing technique”. In: *Pharmaceutics* 12.3 (2020), p. 207.

[46] Kyu-Young Shim et al. “Microfluidic gut-on-a-chip with three-dimensional villi structure”. In: *Biomedical microdevices* 19.2 (2017), p. 37.

[47] Kornphimol Kulthong et al. “Implementation of a dynamic intestinal gut-on-a-chip barrier model for transport studies of lipophilic dioxin congeners”. In: *Rsc Advances* 8.57 (2018), pp. 32440–32453.

[48] Vincenza De Gregorio et al. “Intestine-liver axis on-chip reveals the intestinal protective role on hepatic damage by emulating ethanol first-pass metabolism”. In: *Frontiers in bioengineering and biotechnology* 8 (2020), p. 163.

[49] Aleksander Skardal et al. “Multi-tissue interactions in an integrated three-tissue organ-on-a-chip platform”. In: *Scientific reports* 7.1 (2017), pp. 1–16.

[50] Anna Herland et al. “Quantitative prediction of human pharmacokinetic responses to drugs via fluidically coupled vascularized organ chips”. In: *Nature biomedical engineering* 4.4 (2020), pp. 421–436.

[51] Paul M van Midwoud et al. “A microfluidic approach for in vitro assessment of interorgan interactions in drug metabolism using intestinal and liver slices”. In: *Lab on a Chip* 10.20 (2010), pp. 2778–2786.

[52] Mingsha Jie et al. “An on-chip intestine-liver model for multiple drugs absorption and metabolism behavior simulation”. In: *Science China Chemistry* 61.2 (2018), pp. 236–242.

[53] Jiandong Yang et al. “Multilayered Microfluidic Device for Controllable Flow Perfusion of Gut-Liver on a Chip”. In: *2021 21st International Conference on Solid-State Sensors, Actuators and Microsystems (Transducers)*. IEEE. 2021, pp. 176–179.

[54] Thibault Bricks et al. “Development of a new microfluidic platform integrating co-cultures of intestinal and liver cell lines”. In: *Toxicology in Vitro* 28.5 (2014), pp. 885–895.

[55] Hessel HH Maalderink et al. “3D Printed structural electronics: embedding and connecting electronic components into freeform electronic devices”. In: *Plastics, Rubber and Composites* 47.1 (2018), pp. 35–41.

[56] Salvatore Cuzzocrea et al. “Role of free radicals and poly (ADP-ribose) synthetase in intestinal tight junction permeability”. In: *Molecular Medicine* 6.9 (2000), pp. 766–778.

[57] Paula Blanco et al. “Bacterial multidrug efflux pumps: much more than antibiotic resistance determinants”. In: *Microorganisms* 4.1 (2016), p. 14.

[58] Karine Anselme et al. “Cell/material interfaces: influence of surface chemistry and surface topography on cell adhesion”. In: *Journal of Adhesion Science and Technology* 24.5 (2010), pp. 831–852.

[59] Rachel Stewart et al. “Generation of three induced pluripotent stem cell lines from a patient with KCNQ2 developmental and epileptic encephalopathy as a result of the pathogenic variant c. 638C> T; p. Arg213Gln (NUIGi063-A, NUIGi063-B, NUIGi063-C) and 3 healthy controls (NUIGi064-A, NUIGi064-B, NUIGi064-C)”. In: *Stem Cell Research* (2023), p. 103093.

[60] Leon Chew et al. “Generating cerebral organoids from human pluripotent stem cells”. In: *Neural Progenitor Cells: Methods and Protocols* (2022), pp. 177–199.

[61] Nicoló Milani et al. “Application of a gut–liver-on-a-chip device and mechanistic modelling to the quantitative in vitro pharmacokinetic study of mycophenolate mofetil”. In: *Lab on a Chip* 22.15 (2022), pp. 2853–2868.

[62] Mandy B Esch et al. “Body-on-a-chip simulation with gastrointestinal tract and liver tissues suggests that ingested nanoparticles have the potential to cause liver injury”. In: *Lab on a Chip* 14.16 (2014), pp. 3081–3092.

[63] Lawrence Vernetti et al. “Functional coupling of human microphysiology systems: intestine, liver, kidney proximal tubule, blood-brain barrier and skeletal muscle”. In: *Scientific reports* 7.1 (2017), pp. 1–15.

[64] Rachelle Prantil-Baun et al. “Physiologically based pharmacokinetic and pharmacodynamic analysis enabled by microfluidically linked organs-on-chips”. In: *Annu. Rev. Pharmacol. Toxicol* 58 (2018), pp. 37–64.

[65] Ying I Wang et al. “Multiorgan microphysiological systems for drug development: strategies, advances, and challenges”. In: *Advanced healthcare materials* 7.2 (2018), p. 1701000.

[66] John P Wikswo et al. “Engineering challenges for instrumenting and controlling integrated organ-on-chip systems”. In: *IEEE Transactions on Biomedical Engineering* 60.3 (2013), pp. 682–690.

[67] Mridu Malik et al. “Critical considerations for the design of multi-organ microphysiological systems (MPS)”. In: *Frontiers in Cell and Developmental Biology* 9 (2021).

[68] Sangeeta N Bhatia et al. “Microfluidic organs-on-chips”. In: *Nature biotechnology* 32.8 (2014), pp. 760–772.

[69] Dongeun Huh et al. “Microengineered physiological biomimicry: organs-on-chips”. In: *Lab on a Chip* 12.12 (2012), pp. 2156–2164.

[70] Jong Hwan Sung et al. “Strategies for using mathematical modeling approaches to design and interpret multi-organ microphysiological systems (MPS)”. In: *APL bioengineering* 3.2 (2019), p. 021501.

[71] Lucie A Low et al. “Organs-on-chips: into the next decade”. In: *Nature Reviews Drug Discovery* 20.5 (2021), pp. 345–361.

[72] Martin Trapecar. “Multiorgan microphysiological systems as tools to interrogate interorgan crosstalk and complex diseases”. In: *FEBS letters* 596.5 (2022), pp. 681–695.

[73] John P Wikswo et al. “Scaling and systems biology for integrating multiple organs-on-a-chip”. In: *Lab on a Chip* 13.18 (2013), pp. 3496–3511.

[74] Christopher MoraesEqual contributions et al. “On being the right size: scaling effects in designing a human-on-a-chip”. In: *Integrative Biology* 5.9 (2013), pp. 1149–1161.

[75] Craig R White et al. “Metabolic scaling in animals: methods, empirical results, and theoretical explanations”. In: *Comprehensive Physiology* 4.1 (2011), pp. 231–256.

[76] Christian Maass et al. “Multi-functional scaling methodology for translational pharmacokinetic and pharmacodynamic applications using integrated microphysiological systems (MPS)”. In: *Integrative Biology* 9.4 (2017), pp. 290–302.

[77] James J Feng et al. “A similarity scaling approach for organ-on-chip devices”. In: *Lab on a Chip* (2022).

[78] Alireza Tajeddin et al. “Design and fabrication of organ-on-chips: promises and challenges”. In: *Micromachines* 12.12 (2021), p. 1443.

[79] B Selma Mohammed et al. “Are peristaltic pumps as reliable as syringe pumps for metabolic research? assessment of accuracy, precision, and metabolic kinetics”. In: *Metabolism* 53.7 (2004), pp. 875–878.

[80] Kenta Shinha et al. “A Kinetic Pump Integrated Microfluidic Plate (KIM-Plate) with High Usability for Cell Culture-Based Multiorgan Microphysiological Systems”. In: *Micromachines* 12.9 (2021), p. 1007.

A

2D Drawings and Microfluidic Set-up

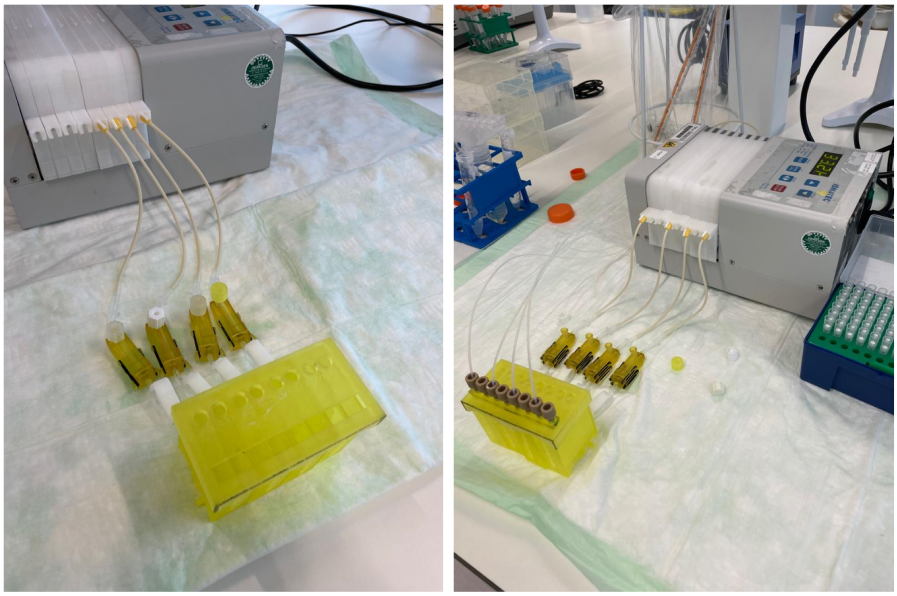

Figure A.1: Microfluidic set-up

HFM Holder

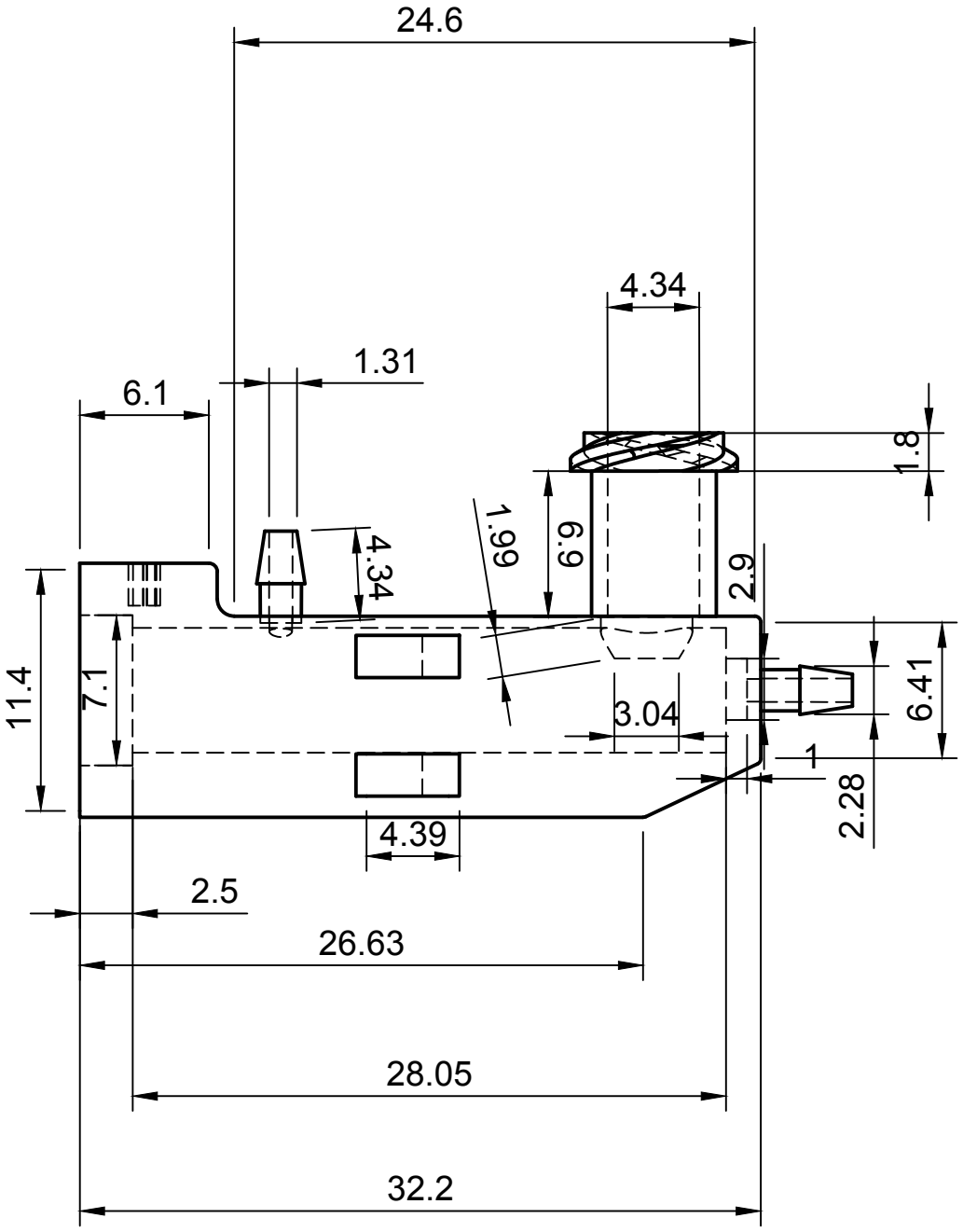

Figure Scale 3:1

Dept.	Technical reference	Created by	Approved by
	mm	Sarah Braem 11/04/2023	
		Document type: Technical Drawing	Document status:
		Title: HFM Chip Final Version HFM Chip Holder Side View	DWG No.: 1
			Rev. / Date of issue: 11/04/2023 / Sheet: 1/1

HFM Holder

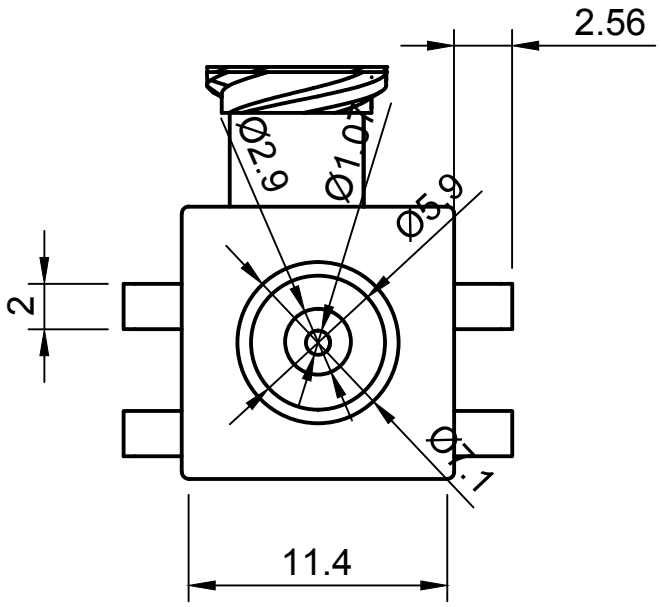

Figure Scale 3:1

Dept.	Technical reference	Created by	Approved by	
	mm	Sarah Braem 11/04/2023		
		Document type	Document status	
		Technical Drawing		
		Title	DWG No.	
		HFM Chip Final Version HFM Chip Holder Frontal View	2	
			Rev.	Date of issue: 11/04/2023 — Sheet: 1/1

HFM Holder

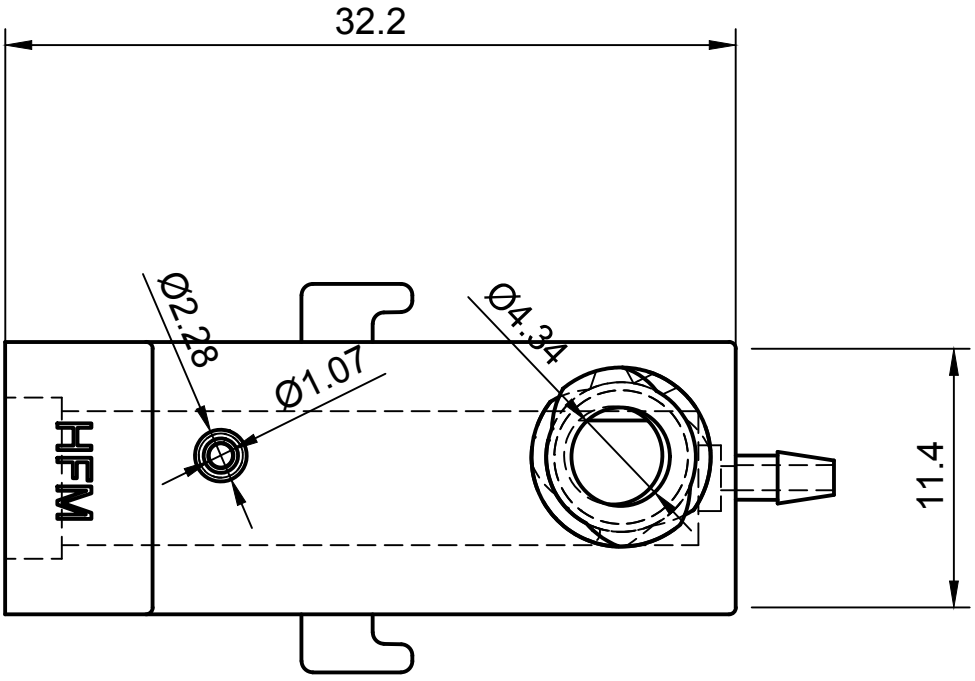

Figure Scale 3:1

Dept.	Technical reference	Created by	Approved by
	mm	Sarah Braem 11/04/2023	
		Document type: Technical Drawing	Document status:
		Title: HFM Chip Final Version HFM Chip Holder Top View	DWG No.: 3
			Rev.: / Date of issue: 11/04/2023 / Sheet: 1/1

HFM CAP

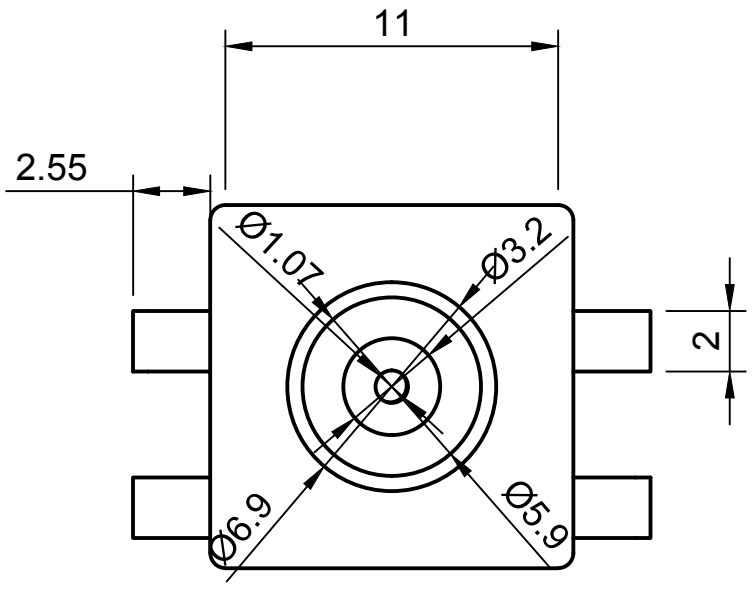

Figure Scale 4:1

Dept.	Technical reference	Created by	Approved by		
	mm	Sarah Braem 11/04/2023			
		Document type	Document status		
		Tecnical Drawing			
		Title	DWG No.		
		HFM Chip Final Design HFM Chip Cap Back View			
			Rev.	Date of issue	Sheet
				11/04/2023	1/1

HFM CAP

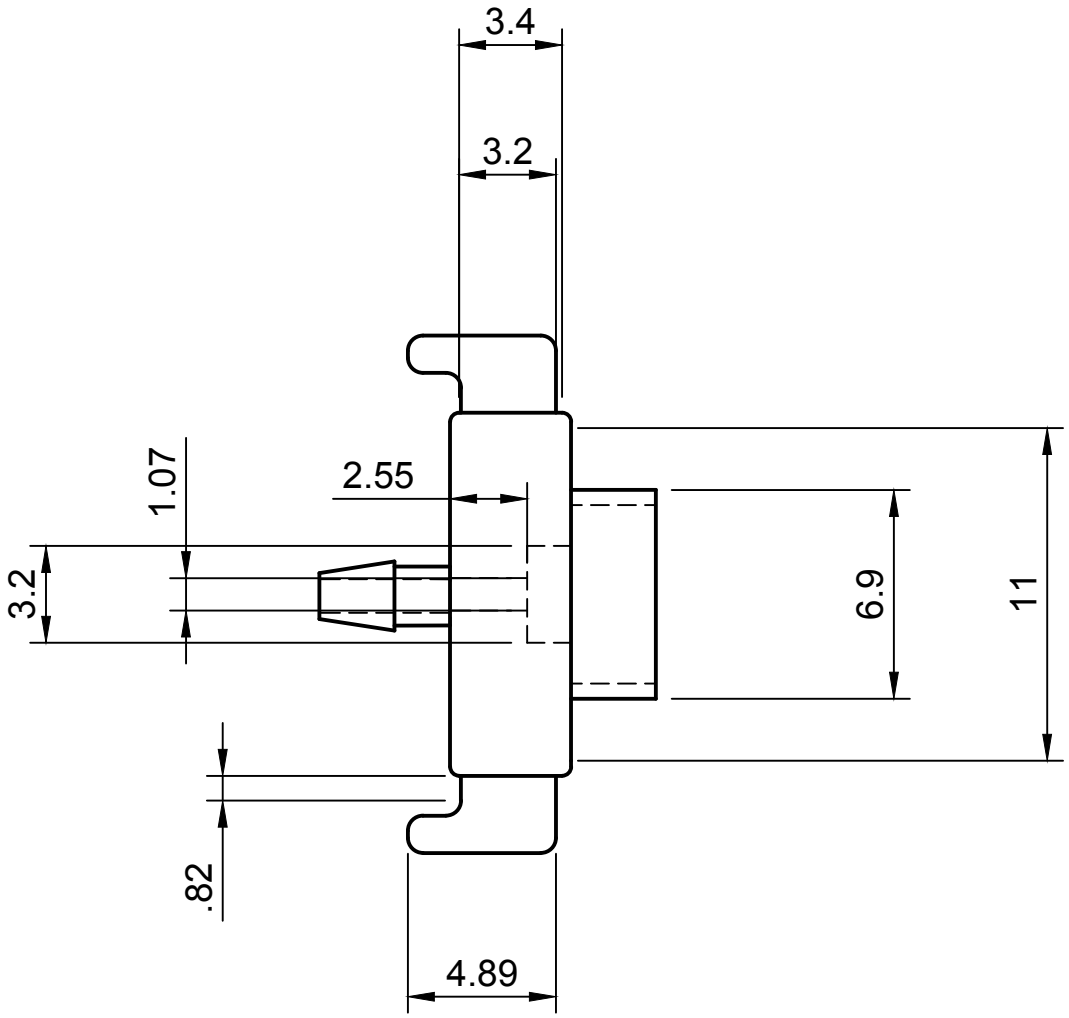

Figure Scale 4:1

Dept.	Technical reference	Created by	Approved by
	mm	Sarah Braem 11/04/2023	
		Document type: Tecnical Drawing	Document status:
		Title: HFM Chip Final Design HFM Chip Cap Top View	DWG No.:
			Rev. / Date of issue: 11/04/2023 / Sheet: 1/1

HFM Insert

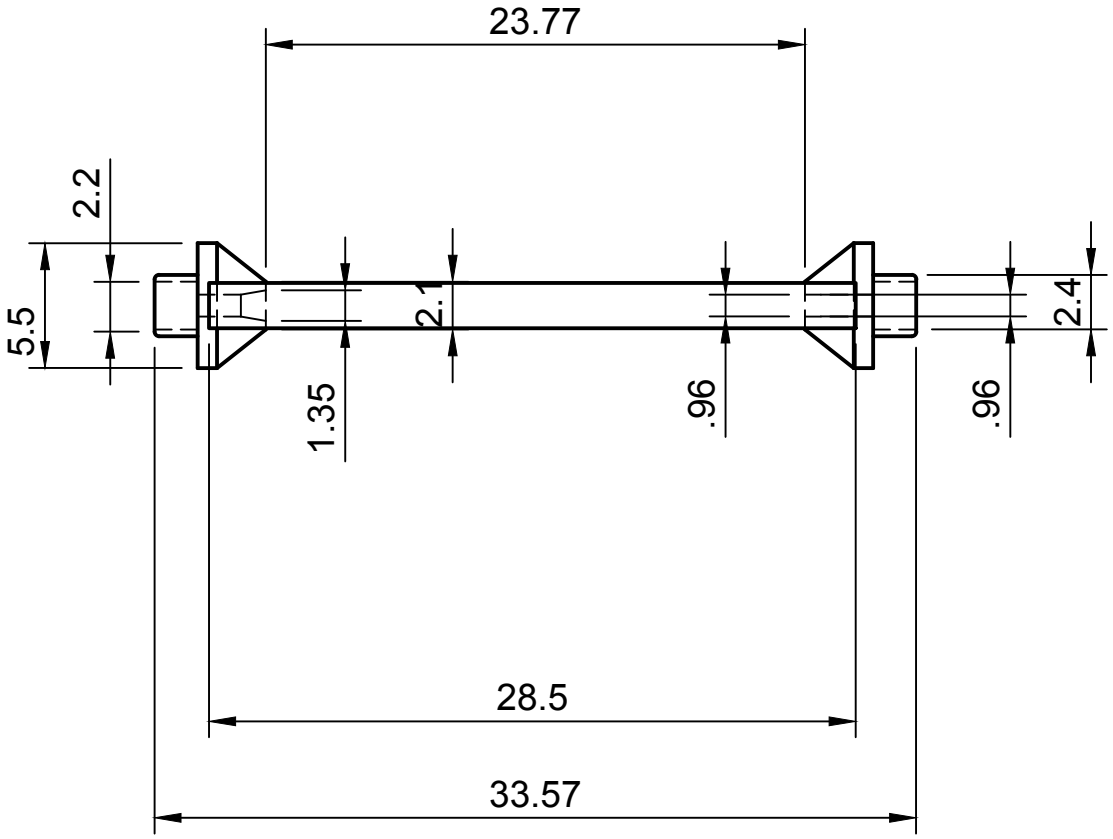

Figure scale 3:1

Dept.	Technical reference	Created by	Approved by
	mm	Sarah Braem 11/04/2023	
		Document type: Technical Drawing	Document status:
		Title: HFM Chip Final Version HFM Chip Insert Side View	DWG No.: 1
			Rev. / Date of issue: 11/04/2023 / Sheet: 1/1

HFM Insert

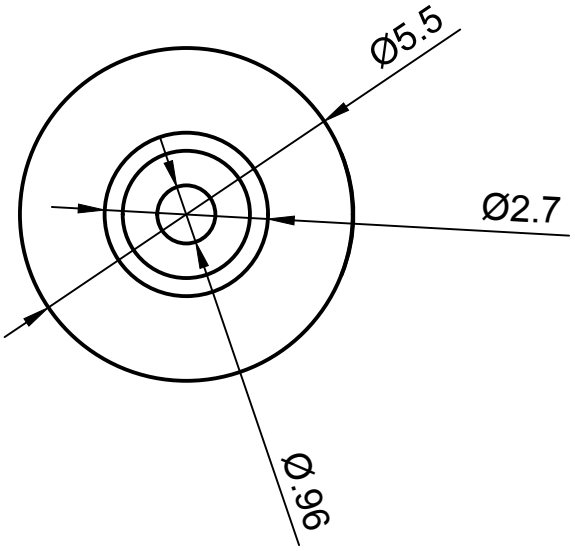

Figure Scale 8:1

Dept.	Technical reference	Created by	Approved by	
	mm	Sarah Braem 11/04/2023		
		Document type	Document status	
		Technical Drawing		
		Title	DWG No.	
		HFM Chip Final Version HFM Chip Insert Front View	2	
			Rev. / Date of issue / Sheet	
			11/04/2023	1/1

B

Design Overview

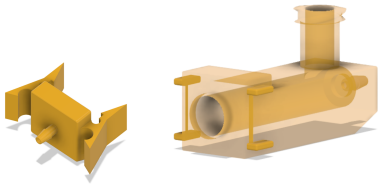

Figure B.1: V1.2. Click system. Cap could not be removed from holder after application.

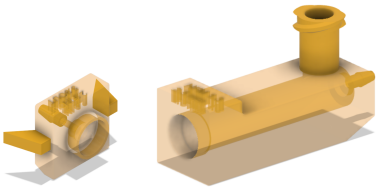

Figure B.2: V2.3 Push system. High leakage because cap was not attached to the system and pressure by the flow pushed cap out of the holder.

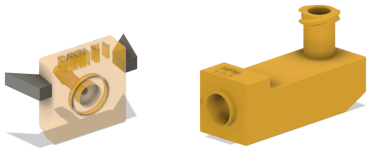

Figure B.3: V2.4. Alternative push system. Same problem as V2.3.

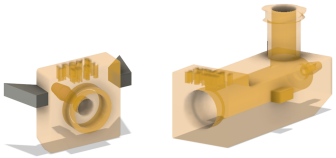

Figure B.4: V2.6. Alternative push system. Same problem as V2.3 and 2.4.

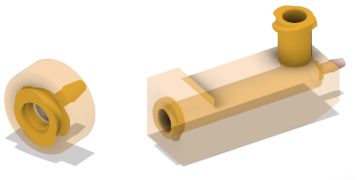

Figure B.5: V3.1. Screw system. Created high torsion on the insert causing it to break.

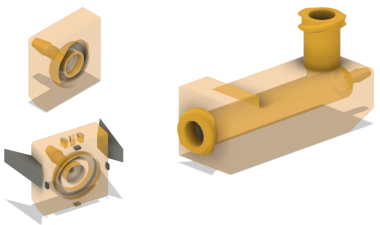

Figure B.6: V3.3. Alternative screw system. Same problem as V3.1.

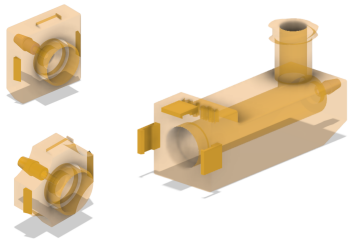

Figure B.7: V4.1. Snap-fit mechanism. Susceptible to breaking.

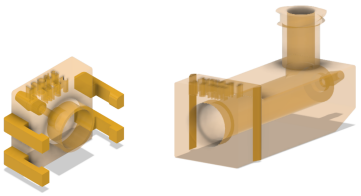

Figure B.8: V4.2. Click-system. Wings cap very susceptible to breaking.

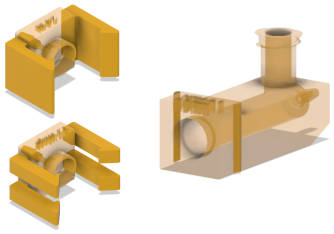

Figure B.9: V4.6. Click-system with rounded edges. Top cap hard to remove, bottom cap easy and intuitive to use, but did not exert enough pressure on the system to stay leak-free when cap was fully cured (and brittle). A more flexible material for the cap could resolve this problem in the future.

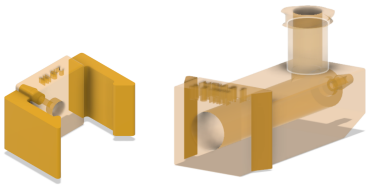

Figure B.10: V4.7. Alternative click-system with rounded edges. Leak-free but very hard to remove cap from holder after experiment.

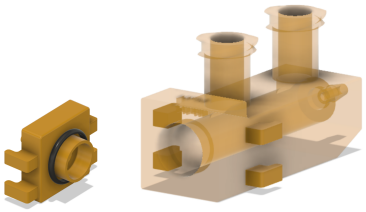

Figure B.11: V5. Alternative final version of the final design (2 sample luers instead of 1 sample luer and 1 TNO connector on top of holder. May be useful for easier sampling.

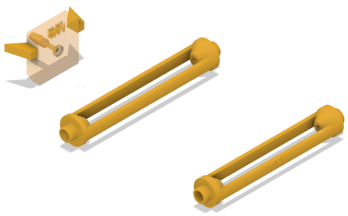

Figure B.12: The design of the insert was primarily changed concerning the inner diameter and inside space of the extremities and the full length. Precise fit in the HFM chip cap was determined by printing a range of different caps like the one on top and fitting the insert.

C

Protocols

Caco-2 & HepaRG culture in Hollow Fiber Membrane (HFM) Holder

Version 2.1 (03-12-2022)

This protocol describes how to seed caco-2 cells on HFMs using the HFM holder and how to perform a perfusion experiment. This protocol is also applicable to other cell types. HFM coating, seeding density and culture time & conditions may vary in that case.

Protocol overview

1. Sterilize and coat HFM's with L-DOPA and Collagen I (or IV)
2. Sterilize holders with EtOH and UV
3. Glue HFMs into holders
4. Seed cells on holder in 2ml tubes with periodic rotation for 4h
5. Move holders with HFMs to 6 well plates
6. Put on shaker after day 7, culture up to 21 days
7. Perform perfusion experiment

Detailed Protocol

Fiber Preparation & Coating

1. Dissolve L-DOPA in 10 mM Tris pH 8.5 (2 mg/mL) overnight at 37°C on a carrousel or rocker
2. After the L-DOPA solution is dissolved the next day, filter sterilize it using a 0.22um syringe filter.
3. Cut HFM's in pieces of 35mm in length
4. Sterilize fibers in 70% ethanol in a sterile tube (2ml – 50ml) for 30 min at RT
5. Wash fibers 3x with 1x PBS, store in 1x PBS
6. Add the L-DOPA solution to fibers and incubate for 4h at 37˚C on a carrousel or rocker
7. Wash fibers 3x with 1x PBS
8. Dilute ECM components (Collagen I/IV 25µg/ml) in PBS (25µl collagen I/5ml PBS with collagen I 5mg/ml).
9. Incubate fibers with the ECM solution for 2h at 37˚C on a carrousel or rocker
10. Remove the solution and dry fibers for 45 min at RT (open lid) in a sterile environment
11. Wash fibers with 1x PBS, use immediately

Fiber Gluing

1. Sterilize HFM holders in 70% ethanol for 30 minutes. Thoroughly wash in PBS 3x and sterilize with UV for 15 minutes.
2. Insert coated HFM's into sterile holders using tweezers (check if the surface of the insert is smooth everywhere and no remaining of a support is present!).
3. Deposit dental glue into HFM holder, making sure not to damage HFM (about 4 holders can be glued sequentially before glue hardens).
    a. Use the mixer nozzle and tips provided by dental glue manufacturer, **OR**
    b. Attach a (blunt end) syringe needle to a 10ml syringe
    c. Remove plunger from the syringe, deposit both glue components into syringe
    d. Briefly mix with a pipette tip, put back the plunger and push through the glue
4. Let glue set for 5 minutes.

5. Cut off excess glue and HFM sticking out flush with the holder using a sterile scalpel blade (make sure HFM does not close by cutting off excess glue).
6. Place HFM holders in sterile 2mL Eppendorf tubes.

Fiber Seeding & Culture

1. Harvest Caco-2 cells from culture, ideally 300k-500k cells per mL.
2. Fill 2ml tubes completely(~1.9mL) of suspended cells(600k-1000k cells in total).
3. Incubate HFM Holders with cells for a total of 4 hours.
    a. Gently tilt left and right to resuspend cells and lay down with a 90 degree rotation every 45 minutes at 37°C.
4. Remove HFM Holders from the 2mL tubes and place in 6 well plates, incubate at 37°C
    a. Up to 3 holders can fit into 1 well of a 6 well plate
    b. 6ml of medium per well, refreshed every other day
5. Fibers can be placed on a rocker from day 7 for better maturation.
6. Tight monolayer is formed after 12 days, full maturity after **21 days** for **Caco-2**; for **HepaRG** tight monolayer after 10 days, afterwards add differentiation medium (medium with 1% DMSO) and let differentiate for 10 days, so full maturity at **20 days**.

Perfusion Experiment

1. In case of long duration experiments, sterilize chip with 70% ethanol for 30 minutes. Thoroughly wash in PBS 3x and sterilize with UV for 15 minutes. In case of short duration experiments without sterilization it is important to make sure that all parts of the chip are saturated with liquid (e.g. PBS) before usage to prevent bubble formation in the chip (never use a dry chip)!
2. Assemble system as shown in figure 1 and wash with Biofilm (30min), PBS (30min) and medium (1h) at a speed of 0.333 µl/min.
3. Put small O-rings on both ends of the HFM insert (figure 2).
4. Check if HFM openings are open on both sides and are not blocked by glue!
5. Insert HFM holder into chip (figure 3).
6. Put on a larger O-ring around the larger opening of the cap. Close off the chip with the cap (figure 4) and attach 2 rubber elastics between the upper and lower connections of the cap and the holder (figure 4b) (in case of old rubber elastics, 4 elastics per connection can be used to create a tight seal).
7. Attach a piece of tubing (approx. 4 cm long) the front of the chip and connect the chip to pump with a clamp in between the reservoir and the chip (figure 5).
8. Add right amount of dose or medium in the basolateral reservoirs (for an experiment of 1 hour, you need 2 ml dose/reservoir).
9. Add 710 µl of medium or dose through the sample port in the apical reservoir of the chip.
10. Close the sampling ports with a clean luer cap.
11. Run for X(~10) min at 33,3 µl/min speed and take the T=0 measurement from the reservoir. This speed is used for the whole duration of the experiment.
12. Start the experiment.
13. Sample through the sampling port and refill holder reservoir until 710 µl after sampling (apical sampling) or sample in the reservoir and refill until 2 ml after sampling (basolateral sampling).
14. After the experiment fiber can be removed from holder to continue incubation at 37C.

Important notes for chip assembly to prevent leakage:

- In case of first use of a chip it is important to make the surfaces of the chip “smoother”:
    - Put the a cap into the holder without an insert in the system and turn the cap around in the system until the surface feels smooth and turning is easy

    - Insert and remove a HFM insert in the holder a couple of times until the insert can smoothly be removed and inserted
    - Put one end of an insert in the cap and turn the insert a couple of times around until the surface feels smooth and turning is easy
- To prevent leakage it is very important that the insert fits smoothly in the cap and the holder. Sometimes, a remaining of a support is still present and prevents this. In that case the remaining of the support should be removed by filing the chip until the surface is completely smooth.

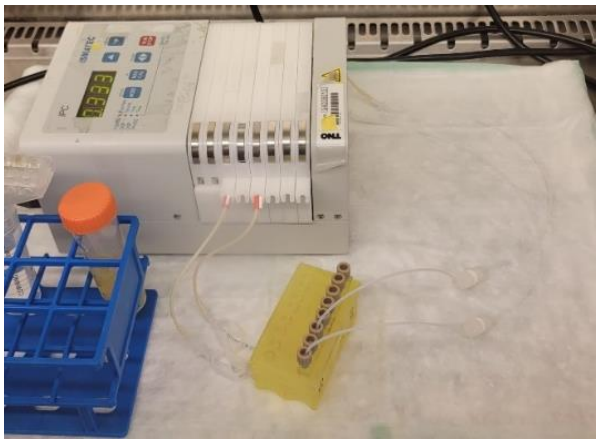

Figure 1. Reservoirs, tubing and luer connectors assembled to form a closed loop for washing.

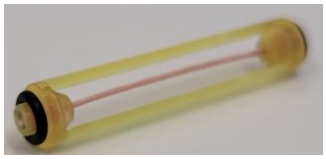

Figure 2. HFM insert with O-Rings.

3. HFM holder in HFM Chip.

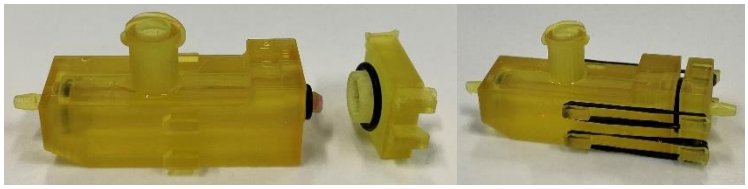

Figure 4. Assembled HFM chip.

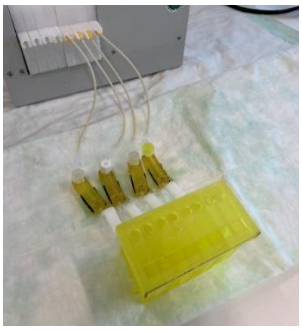

Figure 5. HFM chip connected to pump and reservoir.

D

Theoretical Background Coupling Methods

D.1. Coupling Methods

The design of the microfluidic chip and the specific goals of the research both influence how individual organ models can be coupled. The most common coupling methods for the generation of MOoC devices comprise functional coupling, physical or direct coupling of individual OoC models, and merging of numerous organ models on a single chip. These coupling methods and their most common advantages and disadvantages will be discussed in the following section to determine which is the best method for linking the liver- and intestine-on-a-chip in this particular study. The advantages and disadvantages of each method are summarised in Table D.1.

D.1.1. Single Chip Devices

The vast majority of designs used to couple liver- and gut-on-a-chip models that can be found in the literature are single-chip devices [19, 2, 17, 4, 61, 51, 52, 3, 62, 54, 39, 34]. In this case, the organ models are combined into a single microfluidic platform. This method has the primary benefit of minimizing the dead volume and required medium. Mostly, the chip comprises two organ chambers or layers (an intestine and liver compartment) that are directly interconnected by microfluidic channels [48]. The two-layer design enables direct and effective crosstalk between gut and liver cells by allowing them to be cultured in distinct compartments but in close proximity to one another [2]. This type of design omits the need for off-chip pumps and fluidic connections, contrary to devices that are directly or physically coupled. External pumping systems and fluidic connections create an inherent problem with the complexity and usability of microfluidic devices [2]. These problems are partially resolved by this type of design. Furthermore, the use of external pumping systems makes it more difficult to conduct high-throughput experiments and increases the chance of failures, such as fluid leakage or bacterial contamination [2]. Additionally, fluidically linked devices often fail to reproduce the desired circulation medium volume [53]. By including microfluidic channels in the chip and producing flow in other ways, for example by placing the chip on a tilting device to create gravity-induced flow [2] or utilizing on-chip micropumps, single-chip systems eliminate the need for external pumps and their corresponding disadvantages [53].

One typical example of such a single-chip device to recapitulate the first-pass metabolism was

created by *Choe et al.* [16]. This gut-liver chip is made using two separate layers, one for the gut epithelial cells (Caco-2 cells) and the other for the liver cells (HepG2 cells). [2]. Additionally, the chip is designed so that drugs are passed through the gut chamber to be absorbed before being passed on to the liver chamber, where the metabolic reaction occurs (Figure D.1) [2]. Here, the need for an external pump was eliminated by placing the chip on a tilting stage, thereby creating a gravity-based flow [2]. To further explore the first-pass metabolism in various tissue types, additional chambers can be added to the gut-liver chip [16]. In comparison to traditional models, both cell types found in the liver-gut chip displayed noticeable behavioral changes [11]. This result shows that co-culture systems are needed to enhance the physiological relevance of *in vitro* models [11].

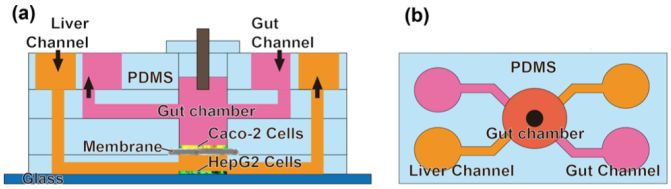

Figure D.1: First-pass metabolism recapitulated by microfluidic gut-liver chip. **a)** side-view of the gut-liver chip showing the separate layers for the gut cells (pink) and liver cells (orange). **b** top-view of the gut-liver chip. Figure adapted from *Choe et al.* [2].

Another example of a single-chip gut-liver device is the MOoC platform created by *Tsamandouras et al*. This platform was created to enable quantitative pharmacology experiments in coupled OoCs involving up to four separate organs [4]. The platform comprises five different compartments to hold a 3D-perfused liver OoC, a transwell-style gut OoC, two additional transwell-style OoCs of interest organs, and a mixing chamber that aims to replicate the systemic circulation compartment. Microfluidic channels and peristaltic micropumps, which are built into the bottom of the fluidic plate, connect the various platform compartments (Figure D.2b) [4]. What is special about this design is that it tries to closely resemble the human organ physiology and flow partition. The OoC interconnection scheme and associated flow partitioning are designed in such a way that they resemble the *in vivo* configuration as close as possible [4]. As a result, the gut and liver OoC compartments were linked together in series, and the total output from the mixing chamber (systemic flow rate) was distributed in a 75:25 ratio to the gut and liver compartments, respectively (Figure D.2a). As a result, the liver OoC receives 3/4 of its input flow from the outflow of the gut OoC compartment and 1/4 of its input flow (which mimics the hepatic artery blood flow) directly from the mixing chamber. The gut OoC receives its complete input flow directly from the mixing chamber (mimicking the portal vein blood flow) [4]. The versatility this platform provides in relation to drug dosage makes this MOoC platform ideal for drug-related studies. In particular, a compound can be supplied to the apical side of the gut OoC (emulating oral administration), where it will be absorbed and then dispersed first to the liver OoC compartment (as in the human body) before being distributed to the mixing chamber. In contrast, it can be given directly into the mixing chamber (mimicking an IV administration)[4].

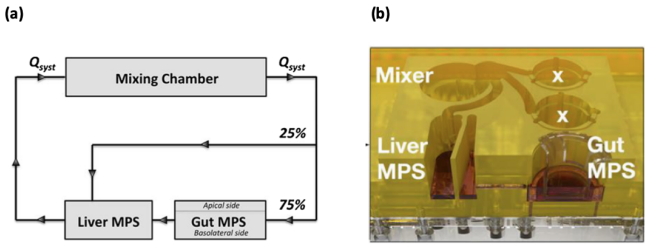

Figure D.2: a Flow pattern of the platform's medium shown schematically. The overall output from the mixing chamber is represented by the systemic flow rate (Qsyst), which was allocated, respectively, to the liver and gut OoC compartments at 75 and 25% of the total flow rate. **b** The platform consists of five different compartments (left top to right bottom): a mixing chamber that aims to replicate the systemic circulation, two transwell-style OoCs of interest organs, a 3D-perfused liver OoC, and a transwell-style gut OoC. Figure adapted from *Tsamandouras et al.* [4]

D.1.2. Direct or Physical Coupling

When using a direct or physical coupling, the individual organ models are connected through tubing systems or connecting channels, and the circulatory perfusion is achieved using an off-chip pumping system [2, 63]. In this way, the medium outflow of one organ (e.g. the gut) is linked to the inflow of another organ (e.g. the liver). Concerning gut-liver-on-a-chip devices, the basolateral compartment of the gut OoC (the gut OoC is mostly divided into an apical and basolateral compartment, see section 2.1.3) is generally fluidically connected to the liver OoC [61]. Individual organ-on-a-chip devices can also be connected through a central fluid-routing bread- or motherboard (Figure D.3) [49]. A crucial advantage of such a *"plug-and-play"* platform arrangement is its high degree of modularity, which enables individual organ modules to be developed and improved before being integrated into the system. Additionally, replacing a single organ model in the event of dysfunction or adding another serially connected tissue type to the system is very straightforward [49].

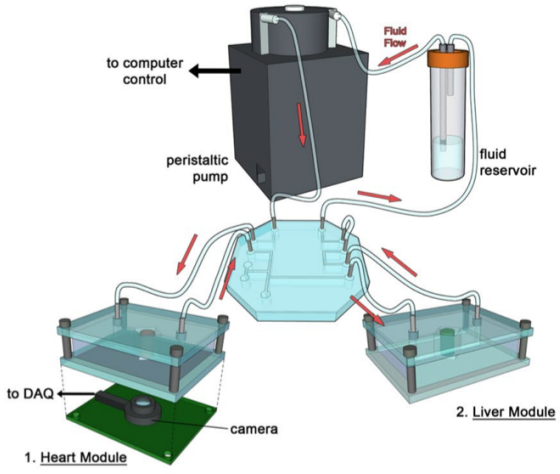

Figure D.3: Example of a plug-and-play system for organ-on-a-chip modules developed by *Skardal et al.* Individual organ modules are connected to each other and to a central motherboard. Figure adapted from *Skardal et al.* [49]

However, one major disadvantage of this configuration is the need for a common or *"universal"* medium [49, 64, 50]. As both the liver and gut organ modules have their own medium in which their cells thrive, the generation of a common medium in which both would thrive is very complicated. One way to overcome this issue is by using vascularised organ chips [50]. *Herland et al.* developed organ chips with endothelium-lined vascular channels [50]. Because of the endothelium-lined vasculature, the complete multi-organ system could be perfused with a common universal medium consisting of an optimized endothelial cell medium with a low quantity of serum [50]. This allows for *in vitro* modeling of normal systemic drug transport between organs. Moreover, the endothelium-lined vasculature supports the long-term survival of cells [50]. Another advantage of this setup is that the parenchymal channel of each organ chip is perfused with a distinct medium that is tailored for the organ-specific endothelium [50]. Besides this, *Herland et al.* incorporated an arteriovenous (AV) reservoir in the fluid stream to allow drug mixing [50]. This reservoir imitates the systemic circulation or bloodstream of the body and can be used to assess drug concentrations in the blood and plasma (Figure D.4 [50]. Using an AV reservoir enables getting around the drawbacks of simple serial linkages between various organ-on-a-chip systems. Serial linking led to cumulative drug loss with each organ linkage because they required the removal of experimental medium samples and replacement with a new medium [50, 64]. Additionally, by maintaining consistent flow and pressure across the system as well as physiologically appropriate drug distributions and organ-organ interactions, this arrangement avoids other drawbacks of serial organ-chip linkage [50].

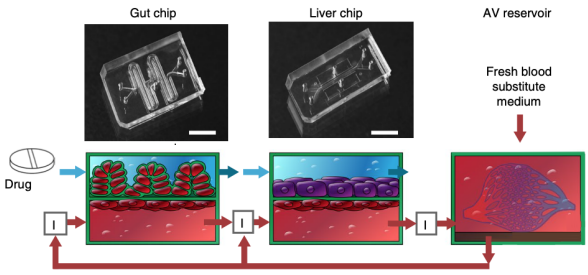

Figure D.4: Illustration of vascularized endothelium channels in the liver- and gut-on-a-chip devices which are linked to an AV reservoir that allows for drug mixing and continuous perfusion. Figure adapted from *Herland et al.* [50]

Next to the urgent need for a universal medium for physical coupling, there are some other disadvantages linked to this method. These include regulating organ-specific flow rates, the difficulty in reducing metabolic wastes to the next organ, proper scaling of the organ modules, and controlling adequate oxygenation of all modules in the system [63]. The best way to overcome these issues is to design and fabricate the organ modules simultaneously in the same lab, but nevertheless, determining the appropriate scaling between organ modules poses a considerable design and computation issue [63]. The issue of scaling organ modules to reproduce maximal biological functions will be further discussed in section D.4.

	Advantages	Disadvantages
One-chip	Omit the need for external pumping systems and their disadvantages Minimizing required medium	Need for a universal medium or vascularised organ system Scaling issues
Physical Coupling	High degree of modularity Plug-and-play system facilitates decoupling of malfunctioning organ modules and coupling of new organ modules	Need for a universal medium or vascularised organ system Need for external pumping systems which increase chances of bacterial contamination, failure, and leads to increased contamination of the system Difficulty to reproduce the desired circulation medium, reproduce organ-specific flow rates, reducing metabolic waste to the next organ, and controlling the oxygenation of all modules Scaling issues
Functional Coupling	Overcoming scaling issues No need for a universal medium Ability to adjust flow rates and medium composition for each module Functional composition of each organ module can be evaluated before medium transfer or ”coupling”	Results are not dynamic or real-time Difficult to sustain and repeat organ-organ interactions Difficult to adopt for industrial drug screening in its current format

Table D.1: Summary of advantages and disadvantages of the three major coupling methods for organ-on-a-chip modules [65, 50, 63, 66].

D.1.3. Functional Coupling

As an alternative to a direct or physical connection, functional coupling is defined as the transfer of media from one organ module to another in a physiological sequence. In other words, in functional coupling, the medium of one organ module is transferred to a consecutive organ module to achieve *in vivo*-like organ-organ interactions [63]. When employing functional coupling, the medium composition is functionally altered based on the distinct metabolic activity of each organ module [63]. This technique enables independent operation of each organ under optimal perfusion conditions [63]. Furthermore, it allows for multilaboratory collaboration as different organ modules can be independently constructed in physically distinct laboratories [65]. This integration technique has the potential to combine the knowledge from several laboratories and incorporate the most advanced single-organ modules into a multiorgan system. Physical decoupling makes it possible to build distinct organ models on various microfluidic platforms and cultivate them in their ideal medium and with their organ-specific perfusion rate. However, the outcomes would not be dynamic or real-time [65]. To what extent the interorgan communication can be sustained and rebuilt after the transfer of medium is a fundamental problem raised by the additional intermediate steps required to connect distant organ modules [65]. Notwithstanding, functional coupling overcomes the greatest issues of physical coupling, which are listed in Table D.1, because all organ modules are individually developed and sustained [63]. In fact, functional coupling can offer crucial information about the ideal scaling parameters for each organ module in a coupled system as well as information about media compatibility between modules, and therefore, it can be used as a first step to resolving the challenges of direct coupling of multiple organs in one continuous fluid stream [63]. So, before a universal platform and a common medium are established to physically connect all organ modules, functional coupling may be a useful technique for building prototype multiorgan models to collect insightful information for future designs. However, in its present state, it would be challenging to use this technique for industrial drug screening [65].

D.2. Medium

Providing each tissue type with a supply of nutrients and growth factors that meets the needs of that particular tissue is a crucial problem to solve when developing MOoC systems. Because of the multitude of available cell types, MOoC culture conditions must comply with a wide variety of cell growth needs [67]. Every organ exists out of a myriad of different cell types and, frequently, all of these cell types require a separate culture medium. Thus, when trying to co-culture cells from several organs, this problem becomes even more significant [16]. The usage of currently available cell culture media in MoOC experiments has turned into a hurdle in the recapitulation of the interaction between different organs because all cell culture media have been customized for a particular cell line [16].

Therefore, as mentioned before in section D.1.2, when coupling organ modules, either in a single chip or via physical coupling, a universal medium or *"blood surrogate"* is required [49, 64, 50]. Similar to how blood nourishes all the organs in the body, a universal blood surrogate is a single culture medium that sustains all of the tissues. The generation of such a medium remains a substantial obstacle, especially because some tissues are grown in a serum-containing medium and others in a serum-free medium and because existing culture media have been tailored for each individual cell type [68]. A universal medium is essential to preserve the viability and differentiated functionalities of numerous connected organ modules. All of the nutrients, chemicals, cytokines, and trophic factors needed by each organ module must be provided by the blood surrogate, together with physiologically realistic *"vascular linkages"* and blood composition (such as plasma protein binding) that accurately mirror drug profiles seen in humans [69]. To address this, the ideal universal medium would have to be serum-free, have no impact on tissue function, and include all the nutrients and growth elements needed for each unique organ. Although a standardized universal medium has not yet been identified, a number of other approaches have been proposed to address the problem [69, 49, 64, 50].

For linking the gut- and liver-on-a-chip devices, there are two common ways to circumvent this problem. The first solution is to develop organ chips with endothelium-lined vascular channels, as previously discussed in section D.1.2 [50]. Another way to mitigate this problem is to combine equal parts of existing cell-type specific media of the target organs. In this way, the universal medium contains vital growth factors for each type and can at least partially cover the needs of the involved organs [70]. However, it is important to note that this method will become less applicable when more than two organs are incorporated in the system [70].

D.3. Cell Sources and Cellular Environment

Cell sources can generally be divided into four categories: stem cell sources, *ex vivo* tissue biopsies, primary cells collected from human donors, and commercially available cell lines (immortalized cell lines) [71]. Although it is widely known that immortalized lines cannot replicate the complicated 3D *in vivo* tissue architecture and function (see section 2.1.3 and 2.2, up until now, most gut-liver-on-a-chip devices are designed to use conventional immortalized cell lines. Mostly, Caco2-cell lines are co-cultured with HT-29 or HepG2/C3A cell lines to simulate the gut and liver tissue, respectively [3, 52, 61, 54, 39]. Although these cell lines are highly appealing because of their wide availability and ease of use, they are not very relevant for drug absorption

studies as they lack the mature and complex microarchitecture of the *in vivo* environment [19]. So, the fact that, up until now, immortalized cell lines are used in most chips rather than higher performing primary cells or induced pluripotent stem cell (iPS)-derived cells may place a restriction on how accurately they may simulate complex reactions and interactions between tissues during drug and toxicity testing [49]. To achieve a more realistic model of the first-pass metabolism, new microfluidic devices are needed that can implement primary cells or 3D arrangements of cells. However, primary cell sources have quite some drawbacks such as being difficult to obtain from a human and the fact that they lose their functionality rapidly when used *in vitro* [3]. In order to solve this issue, the use of human induced pluripotent stem cells (hiPSCs) could be promising [3]. hiPSCs can offer an organ model that more closely resembles the human body [3]. Additionally, the organoids that are generated from iPSCs can close the gap between *in vivo* systems and *in vitro* models [3]. Unfortunately, for precise cell type differentiation, hiPSCs still require a lot of time [3].

Although most groups still use conventional cell lines, there are some examples of research groups that use 3D cell cultures of both the gut and liver cells [48, 3] or for one of both cell types [42]. Furthermore, some groups use intestinal and/or liver slices instead of cell lines inside their microfluidic devices [51]. However, these examples are quite exceptional, so this shows the importance of new devices that can accomplish the aforementioned requirements. Up until now, the gut-on-a-chip (IEBC) incorporated an intestinal tissue explant between its two microchannels, but in future research, this explant can be substituted by human-derived organoid cultures to approach the *in vivo* environment even more realistically [19]. As for the liver chip, liver organoids will be incorporated into the chip. Adult tissue progenitor/stem cells found in the intrahepatic bile ducts are mostly used to create the liver organoids [36]. These organoids are then called intrahepatic cholangiocyte organoids (ICOs). The ICOs can be genetically maintained and grown for several months *in vitro* due to their great proliferative abilities [36]. Additionally, the ICOs have the ability to differentiate into cholangiocyte or hepatocyte lineages after being cultured in specific media compositions [37].

D.4. Scaling

To avoid drug metabolites from one organ being delivered to other organs in excessively high or low quantities, MOoC devices for drug testing purposes must be designed with organ models that have the correct relative sizes and circulatory volumes [66]. For example, if a µOrgan and a mOrgan were connected, the mOrgan may not respond significantly to drugs or toxins provided by or metabolized by the µOrgan. Therefore, the scaling factor that results from a scaling analysis is a key design criterion as it establishes the limits of the dimensions of the microfluidic devices in terms of the sizes of connected organ chambers, the quantity of cellular material that is necessary, and the volume of the microfluidic channels [72]. System engineering faces a significant problem in designing and achieving organ systems that accurately represent the appropriate fraction of an adult human [66]. Although there are multiple scaling methods available to design MOoC devices, all methods have their own advantages and disadvantages, and to this day there is no consensus on which scaling method is the most appropriate to design a MOoc device [37, 73, 74]. In this paper, the most common scaling methods and their accompanying advantages and

disadvantages will be discussed.

D.4.1. Direct Scaling

Direct scaling is the simplest technique used for reducing organ size and is therefore the most used technique to scale and design MOoC devices. In direct scaling, readily available anatomical information, such as tissue volume, metabolic activity, or body mass, is used to proportionally scale down organs of interest [70]. One may, for instance, choose a scaling factor that is appropriate and compatible with the dimensions of the microfluidic device, then divide the size of each target organ by this downsizing factor [70].

D.4.2. Allometric Scaling

Allometry is the discipline that studies the relationships between anatomy, physiology, and body size and shapes [74]. It has been long recognized that numerous biological features vary allometrically with animal size [75]. In contrast to direct scaling, in allometric scaling, organ size does not scale isometrically (proportionally) with body mass (M_b) but rather follows a number of different allometric power laws describing for example blood flow rates, residence times, volumes, and metabolic rates [73, 76]. Organ mass can be computed with the following mathematical relationship:

$$M = AM_b^B \quad (11)$$

Where M is a physiological property, M_b is the mass of the organism, A is a constant, and B is a scaling exponent [74]. When B = 0, M is independent of (M_b); when B = 1 the relationship is isometric and M is proportional to (M_b) (as in direct scaling); when B takes on another value the relationship is allometric [75]. It is possible to normalize the relative sizes of connected organs to the surface area, mass, volumetric flow, or other geometric measurements [73]. If you want to design a physically functional organ in combination with a pharmacodynamic model in a MOoC, the difficulty is to specify the right scaling law(s) for that application [73].

D.4.3. Functional Scaling

Although direct and allometric scaling methods are often used to design MOoC devices, these methods do not systematically take into consideration the numerous interconnected mechanisms and factors in MOoCs [77]. As only the OoC-to-human size or mass ratio is used to calculate the size of the organs on the chip in both methods, these methods cannot guarantee accurate scaling of rate parameters because they do not involve any time scales (e.g., perfusion and metabolic rates) [77]. When applying direct or allometric scaling in a gut-liver device, this would result in drug exposure periods that are orders of magnitude lower than those *in vivo* [77]. Therefore, a more function-based scaling method is needed for the design of MOoCs [76]. When using functional scaling, certain physiological processes or behaviors from the *in vivo* environment are intended to be replicated in the *in vitro* setting [76]. Relating the desired functions of the MOoC to the application or study objective of interest can help identify design parameters for single OoCs

or MOoCs [76]. So, in contrast to the usual factors in direct or allometric scaling approaches, such as relative masses, and flow rates, these designs would be based on recapitulating the functions of the involved organs [76]. For example, for the liver, the most important function would be the metabolic rate [77]. When considering the application of this study (drug testing), biological processes that need to be taken into account in functional scaling would be drug metabolism and excretion [76]. However, the challenge in developing MOoC systems with this method is balancing the frequently incompatible demands of the multiple organs in the system [77].

Although many improvements in scaling methods have been proposed in the last couple of years, there is still no general framework for scaling and it remains one of the most pressing issues to be solved in MOoC device design [77].

D.4.4. Cellular Environment

Making sure that each organ model is included under the best possible conditions is a major challenge in the design of MOoCs. For cellular replication, the appropriate architecture of the tissue itself is of utter importance, but it is also crucial to take into account the microenvironmental impact of the scaffold or extracellular matrix (ECM) [37]. The tissue environment must as accurately as possible mimic the local *in vivo* environment and should be designed to encourage sufficient cell proliferation, support particular tissue properties, and be biocompatible with the intended studies [37]. As mentioned before, organoid cultures are a promising cell source for regenerative medicine, but they often require a 3D platform to recreate the (pato)physiology of their native tissue [36]. For this reason, the organoids that will be used in the liver chip will be cultured onto a polyethersulfone hollow fiber membrane (HFM) [36]. In this way, they can more accurately mimic their native environment by for example, obtaining an anatomical tubular architecture [36]. Furthermore, the HFM will be double-coated to provide the cells with an extracellular matrix (ECM) [65].

D.5. Flow Rates

In order to get relevant and correct results in OoC research, the control of the flow going through the OoC device is of crucial importance [78]. To guarantee similar fluid residence times in the organ modules to that *in vivo*, flow rates should be optimized. Additionally, flow rates should be controlled to ensure that secreted factors can build up to concentration levels above a specific threshold to be both detectable and have an impact on the next organ module in the MOoC sequence [78]. As each tissue type has a distinct metabolic profile and consequently specific perfusion requirements, flow rates are best controlled and altered per individual organ chamber in the MOoC setup. Some important factors that are impacted by the flow rate comprise (shear) stresses, polarity, and concentration gradients (oxygen and nutrients) [78]. Generally, the primary research objective determines the desired experimental flow rate [78]. As the flow rate should be customized for each organ chamber in the device, this makes the flow rate one of the most challenging design criteria for MOoC devices. Shear stress provided by the presence of a fluid flow is one the most important stimuli for developing mature tissue *in vitro* [11]. Therefore, the primary challenge when determining the fluid flow is to figure out the right flow rate that provides just enough stimulus (and thus shear stress) on the cells to allow for efficient transport and maturation but not too much to avoid the risk to damage them [2]. The following formula can be

used to calculate the fluid flow for a particular organ approximately:

$$\tau = \frac{6\eta Q}{wh^2} \quad (12)$$

h stands for the height of the channel in the OoC, w stands for the width, Q stands for the volumetric flow rate, and η stands for viscosity [2]. Other fluid flow values will be required for the liver and gut compartments in the MOoC device for them to function optimally. However, technical difficulties do often not allow to set the flow to a different rate in different organ chambers. Therefore, an appropriate intermediate value should be determined that suits the needs of both to a certain level. Finding this value will be a difficult task, so this will be a process of trial and error when developing the MOoC.

D.6. Fluid Circulation

Fluidic linkages between organ models are frequently required to establish organ-organ interactions *in vitro*. The current integration platforms can be divided into four main categories based on how different organ models are fluidically connected: static microscale platforms, single-pass microfluidic platforms, pump-driven recirculating microfluidic platforms, and pumpless recirculating microfluidic platforms (Figure D.8) [65].

D.6.1. Static Microscale Platforms

Organ-organ interactions in static microscale platforms are mostly accomplished through direct physical contact between tissues and/or passive diffusion of cell metabolites, soluble ligands, or cellular components via a common medium that bridges all organ chambers (Figure D.8A) [65]. The four major configurations of this kind of platform comprise a transwell platform, microtunnel platform, micropattern platform and wells-within-a-well platform [65]. As these configurations are not particularly relevant for connecting OoCs, there will be no further elaboration on these techniques in this paper.

D.6.2. Single-pass Microfluidic Platforms

By applying open-loop sequential medium perfusion through all organ units in a single fluid channel, or multiple separate ones if barrier tissues are included, single-pass microfluidic devices combine various organ models (Figure D.8B). In these systems, organ-organ interactions are often unidirectional [65]. Since there is no feedback path to the upstream organs, drugs, and drug metabolites from upstream organ models are carried along and can only affect the downstream organ units. Due to the absence of feedback, a potentially significant inter-organ interaction pathway may not be detected in this type of configuration [65]. Mostly, the connections in a single-pass microfluidic platform are established by physically linking multiple OoCs with tubing connections [65]. However, alongside the physical integration of different organ models, a special type of single-pass microfluidic platform exists, which is functional coupling [65]. This type of coupling was extensively discussed in section D.1.3. One of the main advantages of functional coupling is that it allows multilaboratory collaboration [65]. For example, *Vernetti et al.* connected

four different organ units that were built in four distinct laboratories [63]. By moving medium effluent from one organ module to the next in a physiological order, linkages between organs were made without physically connecting them [65, 63].

D.6.3. Pump-driven Recirculating Platform

The platforms on which barrier and parenchymal organ models are built often differ. Models of barrier tissues, including the lung, skin, and intestine, are frequently built on microporous membranes that divide the apical and basal area of the barrier, in contrast to parenchymal organ models, which are developed in constrained microchambers or hanging drops [65]. The different platforms for barrier and non-barrier tissues must frequently be integrated into one system in order to incorporate barrier tissues into MOoCs [65]. This integration can be realized by either incorporating OoCs in a single-chip (Figure D.5) or by physically connecting them by tubing (Figure D.6) [65]. The pump-driven recirculating platform is closed-loop and can consist of serial and/or parallel connections between individual OoCs (Figure D.8C) [65]. Furthermore, concerning the pumping systems themselves, these can be externally connected or can be integrated on the board of the chip [78]. The most commonly used external pumping systems are peristaltic or syringe pumps [79]. Both pumping systems have been shown to be very accurate and precise over a wide range of flow rates [79]. Pumps that are frequently used to realize an on-chip circulation system are peristaltic micro-pumps or kinetic pumps [80].

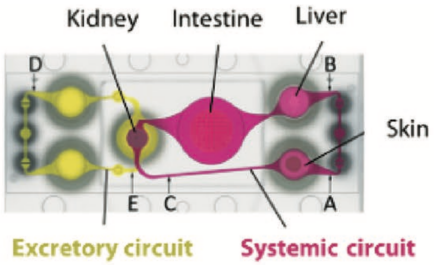

Figure D.5: Example of individual organ models integrated into one device (mostly used for organ models that comprise barrier tissues). Figure adapted from *Wang et al.* [65].

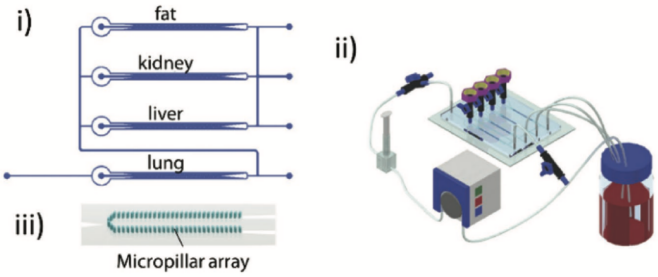

Figure D.6: Example of individual organ models connected by physical tubing (mostly used for organ models with only parenchymal tissues). Figure adapted from *Wang et al.* [65]

D.6.4. Pumpless Recirculating Platform

Contrary to the recirculating multiorgan platforms, which all depend on active fluid pumping to circulate medium among organ models, there also exists a type of microfluidic platform that passively generates flow by combining passive gravity-driven flow and a rocking motion [65]. Recirculating MOoC platforms rely heavily on expensive pumps that have the risk of introducing errors like air bubble formation and the leaking of medium [42]. To overcome these issues, in this configuration, a gravity-induced flow is achieved via an on-chip fluidic network by placing the chip on a tilting rocker platform and periodically changing the tiling direction (Figure D.8D). Instead of closed-loop unidirectional perfusion as occurs *in vivo*, this pumpless configuration offers reciprocating medium circulation [65]. However, the pharmacokinetic profiles of drugs hardly change as a result of the recirculation mode difference [65]. Furthermore, a gravity-driven system allows for exceptionally low liquid volumes because no tubing or pumps need to be refilled with medium [42]. Therefore, this configuration allows for a highly parallel and inexpensive operation while still being reliable [42].

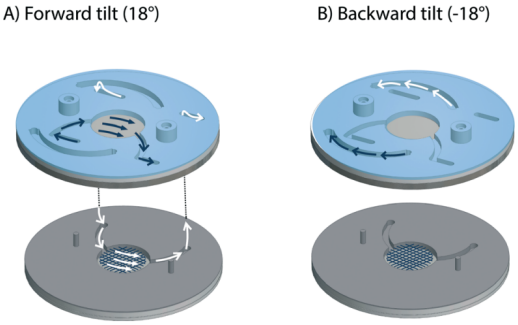

Figure D.7: Example of a pumpless recirculating platform developed by *Esch et al.*. Figure adapted from *Esch et al.* [42]

For example, *Esch et al.* developed a modular and pumpless MOoC system for the co-culture of 3D primary liver tissue and GI tract epithelium [42]. They have created different fluid flow paths through the organ chips for distinct tilting directions [42]. On the one hand, flow is directed through the tissue culture chambers when the chip is tilted at an angle of 18 degrees forward (Figure D.7A). The blue arrows indicate the flow through the apical side of the GI tract and the associated backflow channel, while the white arrows indicate the flow through the liver tissue chamber and the associated backflow channel. On the other hand, when the chip is tilted backward at 18°, the flow is directed through the backflow channels (Figure D.7B). The two fluidic circuits are independent and do not interact [42].

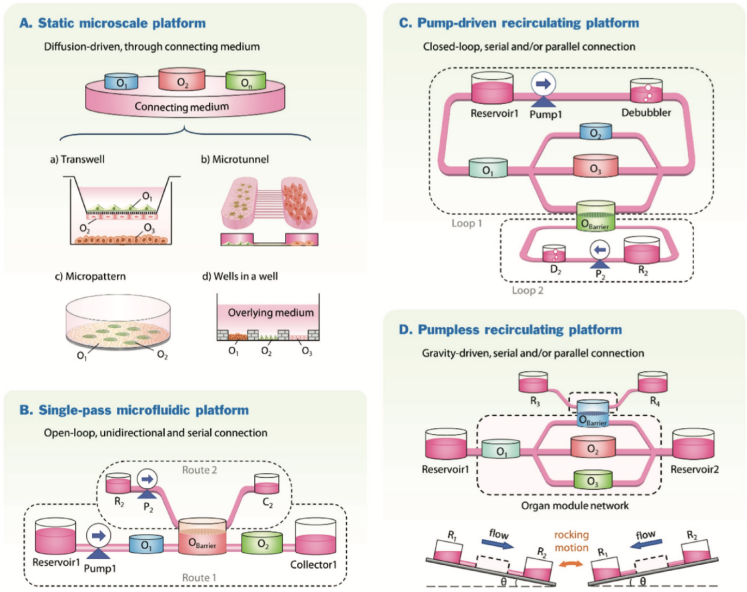

Figure D.8: Four main categories in which current integration platforms can be divided based on how different organ models are fluidically connected: (A) static microscale platforms, (B) single-pass microfluidic platforms, (C) pump-driven recirculating microfluidic platforms, and (D) pumpless recirculating microfluidic platforms. Figure adapted from *Wang et al.* [65]

The IEBC (gut-on-a-chip) that will be used in this study is a pump-driven recirculating platform as it works with a peristaltic pump [19]. This pump moves media back and forth between the reservoirs and the chip, by removing media from the reservoirs through the chip and returning it back to the reservoirs [19]. Therefore, when the chips are connected physically, the connection between the gut- and liver-on-a-chip will most likely also take on this configuration and make use of a peristaltic pump as this will be the most convenient option.